DILUTE SOLUTION PROPERTIES OF SEMIFLEXIBLE STAR POLYMERS(Dissertation_全文)

AUTHOR(S):

Ida, Daichi

DILUTE SOLUTION PROPERTIES OF SEMIFLEXIBLE STAR POLYMERS

DAICHI IDA

2008

Contents

1 Introduction

1.1 Background

Dilute solution behavior of polymers is mainly governed by average chain dimensions of the solute polymers, which are determined by the following three basic factors: primary molecular structures, e.g., linear or branched, chain stiffness, and interactions between segments constituting the polymer chains, the last factor being the so-called excluded-volume effects. Quite a number of theoretical and experimental studies have therefore long been made of the relation between the chain dimension and the three basic factors, and an almost complete understanding has already been built up of the contribution of each individual factor to the chain dimension.[1,2] However, in order to obtain a comprehensive understanding of solution behavior of real polymers having a variety of molecular structures, it is desirable to pursue further the study for cases in which two or more of the factors contribute to the chain dimension. In this thesis, we consider the case in which both the primary molecular structure and chain stiffness are simultaneously concerned, i.e., dilute solution behavior of semiflexible branched polymers.

Although quite a few studies have been made so far of the relation between the primary molecular structure and observable quantities relating to the average dimension of unperturbed chains without excluded volume, e.g., the mean-square radius of gyration $\langle S^2 \rangle$ and intrinsic viscosity $[\eta]$,[1,3–9] almost all of them were of flexible polymers except for the theoretical study by Mansfield and Stockmayer,[7] the Monte Carlo (MC) one by Zimm,[8] and the experimental one by Goodson and Novak.[9] Mansfield and Stockmayer calculated $\langle S^2 \rangle$ of the Kratky–Porod (KP) wormlike[2,10] star chain (without excluded volume) and examined the behavior of its ratio g_S to $\langle S^2 \rangle$ of the corresponding linear one having the same total length of the chain contour (molecular weight). Zimm evaluated $[\eta]$ of "wormlike" four- and six-arm stars by the use of his rigid-body ensemble approximation.[11] Unfortunately, however, his calculation is a preliminary survey, as mentioned by himself. Goodson and Novak synthesized three-arm star poly(*n*-hexyl isocyanate) (PHIC), which is a typical semiflexible polymer, by living titanium-catalized coordination polymerization,[9] and then investigated the behavior of $\langle S^2 \rangle$, $[\eta]$, and g_S as functions of molecular weight. However, they did not examine the behavior of the ratio g_η of $[\eta]$ of the star polymer to that of

the corresponding linear one, since there is no available theory of $[\eta]$ or g_η for semiflexible regular star polymers. Recall that a star polymer with uniform arm length is generally referred to as the regular star (polymer).

As for (perturbed) polymer chains in good solvents, short-ranged repulsive interactions work between segments, expanding the individual chains and yielding an effective volume $V_{\rm E}$ excluded to one chain by the presence of another. The volume $V_{\rm E}$ is another measure of the average chain dimension, although well-defined only in a good solvent system or in the perturbed state, and is proportional to the second virial coefficient A_2, which may be determined simultaneously with $\langle S^2 \rangle$ from light scattering measurements. Of course, there have been several theoretical and experimental studies[5,6,12,13] of A_2 of the flexible star polymers, but none of them has considered the effects of chain stiffness on A_2 for the star polymers.

Under such present situations mentioned above, our attention is necessarily focused on $[\eta]$ and A_2 of the semiflexible regular three-arm star polymers and we make an extensive theoretical and computer simulation study of the effects of chain stiffness on g_η in the unperturbed state and the ratio g_{A_2} of A_2 of the regular three-arm star chain to that of the corresponding linear one in the perturbed state.

For this purpose, we should choose an appropriate model which may well reproduce dimensional behavior of the real regular three-arm star polymers with various chain stiffness in both the unperturbed and perturbed states. Recently, MC studies[14,15] were made of $\langle S^2 \rangle$ and A_2 for flexible linear polymers in dilute solution using the freely rotating chain[1,2] of bond angle $\theta = 109^\circ$ ($\simeq$ tetrahedral bond angle) and with the Lennard–Jones (LJ) 6-12 intra- and intermolecular potential[16] between beads in a cutoff version. It was shown that the behavior of the MC data for $\langle S^2 \rangle$ and A_2 in the unperturbed and perturbed states may be described by the theory on the basis of the KP or helical wormlike[2] chain model as well as the cases of real flexible polymers. We therefore use this model with various values of θ, and calculate g_η and g_{A_2} for the regular three-arm stars with various chain stiffness by MC simulation. Further, it seems to be convenient and useful for an analysis of experimental data to construct a theoretical expression for g_η like the Mansfield–Stockmayer expression for g_S.[7] We then construct an interpolation formula for g_η of the semiflexible regular three-arm star chain on the basis of the KP chain without excluded volume.

The evaluation of $[\eta]$ requires some comments. As is well known, there is no method for the exact theoretical evaluation of $[\eta]$ since the hydrodynamic interaction between the segments composing polymer chains cannot be treated properly. We then use the Kirkwood–Riseman (KR) approximation[1,17] in the MC and theoretical calculations in this study as used in many theories[1,2,4] for polymer hydrodynamics. However, the KR

approximation may not always give a good approximate value of $[\eta]$ because of the preaveraging of the Oseen hydrodynamic tensor. Therefore, in the MC simulation for $[\eta]$ in this study, we also evaluate $[\eta]$ without the preaveraging of the Oseen tensor on the basis of the Zimm rigid-body ensemble approximation[11] and the Fixman method.[18,19] The Zimm method gives an upper bound[18,20] to $[\eta]$ and the Fixman method gives a lower bound.[18] On the basis of the two bounds to $[\eta]$ for the regular three-arm star and linear chains having the same total chain length and chain stiffness, an upper and lower bounds of g_η may be evaluated. Comparing the KR value of g_η with them, we examine the validity of the KR approximation in the evaluation of g_η of semiflexible regular three-arm stars.

The second virial coefficient A_2 of semiflexible or stiff chains having an interaction potential with an attractive tail, e.g., the LJ potential also requires some comments. Schoot and Odijk[21] pointed out that two rigid rods with an attractive tail, which are close to each other, prefer to be parallel rather than perpendicular to each other and their A_2 may therefore be suppressed. This may be also the case with the present MC model chains (the freely rotating chains interacting with the LJ 6-12 potential in a cutoff version) when the chains become stiffer. We therefore examine effects of the attractive tail on A_2 by comparing results for the MC chains with the LJ potential and the hard-sphere one.

1.2 Outline

The plan of this thesis is as follows.

In Chapter 2, Monte Carlo (MC) results of the intrinsic viscosity $[\eta]$ and also of the mean-square radius of gyration $\langle S^2 \rangle$ are presented for regular three-arm star freely rotating chains of bond angles $\theta = 109°$, $165°$, and $175°$ and with the Lennard–Jones (LJ) 6-12 potentials between beads having the parameter values corresponding to the Θ temperature, in the range of the total number n of bonds in the chain from 60 to 300. Three kinds of approximate values of $[\eta]$ are calculated by the use of the Kirkwood–Riseman (KR) approximation, the Zimm rigid-body ensemble approximation which gives an upper bound $[\eta]^{(\mathrm{U})}$ to $[\eta]$, and by the Fixman method which gives a lower bound $[\eta]^{(\mathrm{L})}$, the KR value of $[\eta]$ being designated $[\eta]^{(\mathrm{KR})}$. On the basis of the three kinds of MC values of $[\eta]$ so obtained, the behavior of the ratio g_η of $[\eta]$ for the star chain to that for the linear one, both having the same n, is examined as a function of the reduced contour length λL as defined as the total contour length L of the corresponding Kratky–Porod (KP) wormlike chain divided by its stiffness parameter λ^{-1}, the values of λL being determined from an analysis of the present and previous MC data for $\langle S^2 \rangle$ on the basis of the KP chain. It is found that the KR value $g_\eta^{(\mathrm{KR})}$ of g_η as defined by $[\eta]^{(\mathrm{KR})}(\mathrm{star})/[\eta]^{(\mathrm{KR})}(\mathrm{linear})$ lies between the values of an upper bound $g_\eta^{(\mathrm{U})}$ and a lower one $g_\eta^{(\mathrm{L})}$, which are defined

by $[\eta]^{(\mathrm{U})}$(star)/$[\eta]^{(\mathrm{L})}$(linear) and $[\eta]^{(\mathrm{L})}$(star)/$[\eta]^{(\mathrm{U})}$(linear), respectively, irrespective of the values of λL. Further, the difference between the two bounds becomes very small for small λL, indicating that $g_\eta^{(\mathrm{KR})}$ is a good approximate value for semiflexible or stiff chains.

In Chapter 3, the ratio g_η of $[\eta]$ of the KP wormlike regular three-arm star touched-bead model to that of the KP linear one, both having the same (reduced) total contour length L and (reduced) bead diameter d_b, is numerically evaluated in the KR approximation. Prior to the evaluation of g_η, an interpolation formula for the mean reciprocal of the end-to-end distance of the once-broken KP chain, which is necessary for the theoretical calculation in the KR approximation, is constructed on the basis of the asymptotic forms derived by the use of the Daniels method near the random-coil limit and the ϵ method near the rod limit and also on the basis of the Monte Carlo results. From an examination of the behavior of g_η as a function of L and d_b, it is found that the ratio g_η/g_η^0 of g_η to the rod-limiting value g_η^0 of g_η monotonically increases from 1 to 2.03 with increasing L and is almost independent of d_b for $d_\mathrm{b} \lesssim 0.2$, although the behavior of g_η itself as a function of L remarkably depends on d_b. An empirical interpolation formula is then constructed for g_η/g_η^0 as a function of L, which is considered to be useful for practical purposes.

In Chapter 4, MC results of the second virial coefficient A_2 and also $\langle S^2 \rangle$ are presented for regular three-arm star and linear freely-rotating chains of bond angles θ ranging from 109° (typical flexible chain) to 175° (typical semiflexible or stiff chain) with the LJ 6-12 potentials between beads corresponding to a good solvent system, the range of the total number n of bonds from 30 to 900. On the basis of the MC values of A_2 so obtained, an examination is made of effects of chain stiffness on the ratio g_{A_2} of A_2 of the star chain to that of the linear one, both chains having the same n and θ. It is then found that g_{A_2} is rather insensitive to change in θ (chain stiffness) in contrast to the cases of the ratios g_S and g_η related to $\langle S^2 \rangle$ and $[\eta]$, respectively, which remarkably decrease with increasing θ.

In Chapter 5, MC results of $\langle S^2 \rangle$ and A_2 are presented for the two freely rotating chains with the LJ 6-12 potential and the hard-sphere (HS) one in the range of the bond angle θ from 109° (typical flexible chain) to 175° (typical semiflexible or stiff chain) and in the range of the number n of bonds from 6 to 1000. It is shown that a value may be properly assigned to the collision diameter of the HS potential so that $\langle S^2 \rangle$ of the chain with the HS potential agrees well with that of the chain with the LJ one whose parameter values correspond to a good-solvent condition, irrespective of the chain stiffness. It is then found that A_2 of the latter chain becomes remarkably smaller than that of the former as the chain stiffness is increased. The result implies that the binary cluster approximation does not seem to work well for typical semiflexible and stiff polymers.

References

1. H. Yamakawa, "Modern Theory of Polymer Solutions," Harper & Row, New York, 1971. Its electronic edition is available on-line at the URL: `http://www.molsci.polym.kyoto-u.ac.jp/archives/redbook.pdf`
2. H. Yamakawa, "Helical Wormlike Chains in Polymer Solutions," Springer, Berlin, 1997.
3. B. H. Zimm and W. H. Stockmayer, *J. Chem. Phys.*, **17**, 1301 (1949).
4. B. H. Zimm and R. W. Kilb, *J. Polym. Sci.*, **37**, 19 (1959).
5. J. F. Douglas, J. Roovers, and K. F. Freed, *Macromolecules*, **23**, 4168 (1990), and papers cited therein.
6. Y. Nakamura, *Kobunshi Ronbunshu*, **57**, 530 (2000), and papers cited therein.
7. M. L. Mansfield and W. H. Stockmayer, *Macromolecules*, **13**, 1713 (1980).
8. B. H. Zimm, *Macromolecules*, **17**, 795 (1984).
9. S. H. Goodson and B. M. Novak, *Macromolecules*, **34**, 3849 (2001).
10. O. Kratky and G. Porod, *Recl. Trav. Chim. Pays-Bas.*, **68**, 1106 (1949).
11. B. H. Zimm, *Macromolecules*, **13**, 592 (1980).
12. J. F. Douglas and K. F. Freed, *Macromolecules*, **17**, 1854 (1984).
13. K. Ohno, K. Shida, M. Kimura, and Y. Kawazoe, *Macromolecules*, **29**, 2269 (1946).
14. H. Yamakawa and T. Yoshizaki, *J. Chem. Phys.*, **118**, 2911 (2003).
15. H. Yamakawa and T. Yoshizaki, *J. Chem. Phys.*, **119**, 1257 (2003).
16. J. P. Hansen and I. R. McDonald, "Theory of Simple Liquids," 3rd ed., Academic, London, 1986.
17. J. G. Kirkwood and J. Riseman, *J. Chem. Phys.*, **16**, 565 (1948).
18. M. Fixman, *J. Chem. Phys.*, **78**, 1588 (1983).
19. M. Fixman, *J. Chem. Phys.*, **78**, 1594 (1983).
20. G. Wilemski and G. Tanaka, *Macromolecules*, **14**, 1531 (1981).
21. P. van der Schoot and T. Odijk, *J. Chem. Phys.*, **97**, 515 (1992).

2 Intrinsic Viscosity of Semiflexible Three-Arm Stars: A Monte Carlo Study

2.1 Introduction

In this chapter, we examine effects of chain stiffness on the ratio g_η of the intrinsic viscosity $[\eta]$ of the regular three-arm star chain to that of the corresponding linear one, both having the same total chain length by Monte Carlo (MC) simulation using the freely rotating chain[1,2] with a cutoff version of the Lennard–Jones (LJ) 6-12 potential[3] between beads, which is essentially the same as that used in previous MC studies[4,5] of $\langle S^2 \rangle$ and the second virial coefficient of linear chains. On the basis of sets of sample configurations generated by the use of the Metropolis method[6] with the pivot algorithm[7–9] for the regular three-arm star and linear chains, both having the same total chain length, the values of $[\eta]$ for the two kinds of chains and then g_η may be evaluated.

As mentioned in Chapter 1, there is no method for the exact evaluation of $[\eta]$ since the hydrodynamic interaction between the segments composing polymer chains cannot be treated properly. We therefore evaluate $[\eta]$ in the three approximate ways: the Kirkwood–Riseman (KR) approximation,[1,10] the Zimm rigid-body ensemble approximation,[11] and the Fixman method.[12,13] We note that the Zimm method gives an upper bound to $[\eta]$ and the Fixman method gives a lower bound. On the basis of the three kinds of MC values, we examine the behavior of $[\eta]$ and g_η as functions of the total chain length and the chain stiffness.

2.2 Models and Methods

2.2.1 Models

The MC model used in this study is the regular three-arm star freely rotating chain, each arm composed of m successive bonds of length unity, so that it is composed of $3m$ $(= n)$ bonds, in total, and $3m + 1$ beads whose centers are located at $3m - 3$ junctions of two successive bonds on the arms, at the three terminal ends, and at the branch point (center), as illustrated in Figure 2.1. The angle between each pair of the bonds connected to the center is fixed to be 120°, so that those bonds are on the same plane. For convenience, the

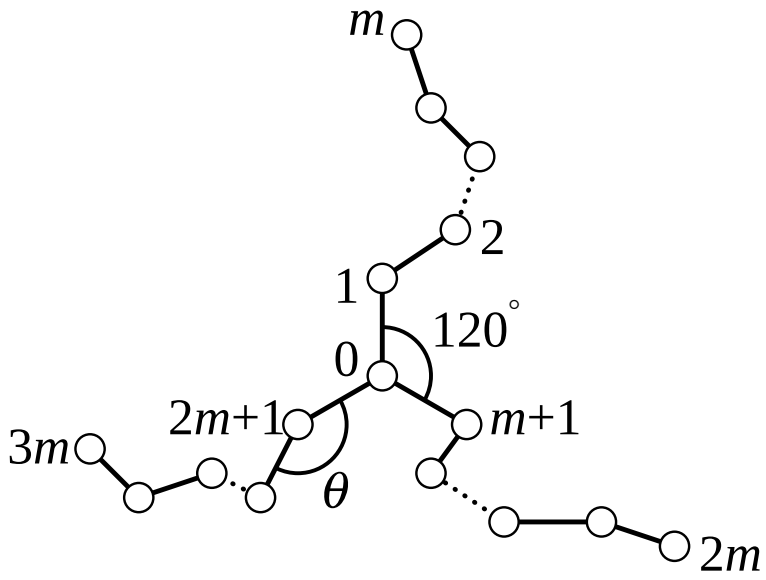

Figure 2.1. Illustration of the Monte Carlo model for the regular three-arm star chain.

three arms are designated the first, second, and third ones and the beads on the ith arm ($i = 1, 2, 3$) are numbered $(i-1)m+1$, $(i-1)m+2$, $\cdots$, im from the center to the end, with the center bead numbered 0. The ith bond vector $\mathbf{l}_i$ ($1 \le i \le 3m$; $i \ne m+1, 2m+1$) connects the centers of the $(i-1)$th and ith beads with its direction from the $(i-1)$th to ith bead, and $\mathbf{l}_{m+1}$ and $\mathbf{l}_{2m+1}$ are from the 0th to the $(m+1)$th and $(2m+1)$th beads, respectively. All the $3m-3$ bond angles θ (not supplement) except for those around the center are fixed, so that the configuration of the entire chain may be specified by the set of $3m-3$ rotation angles $\{\phi_{3m-3}\} = (\phi_1, \cdots, \phi_{m-1}, \phi_{m+1}, \cdots, \phi_{2m-1}, \phi_{2m+1}, \cdots, \phi_{3m-1})$ apart from its position and orientation in an external Cartesian coordinate system, where ϕ_i is the internal rotation angle around $\mathbf{l}_i$.

The linear chain model, the counterpart of the above star one, is the same as that used in refs 4 and 5, i.e., the freely rotating chain composed of n bonds of length unity and $n+1$ beads, whose centers are located at the $n-1$ junctions of two successive bonds and at the two terminal ends. We set n equal to $3m$. The beads are numbered $0, 1, 2, \cdots, n$ from one end to the other, and $\mathbf{l}_i$ ($1 \le i \le n$) connects the centers of the $(i-1)$th and ith beads with its direction from the $(i-1)$th to the ith bead. All the $n-1$ bond angles are fixed at θ, so that the configuration of the linear chain may be specified by the set of $n-2$ internal rotation angles $\{\phi_{n-2}\} = (\phi_2, \phi_3, \cdots, \phi_{n-1})$ apart from its position and orientation in the external Cartesian coordinate system.

The total potential energy U of the regular three-arm star chain as a function of

$\{\phi_{3m-3}\}$ may be given by

$$U(\{\phi_{3m-3}\}) = \sum_{i=0}^{1}\sum_{j=i+1}^{2}\sum_{k,l=1}^{m} h(k+l-4)\,u(R_{(im+k)(jm+l)}) + \sum_{i=0}^{2}\sum_{j=1}^{m-4}\sum_{k=j+4}^{m} u(R_{(im+j)(im+k)}) + \sum_{i=0}^{2}\sum_{j=4}^{m} u(R_{0(im+j)}) \quad \text{(regular three-arm star)} \tag{2.1}$$

and that of the linear chain as a function of $\{\phi_{n-2}\}$ by

$$U(\{\phi_{n-2}\}) = \sum_{i=0}^{n-4}\sum_{j=i+4}^{n} u(R_{ij}) \qquad \text{(linear)} \tag{2.2}$$

where $h(x)$ is a unit step function such that $h(x) = 1$ for $x \geq 0$ and $h(x) = 0$ for $x < 0$ and R_{ij} is the distance between the centers of the ith and jth beads. We note that in eqs 2.1 and 2.2 the interactions between the third-neighbor beads along the chain have been neglected, since they seem to make the chain locally take the *cis* conformation to excess. We adopt as the pair potential $u(R)$ (of mean force) the cutoff version of the LJ 6-12 potential given by

$$\begin{aligned} u(R) &= \infty && \text{for } 0 \leq R < c\sigma \\ &= u^{\mathrm{LJ}}(R) && \text{for } c\sigma \leq R < 3\sigma \\ &= 0 && \text{for } 3\sigma \leq R \end{aligned} \tag{2.3}$$

where $u^{\mathrm{LJ}}(R)$ is the LJ potential[3] given by

$$u^{\mathrm{LJ}}(R) = 4\epsilon\left[\left(\frac{\sigma}{R}\right)^{12} - \left(\frac{\sigma}{R}\right)^{6}\right] \tag{2.4}$$

with σ and ϵ the collision diameter and the depth of the potential well at the minimum of $u^{\mathrm{LJ}}(R)$, respectively. We note that $u(R)$ given by eqs 2.3 is the LJ potential cut off at the upper bound 3σ. The lower bound $c\sigma$ in eqs 2.3 has been introduced for numerical convenience; the factor c is properly chosen so that the Boltzmann factor $e^{-u^{\mathrm{LJ}}/k_{\mathrm{B}}T}$ may be regarded as numerically vanishing compared to unity, where k_{B} is the Boltzmann constant and T is the absolute temperature. In practice, in double-precision computation, we put

$$c = \left[2/\left(1+\sqrt{1+36T^*}\right)\right]^{1/6} \tag{2.5}$$

so that $e^{-u^{\mathrm{LJ}}/k_{\mathrm{B}}T} \lesssim 2 \times 10^{-16}$ for $0 \leq R < c\sigma$, where T^* is the reduced temperature defined by $T^* = k_{\mathrm{B}}T/\epsilon$. Further, we put $\sigma = 1$ for simplicity, as previously[4,5] done.

2.2.2 MC Sampling

The MC simulation algorithm used in this study is the same as that used in refs 4 and 5 and is essentially the same as the Stellman–Gans[8] version of the pivot algorithm[7,9] for a sequential generation of chain configurations. A brief description is given of the algorithm for the regular three-arm star chain, which is in principle the same as that for the linear chain described previously.[4]

First, we generate an initial configuration $\{\mathbf{l}_{3m}\} = (\mathbf{l}_1, \mathbf{l}_2, \cdots, \mathbf{l}_{3m})$ by trial and error. A trial set of the rotation angles $\{\phi_{3m-3}\}$ are randomly generated in the interval $[-\pi, \pi]$. The branch point of the star chain is located at the origin of the external Cartesian coordinate system and the first bond vector $\mathbf{l}_{im+1}$ $(i = 0, 1, 2)$ on the $(i+1)$th arm is laid in the xz plane such that $\mathbf{l}_1^T = (0, 0, 1)$, $\mathbf{l}_{m+1}^T = (\frac{\sqrt{3}}{2}, 0, -\frac{1}{2})$, and $\mathbf{l}_{2m+1}^T = (-\frac{\sqrt{3}}{2}, 0, -\frac{1}{2})$, with the superscript T indicating the transpose. The succeeding bond vector $\mathbf{l}_{im+j}$ $(j = 2, 3, \cdots, m)$ on the $(i+1)$th arm may be given by

$$\mathbf{l}_{im+j} = \mathbf{C}_i \cdot \mathbf{A}(\theta, \phi_{im+1}) \cdot \mathbf{A}(\theta, \phi_{im+2}) \cdots \mathbf{A}(\theta, \phi_{im+j-1}) \cdot (0, 0, 1)^T \tag{2.6}$$

where $\mathbf{C}_i$ $(i = 0, 1, 2)$ is the orthogonal transformation matrix given by

$$\mathbf{C}_i = \begin{pmatrix} -1/2 & 0 & \sqrt{3}/2 \\ 0 & 1 & 0 \\ -\sqrt{3}/2 & 0 & -1/2 \end{pmatrix}^i \tag{2.7}$$

and $\mathbf{A}(\theta, \phi_{i-1})$ is the orthogonal transformation matrix from the ith to the $(i-1)$th localized Cartesian coordinate system[2] given by

$$\mathbf{A}(\theta, \phi) = \begin{pmatrix} \cos\theta\,\cos\phi & \sin\phi & -\sin\theta\,\cos\phi \\ \cos\theta\,\sin\phi & -\cos\phi & -\sin\theta\,\sin\phi \\ -\sin\theta & 0 & -\cos\theta \end{pmatrix} \tag{2.8}$$

The ith localized system associated with $\mathbf{l}_i$ $(2 \le i \le 3m;\ i \ne m+1,\ 2m+1)$ is defined as follows. The z_i axis is taken along $\mathbf{l}_i$, the x_i axis is in the plane of $\mathbf{l}_{i-1}$ and $\mathbf{l}_i$ with its direction chosen at an obtuse angle with $\mathbf{l}_{i-1}$, and the y_i axis completes the right-handed system, so that $\phi_i = 0$ in the *trans* conformation. Since the branch point is located at the origin, the vector position $\mathbf{r}_{im+j}$ $(i = 0, 1, 2;\ j = 1, 2, \cdots, m)$ of the center of the jth bead on the $(i+1)$th arm is given by

$$\mathbf{r}_{im+j} = \sum_{k=1}^{j} \mathbf{l}_{im+k} \tag{2.9}$$

If all the distances between the centers of beads are greater than or equal to $c\sigma$, the above-given trial configuration is adopted as the initial configuration. If not, this trial is repeated until an initial satisfactory configuration is obtained.

Next the initial configuration $\{\mathbf{l}_{3m}\}$ so obtained is sequentially changed by the pivot algorithm. A trial configuration is generated by rotating the chain with a given present configuration by an angle $\Delta\phi$ randomly chosen in the interval $[-\pi, \pi]$ around a bond randomly chosen from the $3m-3$ bonds $\mathbf{l}_i$ ($1 \le i \le 3m-1$; $i \ne m$, $2m$). If the pth bond is chosen, the set of rotation angles $\{\phi'_{3m-3}\}$ in the trial configuration are given by

$$\phi'_i = \phi_i + \delta_{ip}\Delta\phi \quad (1 \le i \le 3m-1;\ i \ne m,\ 2m) \tag{2.10}$$

with δ_{ip} the Kronecker delta. The trial configuration $\{\mathbf{l}'_{3m}\}$ is generated from $\{\phi'_{3m-3}\}$ by the use of the numerical procedure described previously.[4] Practically, the bond vectors (not the vector positions of the centers of beads) are rotated around $\mathbf{l}_p$ to obtain the set of bond vectors $\{\mathbf{l}'_{3m}\}$ in the trial configuration. If $\mathbf{l}_p$ is on the jth arm ($j = 1, 2, 3$), the elements of $\{\mathbf{l}'_{3m}\}$ are given by

$$\begin{aligned}
\mathbf{l}'_i &= \mathbf{l}_i && \text{for } i \le p,\ i > jm \\
&= \mathbf{l}_p\mathbf{l}_p \cdot \mathbf{l}_i + (\cos\Delta\phi)(\mathbf{I} - \mathbf{l}_p\mathbf{l}_p) \cdot \mathbf{l}_i + (\sin\Delta\phi)\mathbf{l}_p \times \mathbf{l}_i \\
&\equiv \mathbf{R}(\mathbf{l}_p; \Delta\phi) \cdot \mathbf{l}_i && \text{for } p < i \le jm
\end{aligned} \tag{2.11}$$

where $\mathbf{I}$ is the unit matrix and the rotation matrix $\mathbf{R}(\mathbf{l}; \Delta\phi)$ is given by

$$\mathbf{R}(\mathbf{l}; \Delta\phi) = (\cos\Delta\phi)\mathbf{I} + (1 - \cos\Delta\phi)\begin{pmatrix} {l_x}^2 & l_x l_y & l_x l_z \\ l_y l_x & {l_y}^2 & l_y l_z \\ l_z l_x & l_z l_y & {l_z}^2 \end{pmatrix} + \sin\Delta\phi \begin{pmatrix} 0 & -l_z & l_y \\ l_z & 0 & -l_x \\ -l_y & l_x & 0 \end{pmatrix} \tag{2.12}$$

with $\mathbf{l}^T = (l_x, l_y, l_z)$. With this rotation, $\mathbf{l}'_i$ ($p < i \le jm$) is renormalized to $\mathbf{l}'_{i(\mathrm{corr})}$ so that $|\mathbf{l}'_{i(\mathrm{corr})}| = 1$, i.e.,

$$\begin{aligned}
\mathbf{l}'_{i(\mathrm{corr})} &= \mathbf{l}'_i/({l'_{i,x}}^2 + {l'_{i,y}}^2 + {l'_{i,z}}^2)^{1/2} \\
&\simeq \left[1 - \frac{1}{2}({l'_{i,x}}^2 + {l'_{i,y}}^2 + {l'_{i,z}}^2 - 1)\right]\mathbf{l}'_i \qquad \text{for } p < i \le jm
\end{aligned}$$

in order to suppress a roundoff error characteristic of computer work. (Note that $|\mathbf{l}'_i - \mathbf{l}'_{i(\mathrm{corr})}| \ll 1$.) The vector position of the centers of beads in the trial configuration are calculated from eq 2.9 with the corrected $\{\mathbf{l}'_{3m}\}$.

Then, the adoption of the trial configuration so generated as the next one is determined by the Metropolis method of importance sampling[6] on the basis of the total potential energy given by eq 2.1 for the trial and present configurations, i.e., the trial configuration is adopted as the next one with the (transition) probability $\tau(\{\phi'_{3m-3}\}|\{\phi_{3m-3}\})$ defined by

$$\tau(\{\phi'_{3m-3}\}|\{\phi_{3m-3}\}) = \min[1, e^{-[U(\{\phi'_{3m-3}\}) - U(\{\phi_{3m-3}\})]/k_{\mathrm{B}}T}] \tag{2.13}$$

If the trial configuration is discarded, the present one is again adopted as the next one. The practical procedure is as follows. If the distance between the centers of beads of a pair is smaller than $c\sigma$, the trial configuration is discarded and the present one is adopted as the next one. If not, the total potential energy $U(\{\phi'_{3m-3}\})$ is calculated from eq 2.1 and the Boltzmann factor in eq 2.13 is evaluated. Then the probability τ is compared with a random number x for $0 \leq x < 1$. If τ is greater than the random number, the trial configuration is adopted as the next one. If not, the present configuration is adopted as the next one. In computing $U(\{\phi'_{3m-3}\})$, the "zippering" method[8,14] has been used for speedy calculation of the double sum in eq 2.1.

By the use of the model and algorithm described above for the regular three-arm star chain and previously for the linear chain,[4] we sample one configuration at every $M_{\rm nom}$ (nominal) pivot steps, and N configurations in total, for both chains. Then, the ensemble average $\langle A \rangle$ of a variable A may be evaluated on the basis of the N sample configurations so generated. If A is independent of the orientation of the chain like the squared radius of gyration S^2, it is a function only of $\{\phi_\alpha\}$ with α being equal to $3m-3$ for the star chain and $n-2$ for the linear one, so that $\langle A \rangle$ may be evaluated from

$$\langle A \rangle = N^{-1} \sum_{\{\phi_\alpha\}} A(\{\phi_\alpha\}) \tag{2.14}$$

where the sum is taken over the N sample configurations. If A is dependent on the orientation, on the other hand, the above average must be evaluated after randomizing the orientation for each sample configuration. Note that $N \times M_{\rm nom}$ pivot steps are required to carry out a MC run in both cases. All the MC runs have been carried out at the reduced temperature $T^* = 3.72$ (Θ) at which $\langle S^2 \rangle / n$ for the linear chains with $\sigma = 1$ and $\theta = 109^\circ$ becomes a constant independent of n for very large n.[4]

All numerical work has been done by the use of a personal computer with an AMD Athlon XP 2600+ CPU. A source program coded in C has been compiled by the GNU C compiler version 2.95.3 with real variables of double precision. For a generation of pseudo-random numbers, we have used the subroutine package MT19937 supplied by Matsumoto and Nishimura[15] instead of the subroutine RAND included in the standard C library.

2.2.3 Mean-Square Radius of Gyration

The mean-square radius of gyration $\langle S^2 \rangle$ has been evaluated from eq 2.14, where S^2 for each sample chain has been calculated from

$$S^2 = \frac{1}{n+1} \sum_{i=0}^{n} {S_i}^2 \tag{2.15}$$

where S_i is the magnitude of the vector distance $\mathbf{S}_i$ of the center of the ith bead from the center of mass of the chain, i.e.,

$$\mathbf{S}_i = \mathbf{r}_i - \mathbf{r}_{\text{c.m.}} \tag{2.16}$$

with $\mathbf{r}_{\text{c.m.}}$ the vector position of the center of mass of the sample chain given by

$$\mathbf{r}_{\text{c.m.}} = \frac{1}{n+1}\sum_{i=0}^{n}\mathbf{r}_i \tag{2.17}$$

2.2.4 Intrinsic Viscosity

The intrinsic viscosity $[\eta]$ of the bead model without the contribution of each single-bead (i.e., without consideration of a distribution of frictional force on the surface of each bead) may be written in terms of the (total) frictional force $\mathbf{F}_i^T = (F_{ix}, F_{iy}, F_{iz})$ exerted by the ith bead on a surrounding solvent and $\mathbf{S}_i^T = (S_{ix}, S_{iy}, S_{iz})$ defined by eq 2.16 as follows,[1]

$$[\eta] = -\frac{N_{\text{A}}}{2M\eta_0 g}\sum_{i=0}^{n}\langle F_{iy}S_{ix} + F_{ix}S_{iy}\rangle \tag{2.18}$$

where N_{A} is the Avogadro constant, M is the molecular weight, η_0 is the viscosity coefficient of the solvent, and g is the velocity gradient of a simple shear flow field. The frictional force $\mathbf{F}_i$ satisfies the following hydrodynamic equations,

$$\mathbf{F}_i = \zeta(\mathbf{u}_i - \mathbf{v}_i^0) - \zeta\sum_{\substack{j=0\\ \neq i}}^{n}\mathbf{T}_{ij}\cdot\mathbf{F}_j \qquad (i = 0, 1, 2, \cdots, n) \tag{2.19}$$

where ζ is the friction coefficient of the bead given by the Stokes relation $\zeta = 3\pi\eta_0 d_{\text{b}}$ with d_{b} the hydrodynamic diameter of the bead, $\mathbf{u}_i$ is the velocity of the ith bead, $\mathbf{v}_i^0$ is the unperturbed velocity of the solvent at the center of the ith bead, and $\mathbf{T}_{ij}$ is the Oseen tensor representing the hydrodynamic interaction between the ith and jth beads.

In the numerical evaluation of $[\eta]$, the linear simultaneous equations 2.19 are first solved for $\mathbf{F}_i$ for the polymer chain immersed in the solvent having the unperturbed flow field,

$$\mathbf{v}_i^0 = g\mathbf{e}_x\mathbf{e}_y\cdot\mathbf{r}_i \tag{2.20}$$

in the external Cartesian coordinate system $(\mathbf{e}_x, \mathbf{e}_y, \mathbf{e}_z)$, and then the ensemble averages on the right-hand side of eq 2.18 are evaluated by the use of the values of $\mathbf{F}_i$ so obtained. Since $[\eta]$ cannot be evaluated exactly, as mentioned already, it has been approximately evaluated in the three ways: the KR approximation,[1,10] the Zimm rigid-body ensemble approximation,[11] and the Fixman method.[12,13] In what follows, we consider the touched-bead model so that $d_{\text{b}} = 1$.

2.2.4.1 KR Approximation

In the KR approximation, the polymer chain in the unperturbed flow filed given by eq 2.20 is assumed to move with the translational velocity equal to that of the unperturbed flow at its center of mass and to rotate around its center of mass with the angular velocity $-\frac{1}{2}g\mathbf{e}_z$, so that $\mathbf{u}_i$ in eq 2.19 may be given by

$$\mathbf{u}_i = \frac{1}{2}g(\mathbf{e}_x\mathbf{e}_y - \mathbf{e}_y\mathbf{e}_x)\cdot\mathbf{S}_i \tag{2.21}$$

Further, the Oseen tensor defined by

$$\mathbf{T}_{ij} = \frac{1}{8\pi\eta_0 R_{ij}}\left(\mathbf{I} + \frac{\mathbf{R}_{ij}\mathbf{R}_{ij}}{{R_{ij}}^2}\right) \tag{2.22}$$

with $\mathbf{I}$ the unit tensor and $\mathbf{R}_{ij} = \mathbf{S}_j - \mathbf{S}_i$ is replaced by its ensemble average $\langle\mathbf{T}_{ij}\rangle$, which may be written in the form,

$$\langle\mathbf{T}_{ij}\rangle = \frac{1}{6\pi\eta_0}\langle {R_{ij}}^{-1}\rangle\mathbf{I} \tag{2.23}$$

In practice, $[\eta]$ in the KR approximation, which we designate $[\eta]^{(\mathrm{KR})}$, has been evaluated numerically as follows: First evaluate the average $\langle {R_{ij}}^{-1}\rangle$ by the use of the N sample chains, then solve the linear simultaneous equations 2.19 with $\langle\mathbf{T}_{ij}\rangle$ so obtained in place of $\mathbf{T}_{ij}$ for each sample chain having a random orientation with respect to the external system, and finally calculate $[\eta]^{(\mathrm{KR})}$ from eq 2.18. We note that this numerical recipe correctly gives $[\eta]^{(\mathrm{KR})}$, although it seems apparently somewhat different from the original one.[1,10]

2.2.4.2 Rigid-Body Ensemble Approximation

The rigid-body ensemble approximation has been proposed by Zimm[11] in order to evaluate $[\eta]$ by MC simulation, in which each sample chain having a rigid conformation immersed in the shear flow given by eq 2.20 is assumed to move with an unknown translational velocity $\mathbf{U}$ and to rotate around its center of mass with the angular velocity $-\frac{1}{2}g\mathbf{e}_z$ under the condition that the total frictional force $\mathbf{F}$ exerted by the chain on the solvent vanishes. Then $\mathbf{u}_i$ in eq 2.19 may be given by

$$\mathbf{u}_i = \mathbf{U} + \frac{1}{2}g(\mathbf{e}_x\mathbf{e}_y - \mathbf{e}_y\mathbf{e}_x)\cdot\mathbf{S}_i \tag{2.24}$$

In this approximation, $\mathbf{F}_i$ and also $\mathbf{U}$ are evaluated for each sample chain having a random orientation by solving the linear simultaneous equations 2.19 with $\mathbf{u}_i$ and $\mathbf{v}_i^0$ given by eqs 2.24 and 2.20, respectively, along with the condition,

$$\mathbf{F} = \sum_{i=0}^{n}\mathbf{F}_i = \mathbf{0} \tag{2.25}$$

Then $[\eta]$ may be calculated from eq 2.18 with $\mathbf{F}_i$ so evaluated.

In the practical evaluation of $[\eta]$, we have used the modified Oseen tensor[16,17] $\mathbf{T}_{\mathrm{m},ij}$ defined by

$$\mathbf{T}_{\mathrm{m},ij} = \mathbf{T}_{ij} + \frac{1}{16\pi\eta_0 R_{ij}}\left(\frac{d_\mathrm{b}}{R_{ij}}\right)^2\left(\frac{1}{3}\mathbf{I} - \frac{\mathbf{R}_{ij}\mathbf{R}_{ij}}{{R_{ij}}^2}\right) \tag{2.26}$$

in place of the (original) Oseen tensor $\mathbf{T}_{ij}$ in order to avoid possible numerical troubles, i.e., the Zwanzig singularities[18,19] associated with the touched-bead model. We note that $\langle\mathbf{T}_{\mathrm{m},ij}\rangle$ becomes identical with $\langle\mathbf{T}_{ij}\rangle$.

Since the rigid-body ensemble approximation gives an upper bound to $[\eta]$, as pointed out by Wilemski and Tanaka[20] and by Fixman,[12] $[\eta]$ obtained in this approximation is designated $[\eta]^{(\mathrm{U})}$.

2.2.4.3 Fixman Method

Fixman[12] has proposed an MC method for evaluating a lower bound $[\eta]^{(\mathrm{L})}$ to $[\eta]$. On the basis of a formal expression for $[\eta]$ by the use of the formal solution of the diffusion equation for the polymer chain, he has derived the following inequality,

$$[\eta] \geq \frac{N_\mathrm{A}}{M\eta_0 g^2 k_\mathrm{B}T}\left[2\langle\mathbf{V}^T\cdot{\mathbf{D}_\mathrm{a}}^{-1}\cdot\mathbf{V}\rangle - \langle\mathbf{V}^T\cdot{\mathbf{D}_\mathrm{a}}^{-1}\cdot\mathbf{D}\cdot{\mathbf{D}_\mathrm{a}}^{-1}\cdot\mathbf{V}\rangle\right] \tag{2.27}$$

where $\mathbf{V}$ is the column matrix with the ith element $\mathbf{V}_i$ given by

$$\mathbf{V}_i = \frac{1}{2}g(\mathbf{e}_x\mathbf{e}_y + \mathbf{e}_y\mathbf{e}_x)\cdot\mathbf{S}_i \tag{2.28}$$

$\mathbf{D}$ is the $3(n+1)\times 3(n+1)$ (true) diffusion matrix whose ij element is the 3×3 matrix $\mathbf{D}_{ij}$ defined by

$$\mathbf{D}_{ij} = k_\mathrm{B}T[\zeta^{-1}\delta_{ij}\mathbf{I} + (1-\delta_{ij})\mathbf{T}_{\mathrm{m},ij}] \tag{2.29}$$

and $\mathbf{D}_\mathrm{a}$ is an approximate expression for $\mathbf{D}$, which is desired to be easier to handle. Both the two tensors $\mathbf{D}$ and $\mathbf{D}_\mathrm{a}$ are required to be positive definite, symmetric, and divergenceless, and the former given by eq 2.29 satisfies the requirements. We note that in eq 2.27 equality holds if $\mathbf{D}_\mathrm{a} = \mathbf{D}$.

For any given expression for $\mathbf{D}_\mathrm{a}$ satisfying the above requirements, the two kinds of averages on the right-hand side of eq 2.27 may be evaluated on the basis of the MC sample configurations. The remaining problem is to find a tractable expression for $\mathbf{D}_\mathrm{a}$, for which Fixman has proposed the following expression,[13]

$${\mathbf{D}_\mathrm{a}}^{-1} = \alpha({\mathbf{D}_\mathrm{p}}^{-1} + {\mathbf{D}'_\mathrm{p}}^{-1}) \tag{2.30}$$

In this expression, $\mathbf{D}_\mathrm{p}$ and $\mathbf{D}'_\mathrm{p}$ the $3(n+1)\times 3(n+1)$ matrices whose ij elements are the 3×3 matrices given by

$$\mathbf{D}_{\mathrm{p},ij} = k_\mathrm{B}T[\zeta^{-1}\delta_{ij}\mathbf{I} + (1-\delta_{ij})\langle\mathbf{T}_{ij}\rangle] \tag{2.31}$$

$$\mathbf{D}'_{\mathrm{p},ij} = k_\mathrm{B}T[(\beta\zeta)^{-1}\delta_{ij}\mathbf{I} + (1-\delta_{ij})\langle\mathbf{T}_{ij}\rangle] \tag{2.32}$$

respectively, α is a constant chosen so that the right-hand side of eq 2.27 becomes the maximum, and β is a constant properly chosen in the range of $0 < \beta < 1$. Then the desired expression for $[\eta]^{(\mathrm{L})}$ is given by the maximum of the the right-hand side of eq 2.27 with eq 2.30 and may be written in the form,

$$[\eta]^{(\mathrm{L})} = \frac{N_{\mathrm{A}}}{M\eta_0 g^2 k_{\mathrm{B}} T}\left[\frac{\langle \mathbf{V}^T \cdot (\mathbf{D}_{\mathrm{p}}{}^{-1} + \mathbf{D}'_{\mathrm{p}}{}^{-1}) \cdot \mathbf{V}\rangle^2}{\langle \mathbf{V}^T \cdot (\mathbf{D}_{\mathrm{p}}{}^{-1} + \mathbf{D}'_{\mathrm{p}}{}^{-1}) \cdot \mathbf{D} \cdot (\mathbf{D}_{\mathrm{p}}{}^{-1} + \mathbf{D}'_{\mathrm{p}}{}^{-1}) \cdot \mathbf{V}\rangle}\right] \tag{2.33}$$

As for the value of the constant β, it has been shown by Freire and Rey[21] that in the case of Gaussian star chains $[\eta]^{(\mathrm{L})}$ given by eq 2.33 is insensitive to the value in the range of $0 < \beta < 1$ and therefore β may be set equal to 0.5. Following them, we have put $\beta = 0.5$.

2.3 Results and Discussion

We have carried out MC runs to generate sample configurations for the regular three-arm star and linear freely rotating chains with n $(= 3m) = 60$—300 and $\theta = 109°$, $165°$, and $175°$, with the parameters σ and T^* for the LJ potential being fixed to be 1 and 3.72, respectively. The freely rotating chain with $\theta = 109°$ corresponds to a flexible polymer and that with $\theta = 165°$ or $175°$ to a semiflexible or stiff polymer. The value 3.72 of T^* was previously[4] determined so that $\langle S^2\rangle/n$ became a constant independent of n for very large n, and therefore it corresponds to the Θ temperature, as mentioned in the previous section. For each chain, 5 MC runs have been carried out to obtain 10^4 sample configurations, so that 5×10^4 sample configurations have been generated in total. We note that we have adopted $N = 10^4$ in the present study of $[\eta]$, which is one order of magnitude smaller than 10^5 adopted in the previous study of $\langle S^2\rangle$,[4] since the computation time necessary for each sample configuration is much longer for $[\eta]$ than for $\langle S^2\rangle$.

On the basis of the sample configurations so generated, we first examine the behavior of the MC values of $\langle S^2\rangle$ as a function of n and compare them with the theoretical values for the *ideal* freely rotating chain without interactions between beads, which we call the ideal chain hereafter, and for the corresponding Kratky–Porod (KP) wormlike chain.[2,22] Then we examine the behavior of g_S as a function of the reduced contour length λL, i.e., the total contour length L of the corresponding KP chain divided by the stiffness parameter λ^{-1} having the dimension of length. Finally, we examine the behavior of g_η as a function of λL, which is the main purpose of the present study.

2.3.1 Mean-Square Radius of Gyration

In Table 2.1 are given the MC values of $\langle S^2\rangle/n$ for both the regular three-arm star and linear chains along with the values of the acceptance fraction, i.e., the mean number of

Table 2.1. Results of Monte Carlo simulations for $\langle S^2 \rangle / n$

	three-arm star		linear	
n	$\langle S^2 \rangle / n$ (error %)	Acceptance fraction	$\langle S^2 \rangle / n$ (error %)	Acceptance fraction
		$\theta = 109^\circ$		
60	0.296_4 (0.5)	59/200	0.367_2 (0.6)	60/100
120	0.307_2 (0.4)	174/1000	0.383_2 (0.3)	151/300
180	0.309_9 (0.4)	243/2000	0.389_6 (0.7)	226/500
240	0.309_0 (0.7)	459/5000	0.395_1 (0.3)	416/1000
300	0.310_8 (0.9)	363/5000	0.396_0 (0.4)	388/1000
		$\theta = 165^\circ$		
60	1.88_6 (0.1)	199/200	3.57_1 (0.1)	99/100
120	3.02_8 (0.2)	995/1000	5.28_5 (0.2)	299/300
180	3.81_6 (0.1)	1979/2000	6.26_7 (0.3)	498/500
240	4.38_0 (0.1)	4919/5000	6.91_0 (0.4)	993/1000
300	4.80_1 (0.2)	4888/5000	7.34_9 (0.5)	989/1000
		$\theta = 175^\circ$		
60	2.29_2 (0.0)	199/200	4.93_4 (0.0)	100/100
120	4.34_2 (0.0)	999/1000	9.29_6 (0.0)	300/300
180	6.28_9 (0.0)	1999/2000	13.2_9 (0.1)	500/500
240	8.14_1 (0.0)	4999/5000	16.9_7 (0.0)	999/1000
300	9.89_8 (0.1)	4999/5000	20.3_4 (0.1)	999/1000

changes in configuration in the $M_{\rm nom}$ pivot steps divided by $M_{\rm nom}$. Specifically, for example, for the regular three-arm star chain with $n = 60$ ($m = 20$), 5 independent MC runs have been repeated, in each of which 200×10^4 pivot steps have resulted in 59×10^4 changes in configuration. The values of $\langle S^2 \rangle / n$ and its statistical error given in the second column for the star and the fourth for the linear are those of the mean and the standard deviation, respectively, of the results of the 5 independent MC runs.

Figure 2.2 shows double-logarithmic plots of $\langle S^2 \rangle / n$ against n with the present MC data given in Table 2.1 for the regular three-arm star ($\bigcirc$) and linear ($\triangle$) chains with $\theta = 109^\circ$ along with the previous MC data for the linear chains ($\blacktriangle$).[4] Although the present number of sample configurations is smaller than the previous one, the unfilled and filled triangles seem to form a single-composite curve, indicating that the present data are so accurate as the previous ones.

In the figure, the lower and upper solid line segments connect the theoretical values for the regular three-arm star and linear ideal chains, respectively. The former values have

been calculated from

$$\begin{aligned}\langle S^2\rangle = {} & \frac{7}{54}\frac{1-\cos\theta}{1+\cos\theta}n + \frac{1}{54}\frac{31+90\cos\theta-13\cos^2\theta}{(1+\cos\theta)^2} \\ & + \frac{1}{18}\frac{19+49\cos\theta+71\cos^2\theta+5\cos^3\theta}{(1+\cos\theta)^3}\frac{1}{n+1} \\ & - \frac{2(1+2\cos\theta)}{(1+\cos\theta)^3}\frac{1-(-\cos\theta)^{n/3+1}}{n+1} \\ & + \frac{1}{27}\frac{(1-\cos\theta)(37-16\cos\theta+\cos^2\theta)}{(1+\cos\theta)^3}\frac{1}{(n+1)^2} \\ & - \frac{2(2+\cos^2\theta)}{(1+\cos\theta)^4}\frac{1-(-\cos\theta)^{n/3+1}}{(n+1)^2} \\ & + \frac{3}{(1+\cos\theta)^4}\frac{\left[1-(-\cos\theta)^{n/3+1}\right]^2}{(n+1)^2} \quad \text{(regular three-arm star)}\end{aligned} \tag{2.34}$$

which is a special case of the theoretical expression obtained by Guenza *et al.*[23] for the regular f-arm star freely rotating chain, and the latter from

$$\begin{aligned}\langle S^2\rangle = {} & \frac{1}{6}\frac{1-\cos\theta}{1+\cos\theta}n + \frac{1}{6}\frac{1+6\cos\theta-\cos^2\theta}{(1+\cos\theta)^2} \\ & + \frac{1}{6}\frac{-1-7\cos\theta+7\cos^2\theta+\cos^3\theta}{(1+\cos\theta)^3}\frac{1}{n+1} \\ & - \frac{2\cos^2\theta}{(1+\cos\theta)^4}\frac{1-(-\cos\theta)^{n+1}}{(n+1)^2} \quad \text{(linear)}\end{aligned} \tag{2.35}$$

It is seen for both the regular three-arm star and linear chains that the MC values are ca. 20% larger than the corresponding ideal-chain values in the limit of $n \to \infty$. This is due to the fact that the unperturbed (Θ) dimension of a polymer chain may be considerably enlarged by nonbonded interactions.[24]

In Figure 2.2 are also shown the theoretical values for the KP regular three-arm star and linear chains, the lower and upper dashed curves representing the respective values. The former values have been calculated from

$$\langle S^2\rangle = \frac{7L}{54\lambda} - \frac{1}{3\lambda^2} + \frac{1}{4\lambda^3 L} + \frac{1}{4\lambda^3 L}(1-e^{-2\lambda L/3}) - \frac{3}{16\lambda^4 L^2}(1-e^{-4\lambda L/3}) \quad \text{(KP regular three-arm star)} \tag{2.36}$$

which is a special case of the theoretical expression obtained by Mansfield and Stockmayer[25] for a general KP star chain, and the latter from[26]

$$\langle S^2\rangle = \frac{L}{6\lambda} - \frac{1}{4\lambda^2} + \frac{1}{4\lambda^3 L} - \frac{1}{8\lambda^4 L^2}(1-e^{-2\lambda L}) \quad \text{(KP linear)} \tag{2.37}$$

In order to plot the KP theoretical values in the figure, we have converted L to n by the use of the relation

$$\log n = \log(\lambda L) + \log(\lambda^{-1} n_{\mathrm{L}}) \tag{2.38}$$

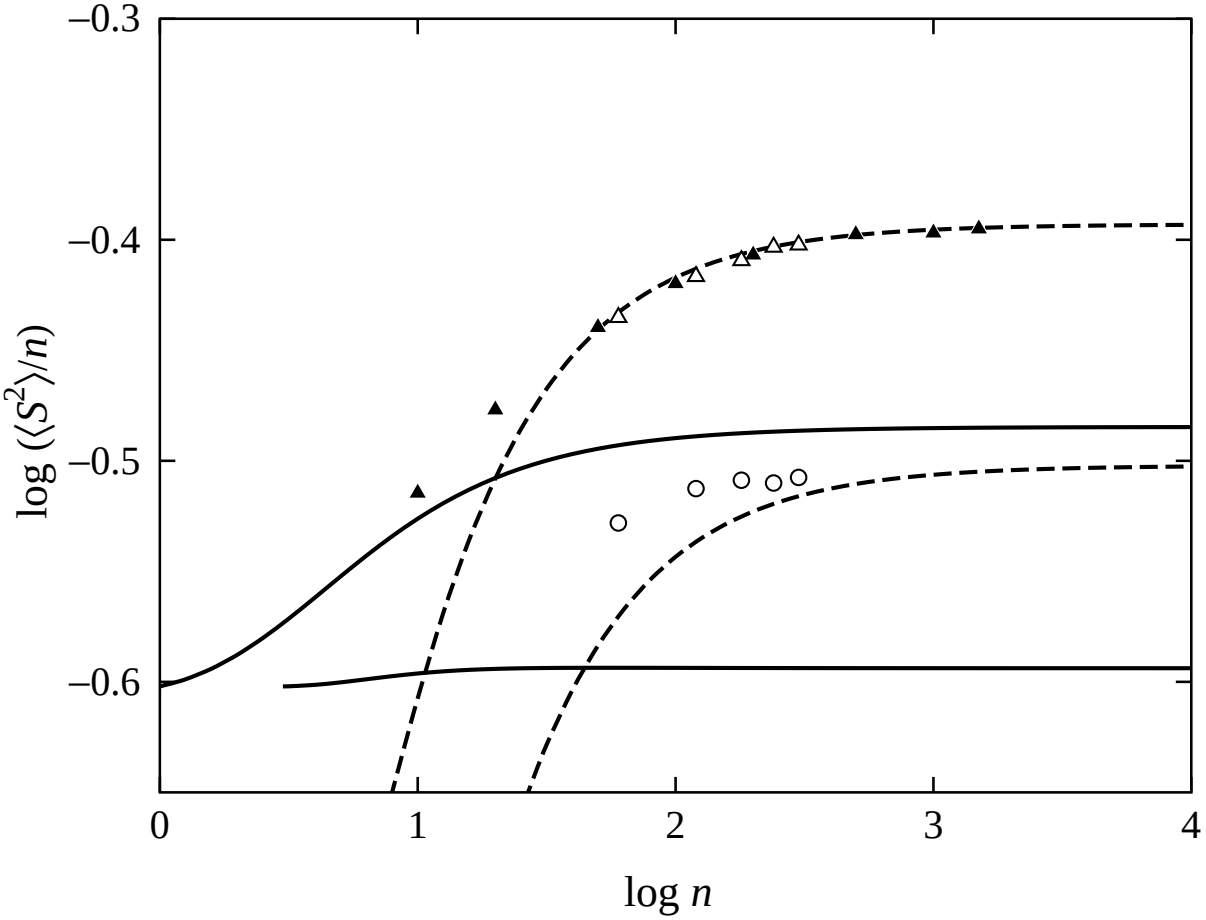

Figure 2.2. Double-logarithmic plots of $\langle S^2 \rangle / n$ against n for the regular three-arm star and linear chains, both with $\theta = 109°$ and $\sigma = 1$ at $T^* = 3.72$. The unfilled circles and triangles represent the present MC data for the regular three-arm star and the linear chains, respectively, and the filled triangles represent the previous MC data[4] for the latter. The lower and upper solid line segments connect the theoretical values of the regular three-arm star and linear ideal freely rotating chains, respectively. The lower and upper dashed curve represent the theoretical values of the corresponding KP regular three-arm star and linear chains, respectively.

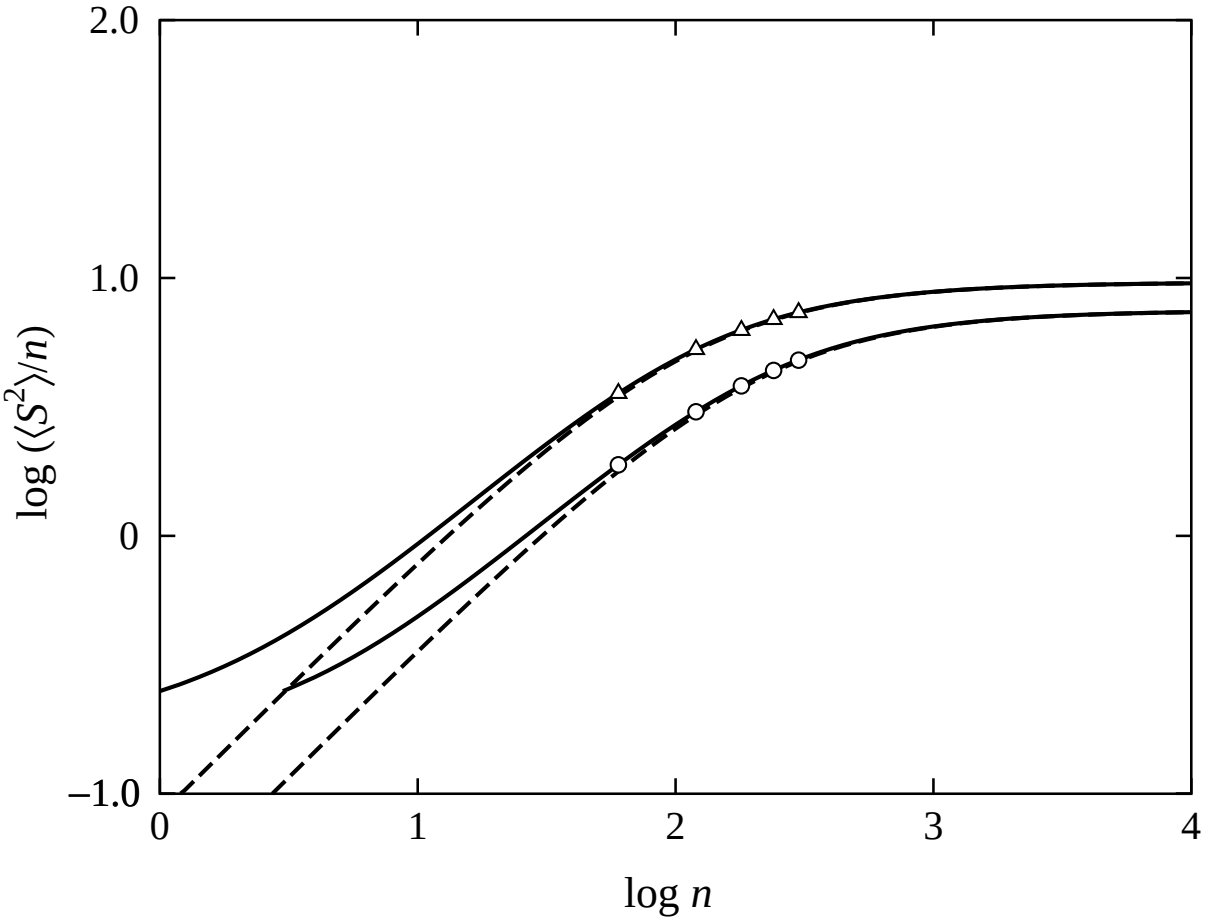

Figure 2.3. Double-logarithmic plots of $\langle S^2 \rangle / n$ against n for the regular three-arm star and linear chains, both with $\theta = 165°$ and $\sigma = 1$ at $T^* = 3.72$. All the symbols, line segments, and curves have the same meaning as those in Figure 2.2.

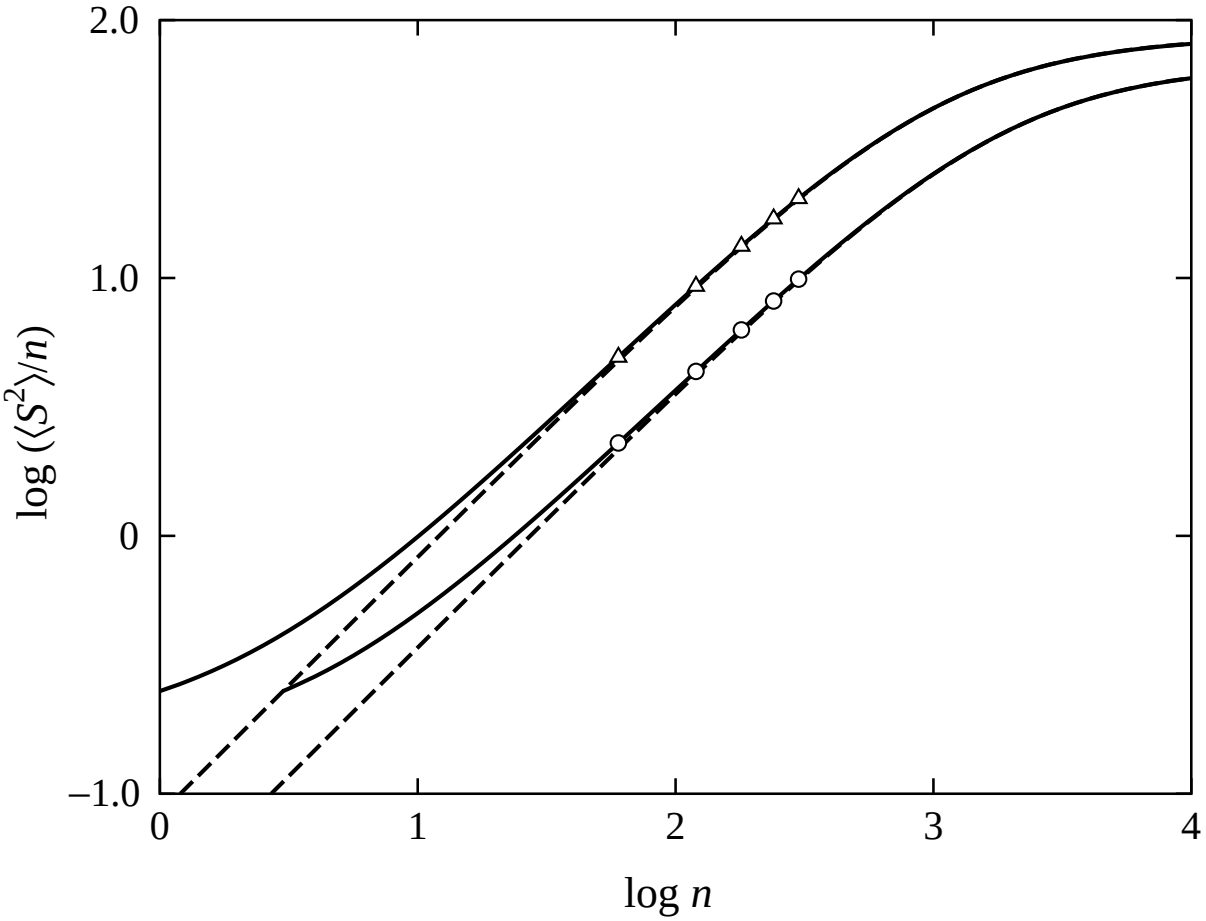

Figure 2.4. Double-logarithmic plots of $\langle S^2 \rangle / n$ against n for the regular three-arm star and linear chains, both with $\theta = 175^\circ$ and $\sigma = 1$ at $T^* = 3.72$. All the symbols, line segments, and curves have the same meaning as those in Figure 2.2.

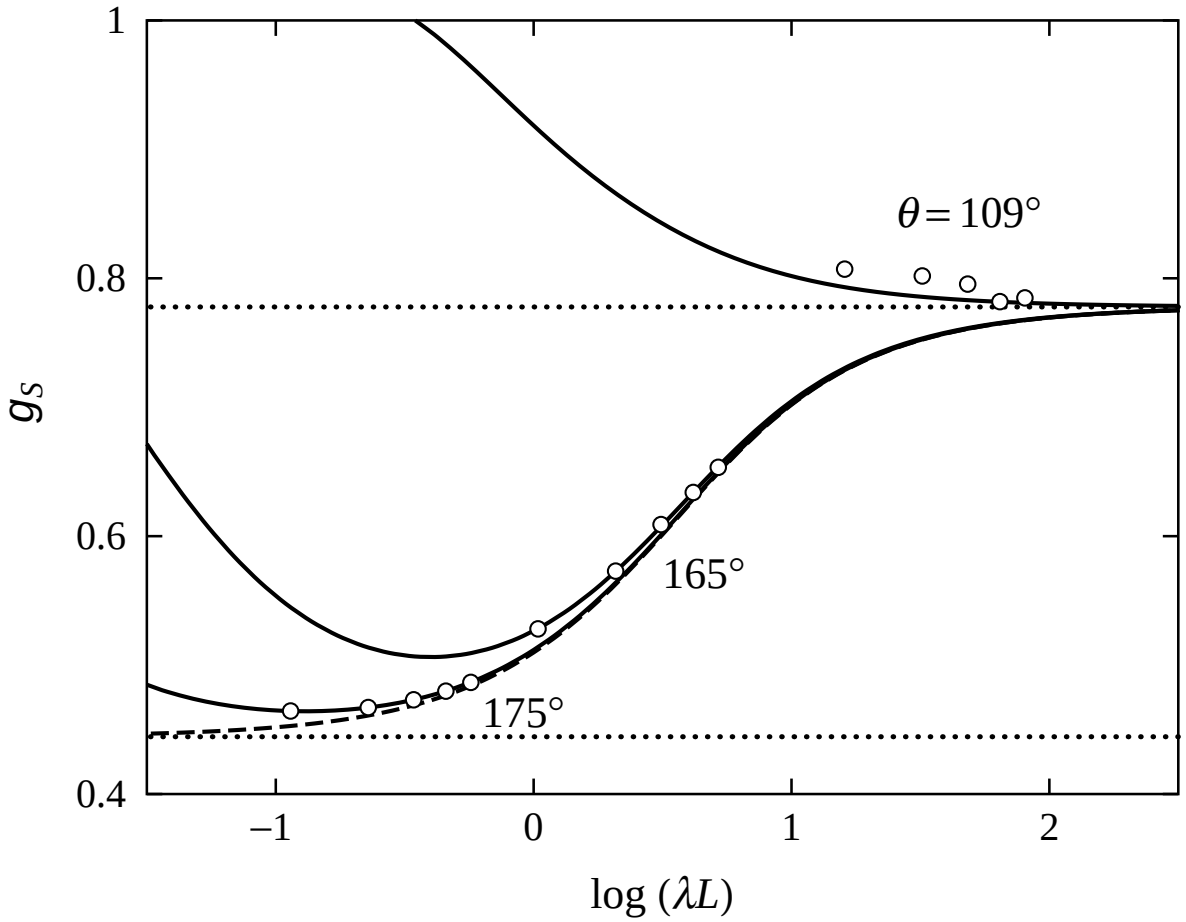

Figure 2.5. Plots of g_S against $\log(\lambda L)$ for the regular three-arm star. The three sets of the five unfilled circles represent the MC values with the indicated values of θ. The solid line segments associated with each set of the MC data points connect the corresponding theoretical values of the ideal freely rotating and the dashed curve represents the KP theoretical values.[25] The upper and lower dotted horizontal lines represent the asymptotic value 7/9 in the (ideal) random-coil limit[27] and 4/9 in the rigid-rod limit, respectively.

Table 2.2. Values of the KP model parameters

θ	λ^{-1}	n_{L}
109°	3.0_1 [a]	1.2_4 [a]
165°	$5.7_7 \times 10$	1.0_0
175°	$5.2_6 \times 10^2$	1.0_0

[a] These values have been determined in the previous study.[4]

where $n_{\mathrm{L}} = n/L$ is the number of bonds per unit contour length, and used the values 3.0_1 and 1.2_4 of λ^{-1} and n_{L}, respectively, which values were previously[4] determined in such a way that the theoretical values of the KP linear chain could most closely reproduce the previous MC values for the linear chain (▲) with $n \gtrsim 50$.

Figures 2.3 and 2.4 show similar plots for the regular three-arm star and linear chains with $\theta = 165°$ and 175°, respectively, which values of θ correspond to a semiflexible or stiff chain. All the symbols, line segments, and curves in the figures have the same meaning as those in Figure 2.2. It is seen that the MC values in each figure are almost identical with the corresponding ideal-chain values in contrast to the case of $\theta = 109°$ which corresponds to a flexible chain. This may be arising from the fact that effects of intramolecular interactions between beads become small with increasing chain stiffness if the total chain length is not very long. We therefore determine the values of the parameters λ^{-1} and n_{L} of the corresponding KP chain in each case of θ from an analysis of the linear ideal-chain values with $n \gtrsim 10^2$. In each of Figures 2.3 and 2.4, the upper dashed curve represents the best-fit KP values calculated from eqs 2.37 and 2.38 with the parameter values given in Table 2.2. It is seen that the theoretical values for the KP regular three-arm star (the lower dashed curve in each figure) calculated from eqs 2.36 and 2.38 with those parameter values may well reproduce the corresponding MC values. We note that the λ^{-1} value so determined is 1.3% larger than the λ^{-1} value calculated from the (ideal) relation $\lambda^{-1} = 2/(1+\cos\theta)$ in the case of $\theta = 109°$ and becomes identical with the latter value for $\theta \geq 165°$.

Now we proceed to examine the behavior of g_S as a function of λL. Values of g_S are plotted against $\log(\lambda L)$ in Figure 2.5. The three sets of the five open circles represent the MC values with the indicated values of θ, calculated from the $\langle S^2 \rangle$ values for the regular three-arm star and linear chains given in Table 2.1 with n converted to λL by the use of eq 2.38 with the values of λ^{-1} and n_{L} given in Table 2.2. The solid line segments associated with each set of the MC data points connect the corresponding ideal-chain values calculated from eqs 2.34 and 2.35 with n converted to λL in the above-mentioned manner. The dashed curve represents the KP theoretical values calculated from eq 2.36 and 2.37, with the upper and lower dotted horizontal lines representing the asymptotic

values 7/9 in the (ideal) random-coil limit[27] and 4/9 in the rigid-rod limit, respectively.

In the cases of $\theta = 165°$ and 175° (semiflexible chain), the MC and ideal-chain values are almost identical with each other as a necessary consequence of the good agreement between the MC and ideal-chain values of $\langle S^2 \rangle$ (see Figures 2.3 and 2.4). A remarkable point is that the two kinds of g_S values for $\theta = 109°$ semiquantitatively agree with each other in spite of the rather large disagreement between the MC and ideal-chain values of $\langle S^2 \rangle$ (see Figure 2.2). Both the MC and ideal-chain values for $\theta = 109°$ monotonically decrease with increasing n and approach the asymptotic value 7/9 in the limit of $n \to \infty$, while the KP value monotonically increases.

2.3.2 Intrinsic Viscosity

It is convenient to present MC results for $[\eta]$ in terms of the dimensionless quantity X_η defined by

$$[\eta] = \frac{3\pi N_{\mathrm{A}} n^{3/2}}{2M} X_\eta \tag{2.39}$$

As in the case of $[\eta]$, the superscript (KR), (U), and (L) are used to indicate that the X_η values have been evaluated in the KR approximation, the Zimm rigid-body ensemble approximation, and the Fixman method, respectively. In Table 2.3 are given the values of $X_\eta^{(\mathrm{KR})}$, $X_\eta^{(\mathrm{U})}$, and $X_\eta^{(\mathrm{L})}$ along with their statistical errors, which are the mean and the standard deviation, respectively, of the results of the 5 independent MC runs, for both the regular three-arm star and linear chains.

Corresponding to the three kinds of X_η (or $[\eta]$), we may consider the three kinds of g_η, i.e., $g_\eta^{(\mathrm{KR})}$, $g_\eta^{(\mathrm{Z})}$, and $g_\eta^{(\mathrm{F})}$ defined by

$$g_\eta^{(\mathrm{KR})} = \frac{[\eta]^{(\mathrm{KR})}(\mathrm{star})}{[\eta]^{(\mathrm{KR})}(\mathrm{linear})}, \qquad g_\eta^{(\mathrm{Z})} = \frac{[\eta]^{(\mathrm{U})}(\mathrm{star})}{[\eta]^{(\mathrm{U})}(\mathrm{linear})}, \qquad g_\eta^{(\mathrm{F})} = \frac{[\eta]^{(\mathrm{L})}(\mathrm{star})}{[\eta]^{(\mathrm{L})}(\mathrm{linear})} \tag{2.40}$$

We note that $g_\eta^{(\mathrm{Z})}$ is not an upper bound to g_η, nor is $g_\eta^{(\mathrm{F})}$ a lower bound. Figure 2.6 shows plots of $g_\eta^{(\mathrm{KR})}$ ($\bigcirc$), $g_\eta^{(\mathrm{Z})}$ ($\triangle$), and $g_\eta^{(\mathrm{F})}$ ($\bigtriangledown$) against $\log(\lambda L)$. Three sets of the data points represent the MC values with the indicated values of θ, calculated from eqs 2.39 and 2.40 with the three kinds of X_η values given in Table 2.3 and with n converted to λL in the above-mentioned manner. It is interesting to see that the $g_\eta^{(\mathrm{Z})}$ and $g_\eta^{(\mathrm{F})}$ values almost completely agree with each other irrespective of the value of λL, i.e., chain stiffness (θ) and total chain length (n), although the $X_\eta^{(\mathrm{U})}$ and $X_\eta^{(\mathrm{L})}$ values themselves do not. As for $g_\eta^{(\mathrm{KR})}$, its value agrees well with the $g_\eta^{(\mathrm{Z})}$ and $g_\eta^{(\mathrm{F})}$ values for very small λL, i.e., for $\theta = 175°$ with small n, but deviates upward from those with increasing λL. In the case of $\theta = 109°$ (flexible chain), $g_\eta^{(\mathrm{KR})}$ values are ca. 5% larger than the corresponding $g_\eta^{(\mathrm{Z})}$ and $g_\eta^{(\mathrm{F})}$ values.

Table 2.3. Values of $X_\eta^{(\mathrm{KR})}$, $X_\eta^{(\mathrm{U})}$, and $X_\eta^{(\mathrm{L})}$

	three-arm star			linear		
n	$X_\eta^{(\mathrm{KR})}$ (error %)	$X_\eta^{(\mathrm{U})}$ (error %)	$X_\eta^{(\mathrm{L})}$ (error %)	$X_\eta^{(\mathrm{KR})}$ (error %)	$X_\eta^{(\mathrm{U})}$ (error %)	$X_\eta^{(\mathrm{L})}$ (error %)
			$\theta = 109°$			
60	0.304_1 (0.3)	0.272_4 (0.5)	0.250_6 (0.4)	0.333_3 (0.3)	0.306_9 (0.3)	0.283_0 (0.3)
120	0.321_2 (0.4)	0.284_4 (0.4)	0.255_9 (0.4)	0.352_8 (0.4)	0.321_1 (0.4)	0.289_8 (0.5)
180	0.329_0 (0.4)	0.288_3 (0.4)	0.256_6 (0.6)	0.363_2 (0.5)	0.329_3 (0.6)	0.293_1 (0.6)
240	0.332_9 (0.5)	0.290_3 (0.6)	0.255_4 (0.8)	0.369_7 (0.2)	0.335_0 (0.3)	0.295_1 (0.3)
300	0.336_0 (0.7)	0.293_3 (0.8)	0.255_5 (0.9)	0.374_3 (0.5)	0.338_7 (0.5)	0.295_7 (0.6)
			$\theta = 165°$			
60	1.76_3 (0.3)	1.77_8 (0.2)	1.72_6 (0.3)	2.91_1 (0.5)	2.96_1 (0.5)	2.88_0 (0.5)
120	3.21_7 (0.2)	3.23_7 (0.3)	3.11_9 (0.2)	5.02_2 (0.3)	5.13_5 (0.3)	4.95_0 (0.3)
180	4.45_5 (0.3)	4.47_8 (0.2)	4.28_7 (0.3)	6.63_4 (0.3)	6.76_5 (0.4)	6.49_1 (0.4)
240	5.51_0 (0.4)	5.52_1 (0.2)	5.26_4 (0.4)	7.94_6 (0.7)	8.07_1 (0.7)	7.72_1 (0.7)
300	6.41_3 (0.3)	6.37_9 (0.3)	6.08_8 (0.3)	9.06_2 (0.5)	9.16_1 (0.5)	8.74_5 (0.5)
			$\theta = 175°$			
60	2.12_9 (0.1)	2.12_7 (0.1)	2.08_7 (0.1)	3.98_8 (0.6)	4.02_0 (0.5)	3.89_9 (0.5)
120	4.57_2 (0.2)	4.59_5 (0.1)	4.46_8 (0.2)	8.70_8 (0.3)	8.83_2 (0.4)	8.51_6 (0.4)
180	7.26_3 (0.2)	7.32_7 (0.2)	7.09_2 (0.2)	13.8_0 (0.4)	14.0_6 (0.3)	13.5_2 (0.3)
240	10.0_8 (0.2)	10.2_3 (0.2)	9.84_8 (0.3)	19.0_6 (0.2)	19.4_9 (0.3)	18.7_0 (0.3)
300	13.0_1 (0.2)	13.2_4 (0.2)	12.7_1 (0.3)	24.2_8 (0.3)	24.9_3 (0.4)	23.8_7 (0.4)

Available theoretical asymptotic values of g_η in the (ideal) random-coil limit ($n \to \infty$ or $\lambda L \to \infty$) are 0.90_7 obtained by Zimm and Kilb[28] for the (dynamic) Gaussian spring-bead model with the preaveraged Oseen tensor and 0.90 obtained by Irurzun[29] for the Gaussian chain in the KR approximation. In Figure 2.6, the dotted horizontal line represents the Zimm–Kilb value 0.90_7. Naturally, the $g_\eta^{(\mathrm{KR})}$ values for $\theta = 109°$ agree well with the Zimm–Kilb value and also with the Irurzun one. If those MC values were appreciably different from the theoretical asymptotic values, the sample configurations of the regular three-arm star might not have been properly generated.

The approximate relation $g_\eta \simeq {g_S}^{1/2}$ proposed by Zimm and Kilb[28] for Gaussian branched chains has been often used in analyses of experimental data. The dashed curve in Figure 2.6 represents the values of ${g_S}^{1/2}$ for the KP regular three-arm star chain calculated from eqs 2.36 and 2.37. It is seen that the approximate relation overestimates g_η for semiflexible or stiff polymers.

Finally, we consider upper and lower bounds to g_η. From the inequality $[\eta]^{(\mathrm{L})} \le [\eta] \le [\eta]^{(\mathrm{U})}$ that holds for both the regular three-arm star and linear chains, we have the following two inequalities,

$$g_\eta \le g_\eta^{(\mathrm{U})} = \frac{[\eta]^{(\mathrm{U})}(\mathrm{star})}{[\eta]^{(\mathrm{L})}(\mathrm{linear})}, \qquad g_\eta \ge g_\eta^{(\mathrm{L})} = \frac{[\eta]^{(\mathrm{L})}(\mathrm{star})}{[\eta]^{(\mathrm{U})}(\mathrm{linear})} \tag{2.41}$$

Figure 2.7 shows the plots of $g_\eta^{(\mathrm{KR})}$ (○) against $\log(\lambda L)$ reproduced from Figure 2.6, where the upper and lower ends of each vertical error bar represent the $g_\eta^{(\mathrm{U})}$ and $g_\eta^{(\mathrm{L})}$ values, respectively, calculated from eqs 2.39 and 2.41 with the values of $X_\eta^{(\mathrm{U})}$ and $X_\eta^{(\mathrm{L})}$given in Table 2.3 and with n converted to λL in the above-mentioned manner. The difference between the upper and lower bounds increases with increasing λL. Although the differences are unexpectedly large for flexible chains ($\theta = 109°$), they are sufficiently small for semiflexible or stiff chains ($\theta = 165°$, $175°$) to let us conclude that $g_\eta^{(\mathrm{KR})}$ may give a good approximate value for the latter chains.

2.4 Concluding Remarks

We have examined the behavior of the ratio g_η of the intrinsic viscosity $[\eta]$ for the regular three-arm star chain to that for the linear one, both in the Θ state and having the same total chain length, by MC simulation of freely rotating chains with the LJ 6-12 potentials between beads in a cutoff version. On the basis of the values of the upper bound $[\eta]^{(\mathrm{U})}$ and lower one $[\eta]^{(\mathrm{L})}$ to $[\eta]$ evaluated by the Zimm rigid-body approximation and by the Fixman method, respectively, the values of the upper bound $g_\eta^{(\mathrm{U})}$ and lower one $g_\eta^{(\mathrm{L})}$ to g_η have been estimated. It has then been found that the KR value $g_\eta^{(\mathrm{KR})}$ of g_η lies between the two bounds irrespective of the number n of bonds and the bond angle θ (or the reduced

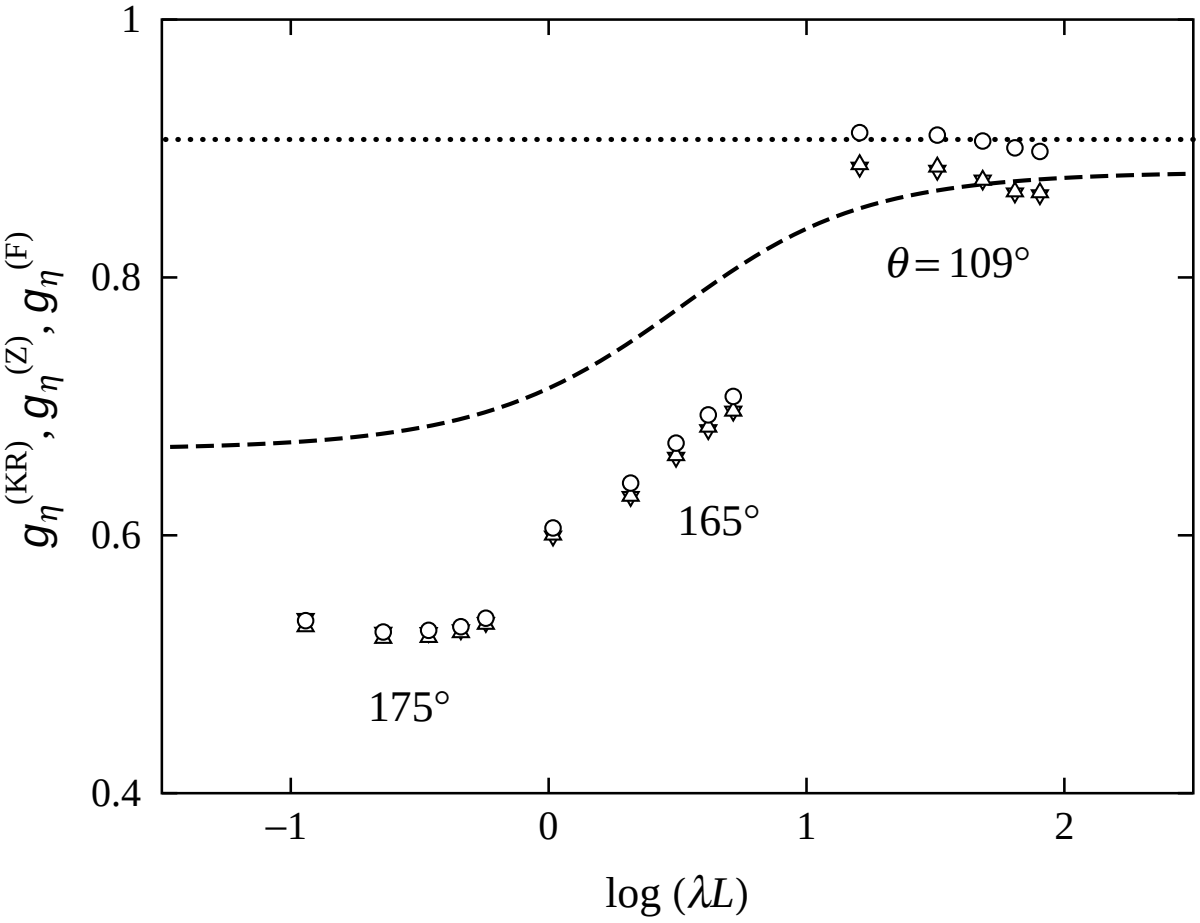

Figure 2.6. Plots of $g_\eta^{(\mathrm{KR})}$, $g_\eta^{(\mathrm{Z})}$, and $g_\eta^{(\mathrm{F})}$ against $\log(\lambda L)$. Three sets of the five unfilled circles, the five unfilled triangles, and the five unfilled inverted triangles represent the MC data of $g_\eta^{(\mathrm{KR})}$, $g_\eta^{(\mathrm{Z})}$, and $g_\eta^{(\mathrm{F})}$, respectively, with the indicated values of θ. The dotted horizontal line represents the Zimm–Kilb[28] value 0.90_7 for the Gaussian chain and the dashed curve the values of ${g_S}^{1/2}$ for the KP chain.

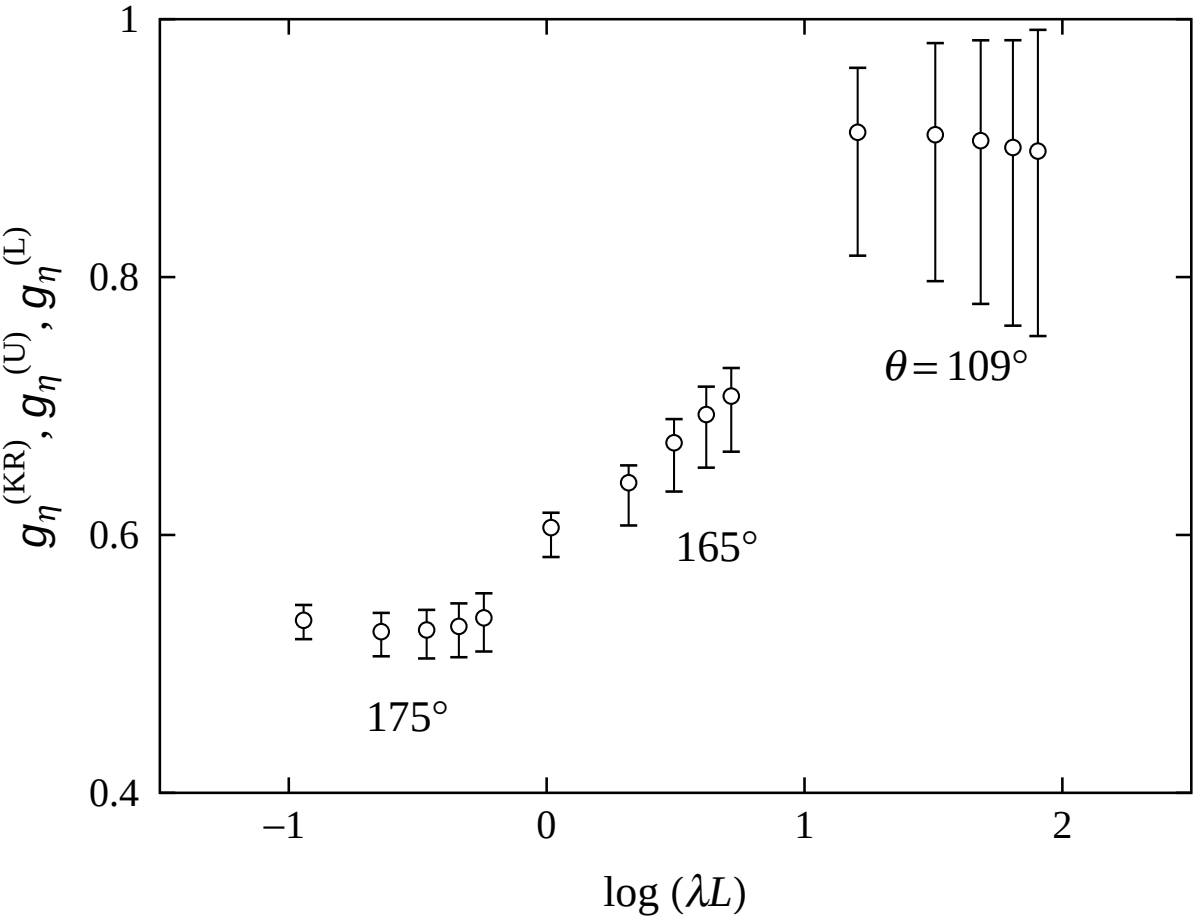

Figure 2.7. Plots of $g_\eta^{(\mathrm{KR})}$, $g_\eta^{(\mathrm{U})}$, and $g_\eta^{(\mathrm{L})}$ against $\log(\lambda L)$. The unfilled circles have the same meaning as those in Figure 2.6. The upper and lower ends of each vertical error bar represent the MC values of $g_\eta^{(\mathrm{U})}$ and $g_\eta^{(\mathrm{L})}$, respectively (see the text).

contour length λL). Although the differences between the two bounds are unexpectedly large for flexible chains ($\theta = 109°$), they are sufficiently small for semiflexible or stiff chains ($\theta = 165°, 175°$) to let us conclude that $g_\eta^{(\mathrm{KR})}$ gives a good approximate value for the latter chains. We therefore proceed to make a theoretical study of g_η for the unperturbed KP chain in the KR approximation and to construct an interpolation formula useful for an analysis of experimental data.

References

1. H. Yamakawa, "Modern Theory of Polymer Solutions," Harper & Row, New York, 1971. Its electronic edition is available on-line at the URL: `http://www.molsci.polym.kyoto-u.ac.jp/archives/redbook.pdf`
2. H. Yamakawa, "Helical Wormlike Chains in Polymer Solutions," Springer, Berlin, 1997.
3. J. P. Hansen and I. R. McDonald, "Theory of Simple Liquids," 3rd ed., Academic, London, 2006.
4. H. Yamakawa and T. Yoshizaki, *J. Chem. Phys.*, **118**, 2911 (2003).
5. H. Yamakawa and T. Yoshizaki, *J. Chem. Phys.*, **119**, 1257 (2003).
6. N. Metropolis, A. W. Rosenbluth, M. N. Rosenbluth, A. H. Teller, and E. Teller, *J. Chem. Phys.*, **21**, 1087 (1953).
7. M. Lal, *Mol. Phys.*, **17**, 57 (1969).
8. S. D. Stellman and P. J. Gans, *Macromolecules*, **5**, 516 (1972).
9. N. Madras and A. D. Sokal, *J. Stat. Phys.*, **50**, 109 (1988).
10. J. G. Kirkwood and J. Riseman, *J. Chem. Phys.*, **16**, 565 (1948).
11. B. H. Zimm, *Macromolecules*, **13**, 592 (1980).
12. M. Fixman, *J. Chem. Phys.*, **78**, 1588 (1983).
13. M. Fixman, *J. Chem. Phys.*, **78**, 1594 (1983).
14. S. D. Stellman, M. Froimowitz, and P. J. Gans, *J. Comput. Phys.*, **7** 178 (1971).
15. M. Matsumoto and T. Nishimura, *ACM Trans. Model. Comput. Simul.*, **8**, 3 (1998), see also the URL: `http://www.math.keio.ac.jp/matsumoto/emt.html`
16. J. Rotne and S. Prager, *J. Chem. Phys.*, **50**, 4831 (1969).
17. H. Yamakawa, *J. Chem. Phys.*, **53**, 436 (1970).
18. R. E. DeWames, W. F. Hall, and M. C. Shen, *J. Chem. Phys.*, **46**, 2782 (1967).
19. R. Zwanzig, J. Kiefer, and G. H. Weiss, *Proc. Natl. Acad. Sci. USA*, **60**, 381 (1968).
20. G. Wilemski and G. Tanaka, *Macromolecules*, **14**, 1531 (1981).
21. J. J. Freire and A. Rey, *Comput. Phys. Commum.*, **61**, 297 (1990).
22. O. Kratky and G. Porod, *Recl. Trav. Chim. Pays-Bas.*, **68**, 1106 (1949).

23. M. Guenza, M. Mormino, and P. Perico, *Macromolecules*, **24**, 6168 (1991).
24. H. Yamakawa and T. Yoshizaki, *J. Chem. Phys.*, **121**, 3295 (2004).
25. M. L. Mansfield and W. H. Stockmayer, *Macromolecules*, **13**, 1713 (1980).
26. H. Benoit and P. Doty, *J. Phys. Chem.*, **57**, 958 (1953).
27. B. H. Zimm and W. H. Stockmayer, *J. Chem. Phys.*, **17**, 1301 (1949).
28. B. H. Zimm and R. W. Kilb, *J. Polym. Sci.*, **37**, 19 (1959).
29. I. M. Irurzun, *J. Polym. Sci. B*, *Polym. Phys.*, **37**, 563 (1997).

3 Intrinsic Viscosity of Semiflexible Three-Arm Stars: A Theoretical Study

3.1 Introduction

In Chapter 2, effects of chain stiffness on the ratio g_η of the intrinsic viscosity $[\eta]$ of a regular three-arm star polymer chain to that of the corresponding linear one, both having the same total chain length and chain stiffness, have been examined by Monte Carlo (MC) simulation on the basis of the freely rotating chain with the Lennard–Jones 6-12 intramolecular potential between beads.[1] Since there is no theoretical method of obtaining $[\eta]$ without any approximations, we have evaluated it in the three approximate ways: the Kirkwood–Riseman (KR) approximation,[2,3] the Zimm rigid-body ensemble approximation,[4] and the Fixman method.[5,6] We note that upper and lower bounds to $[\eta]$ may be obtained by the Zimm and Fixman methods, respectively, and we have ignored the contribution of the Einstein spheres.[7,8] By combining the two bounds to $[\eta]$ so obtained, we have evaluated upper and lower bounds to g_η and then shown that the KR approximation may give a good approximate g_η value for semiflexible or stiff polymer chains. It is therefore convenient and useful for an analysis of experimental data to construct a theoretical expression for g_η in the KR approximation on the basis of a proper model for semiflexible and stiff polymer chains. The purpose in this chapter is to construct an interpolation formula for g_η of the semiflexible regular three-arm star chain in the KR approximation on the basis of the Kratky–Porod (KP) wormlike chain[7,9] without excluded volume.

For an evaluation of $[\eta]$ for both the KP regular three-arm star and linear chains, we adopt the touched-bead hydrodynamic model so that $[\eta]$ may be written as a sum of the solution $[\eta]_{\mathrm{KR}}$ of the KR equation and the contribution $[\eta]_{\mathrm{E}}$ of the Einstein spheres.[7,8] In order to complete the necessary KR equation, i.e., a set of linear simultaneous equations for the hydrodynamic force balance at each bead with the preaveraged Oseen hydrodynamic interaction tensor,[2,3] we need an appropriate approximate expression for the mean reciprocal $\langle R^{-1} \rangle$ of the distance between the centers of two beads, where $\langle \cdots \rangle$ denotes an equilibrium configurational average. Although such an expression is available for a pair of beads on the KP linear chain,[10,11] there are none for a pair of beads on different two arms of the KP star. Prior to the evaluation of $[\eta]$ and g_η, we must therefore derive an approx-

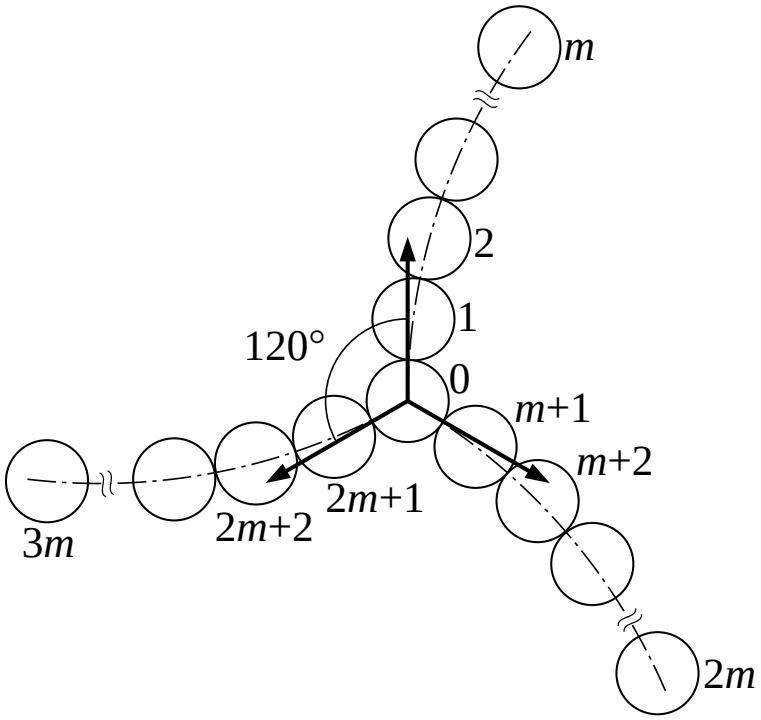

Figure 3.1. Illustration of the KP regular three-arm star touched-bead model.

imate expression for $\langle R^{-1} \rangle$ between the two beads on different parts of the once-broken KP chain as a function of the two contour distances from the broken point to the centers of the respective beads. We carry out the task by the use of the two asymptotic methods, i.e., the Daniels method[7,12–14] near the random-coil limit and the ϵ method[7,15,16] near the rod limit, and also of the MC results for the once-broken KP chain.

3.2 Basic Equations

Consider a regular three-arm star touched-bead model composed of $3m + 1$ identical spherical beads of (hydrodynamic) diameter d_b whose centers are located on the KP regular three-arm star chain contour, as illustrated in Figure 3.1. For convenience, the three arms are designated the first, second, and third ones and the m beads on the ith ($i = 1, 2, 3$) arm are numbered $(i-1)m+1$, $(i-1)m+2$, $\cdots$, im from the branch point (center) to the terminal end, with the center bead numbered 0. The angle between each pair of the unit vectors tangent to the KP contours at the branch point is fixed to be 120°, so that the three vectors are on the same plane. The linear touched-bead model, the counterpart of the above star one, is the KP touched-bead model composed of $n + 1$ identical beads of diameter d_b whose centers are located on the KP linear chain contour. We set $n + 1$ equal to $3m + 1$, so that $n = 3m$. The $n + 1$ beads are numbered 0, 1, 2, $\cdots$, n from one end to the other. For both the star and linear touched-bead models, the

contour distance between the two adjacent beads is set equal to d_b.

The intrinsic viscosity $[\eta]$ of the touched-bead model composed of $n+1$ identical spherical beads of diameter d_b may be written as the sum of the solution $[\eta]_\mathrm{KR}$ of the KR equation and the contribution $[\eta]_\mathrm{E}$ of the Einstein spheres,[7,8] i.e.,

$$[\eta] = [\eta]_\mathrm{KR} + [\eta]_\mathrm{E} \tag{3.1}$$

where

$$[\eta]_\mathrm{KR} = \frac{N_\mathrm{A}}{M} \sum_{i=0}^{n} \phi_{ii} \tag{3.2}$$

$$[\eta]_\mathrm{E} = \frac{5\pi N_\mathrm{A}(n+1){d_\mathrm{b}}^3}{12M} \tag{3.3}$$

with N_A the Avogadro constant and M the polymer molecular weight. In eq 3.2, ϕ_{ij} is the solution of the following linear simultaneous equations,

$$\phi_{ij} + \frac{d_\mathrm{b}}{2} \sum_{\substack{k=0 \\ \neq i}}^{n} \langle {R_{ik}}^{-1} \rangle \, \phi_{kj} = \frac{\pi d_\mathrm{b}}{2} \langle \mathbf{S}_i \cdot \mathbf{S}_j \rangle \tag{3.4}$$

where $\langle {R_{ij}}^{-1} \rangle$ is the mean reciprocal of the distance between the centers of the ith and jth beads and $\mathbf{S}_i$ is the vector distance from the center of mass of the chain to the center of the ith bead. In order to complete the KR equation 3.4, we need an appropriate approximate expression for $\langle {R_{ij}}^{-1} \rangle$ along with the theoretical expression for the equilibrium average $\langle \mathbf{S}_i \cdot \mathbf{S}_j \rangle$. We first give the latter and then consider the former. In what follows, all lengths are measured in units of the stiffness parameter λ^{-1} of the KP chain unless otherwise specified.

3.3 Average $\langle \mathbf{S}_i \cdot \mathbf{S}_j \rangle$

As in the previous study of $[\eta]$ of the linear touched-bead model,[8] where we have adopted the value of $\langle \mathbf{S}_i \cdot \mathbf{S}_j \rangle$ of the (continuous) KP chain of total contour length $L = (n+1)d_\mathrm{b}$ as that of the (discrete) touched-bead model, we adopt the value of $\langle \mathbf{S}_i \cdot \mathbf{S}_j \rangle$ of the KP regular three-arm star chain of total contour length $L = (3m+1)d_\mathrm{b}$ as that of the regular three-arm star touched-bead model. Here, L has consistently been set equal to the total number $n+1$ or $3m+1$ of beads multiplied by d_b for both the linear and star chains. The relation $L = (3m+1)d_\mathrm{b}$ leads to the relation $L_\mathrm{a} = (m + \frac{1}{3})d_\mathrm{b}$ between the contour length $L_\mathrm{a} = \frac{1}{3}L$ of each arm and d_b. Although the latter relation seems somewhat awkward because of the inclusion of the non-integer term $\frac{1}{3}$, it only reflects the fact that the center bead belongs to all the three arms.

For the $[(i-1)m+k]$th and $[(j-1)m+l]$th beads (i, $j = 1, 2, 3$; k, $l = 1, 2, \cdots, m$) of the regular three-arm star chain, i.e., the kth bead on the ith arm and the lth bead on the jth arm, respectively, $\langle \mathbf{S}_{(i-1)m+k} \cdot \mathbf{S}_{(j-1)m+l} \rangle$ may then be given by

$$\langle \mathbf{S}_{(i-1)m+k} \cdot \mathbf{S}_{(j-1)m+l} \rangle = \langle \mathbf{S}(t_k^{(i)}) \cdot \mathbf{S}(t_l^{(j)}) \rangle \tag{3.5}$$

where $\mathbf{S}(t_k^{(i)})$ is the vector distance from the center of mass of the KP regular three-arm star chain to the contour point on the ith arm with the contour distance $t_k^{(i)}$ from the branch point, so that

$$t_k^{(i)} = k d_\mathrm{b} \tag{3.6}$$

The average $\langle \mathbf{S}(t_k^{(i)}) \cdot \mathbf{S}(t_l^{(j)}) \rangle$ may be given by (see Appendix 3.A)

$$\begin{aligned}\langle \mathbf{S}(t_k^{(i)}) \cdot \mathbf{S}(t_l^{(j)}) \rangle = {} & \frac{L}{27} + \frac{(t_k^{(i)})^2 + (t_l^{(j)})^2}{2L} + \frac{t_k^{(i)} + t_l^{(j)}}{6} - \frac{u_{kl}^{(ij)}}{2} \\ & + \frac{1}{24}(1 - 3\delta_{ij})\big[1 - \exp(-2t_k^{(i)}) - \exp(-2t_l^{(j)})\big] - \frac{1}{8}(1 + \delta_{ij}) \exp(-2u_{kl}^{(ij)}) \\ & + \frac{1}{4L} - \frac{1}{4L} e^{-2L/3}\big[\cosh(2t_k^{(i)}) + \cosh(2t_l^{(j)})\big] + \frac{3}{16L^2}(1 - e^{-4L/3})\end{aligned} \tag{3.7}$$

where δ_{ij} is the Kronecker delta and $u_{kl}^{(ij)}$ is defined by

$$u_{kl}^{(ij)} = \big[(t_k^{(i)})^2 + (t_l^{(j)})^2 + 2(1 - 2\delta_{ij}) t_k^{(i)} t_l^{(j)}\big]^{1/2} \tag{3.8}$$

We note that $\langle \mathbf{S}_{(i-1)m+k} \cdot \mathbf{S}_0 \rangle = \langle \mathbf{S}(t_k^{(i)}) \cdot \mathbf{S}(0) \rangle$ and $\langle \mathbf{S}_0 \cdot \mathbf{S}_0 \rangle = \langle \mathbf{S}(0) \cdot \mathbf{S}(0) \rangle$ are also given by eq 3.7 with $u_{kl}^{(ij)} = t_k^{(i)}$ and 0, respectively. In the rod limit, i.e., the limit of L (in units of λ^{-1}) $\to 0$, eq 3.7 reduces to

$$\langle \mathbf{S}(t_k^{(i)}) \cdot \mathbf{S}(t_l^{(j)}) \rangle = \frac{1}{2}(3\delta_{ij} - 1)\, t_k^{(i)} t_l^{(j)} \qquad \text{(rod limit)} \tag{3.9}$$

As for the linear touched-bead model, $\langle \mathbf{S}_i \cdot \mathbf{S}_j \rangle$ (i, $j = 0, 1, 2, \cdots, n$) may be given by

$$\langle \mathbf{S}_i \cdot \mathbf{S}_j \rangle = \langle \mathbf{S}(t_i) \cdot \mathbf{S}(t_j) \rangle \tag{3.10}$$

where $\mathbf{S}(t_i)$ is the vector distance from the center of mass of the KP linear chain to its contour point with the contour distance t_i from one end, so that

$$t_i = \big(i + \tfrac{1}{2}\big) d_\mathrm{b} \tag{3.11}$$

The average $\langle \mathbf{S}(t) \cdot \mathbf{S}(t') \rangle$ is given by eq 19 in ref 17 and may be written in the form,

$$\begin{aligned}\langle \mathbf{S}(t) \cdot \mathbf{S}(t') \rangle = {} & \frac{L}{3} + \frac{t^2 + t'^2}{2L} - \frac{t + t'}{2} - \frac{|t - t'|}{2} - \frac{e^{-2|t-t'|}}{4} \\ & + \frac{1}{8L}\big[2 - e^{-2t} - e^{-2t'} - e^{-2(L-t)} - e^{-2(L-t')}\big] + \frac{1}{8L^2}\big(1 - e^{-2L}\big)\end{aligned} \tag{3.12}$$

In the rod limit, it reduces to

$$\langle \mathbf{S}(t) \cdot \mathbf{S}(t') \rangle = \frac{1}{4}(2t - L)(2t' - L) \qquad \text{(rod limit)} \tag{3.13}$$

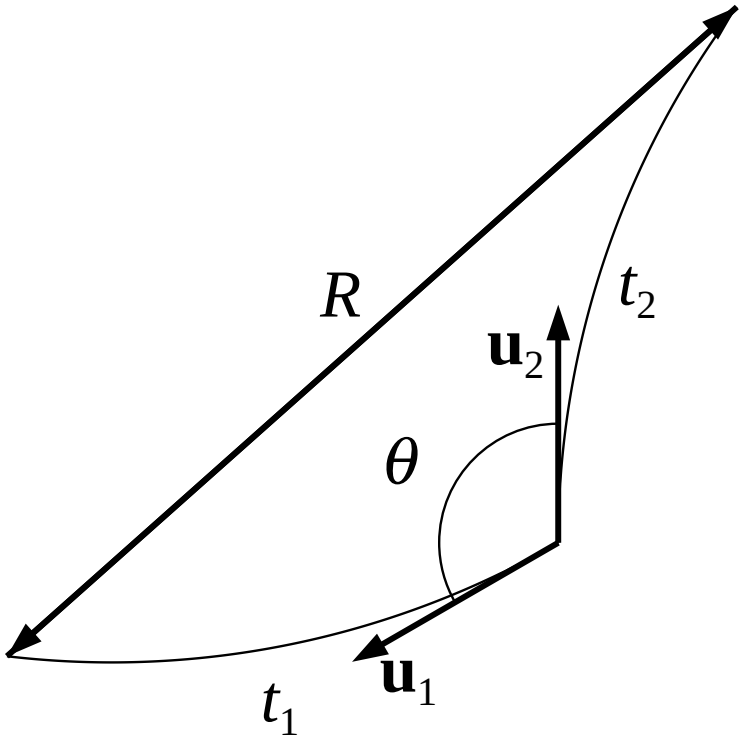

Figure 3.2. Illustration of the once-broken KP chain.

3.4 Mean Reciprocal $\langle R^{-1} \rangle$ of the End-to-End Distance

The mean reciprocal $\langle {R_{[(i-1)m+k][(j-1)m+l]}}^{-1} \rangle$ of the distance $R_{[(i-1)m+k][(j-1)m+l]}$ between the centers of the kth bead on the ith arm and lth bead on the jth arm may be given by

$$\langle {R_{[(i-1)m+k][(j-1)m+l]}}^{-1} \rangle = \langle R^{-1}\big(t_k^{(i)}, t_l^{(j)}\big) \rangle \tag{3.14}$$

where $\langle R^{-1}\big(t_k^{(i)}, t_l^{(j)}\big) \rangle$ is the mean reciprocal of the distance between the contour points $t_k^{(i)}$ and $t_l^{(j)}$ on the KP regular three-arm star chain.

We first consider asymptotic forms for the mean reciprocal $\langle R^{-1}(t_1, t_2, \theta) \rangle$ of the end-to-end distance of the once-broken KP chain of total contour length $t_1 + t_2$ such that two KP subchains 1 and 2 of contour lengths t_1 and t_2, respectively, are connected with a bending angle θ, i.e., the angle between the unit vectors $\mathbf{u}_1$ and $\mathbf{u}_2$ tangent to the contours of the subchains 1 and 2, respectively, at the broken point, as illustrated in Figure 3.2. We then construct an interpolation formula for the case of $\theta = 120^\circ$ on the basis of the asymptotic forms so obtained and also of MC results for the once broken KP chain.

3.4.1 Asymptotic Forms

The asymptotic forms for $\langle R^{-1}(t_1,t_2,\theta)\rangle$ in the cases of $t_1 \gg 1$ and $t_2 \gg 1$, $t_1 \gg 1$ and $t_2 \ll 1$, $t_1 \ll 1$ and $t_2 \gg 1$, and $t_1 \ll 1$ and $t_2 \ll 1$ may be written in the form (see Appendix 3.B),

$$\begin{aligned}\langle R^{-1}(t_1,t_2,\theta)\rangle &= \langle R^2\rangle^{-1/2} f_{\mathrm{DD}}(t_1,t_2,\theta) \qquad \text{for } t_1 \gg 1,\ t_2 \gg 1\\ &= \langle R^2\rangle^{-1/2} f_{\mathrm{D}\epsilon}(t_1,t_2,\theta) \qquad \text{for } t_1 \gg 1,\ t_2 \ll 1\\ &= \langle R^2\rangle^{-1/2} f_{\epsilon\mathrm{D}}(t_1,t_2,\theta) \qquad \text{for } t_1 \ll 1,\ t_2 \gg 1\\ &= \langle R^2\rangle^{-1/2} f_{\epsilon\epsilon}(t_1,t_2,\theta) \qquad \text{for } t_1 \ll 1,\ t_2 \ll 1\end{aligned} \tag{3.15}$$

where

$$f_{\mathrm{DD}}(t_1,t_2,\theta) = \left(\frac{6}{\pi}\right)^{1/2}\left\{1 - \frac{11}{40\langle R^2\rangle} + \frac{1}{80\langle R^2\rangle^2}\left[\frac{431}{56} + 11(1+\cos\theta) + \frac{11}{2}(1-\cos^2\theta)\right]\right\} \tag{3.16}$$

$$f_{\mathrm{D}\epsilon}(t_1,t_2,\theta) = \left(\frac{6}{\pi}\right)^{1/2}\left\{1 - \frac{11}{40\langle R^2\rangle} + \frac{1}{40\langle R^2\rangle^2}\left[\frac{431}{112} + 9{t_2}^2(1-\cos^2\theta)\right]\right\} \tag{3.17}$$

$$f_{\epsilon\epsilon}(t_1,t_2,\theta) = 1 + \frac{3}{8}\left(\frac{\langle R^4\rangle}{\langle R^2\rangle^2} - 1\right) \tag{3.18}$$

and $f_{\epsilon\mathrm{D}}(t_1,t_2,\theta) = f_{\mathrm{D}\epsilon}(t_2,t_1,\theta)$. In eqs 3.15—3.18, $\langle R^2\rangle = \langle R^2(t_1,t_2,\theta)\rangle$ and $\langle R^4\rangle = \langle R^4(t_1,t_2,\theta)\rangle$ are the second and fourth moments, respectively, of the end-to-end distance of the once-broken KP chain given by

$$\langle R^2(t_1,t_2,\theta)\rangle = t_1 + t_2 - \frac{1}{2}\left[1 - e^{-2(t_1+t_2)}\right] - \frac{1}{2}\left(1 - e^{-2t_1}\right)\left(1 - e^{-2t_2}\right)(1+\cos\theta) \tag{3.19}$$

$$\begin{aligned}\langle R^4(t_1,t_2,\theta)\rangle = {}& \frac{5}{3}(t_1+t_2)^2 - (t_1+t_2)\left[\frac{26}{9} + e^{-2(t_1+t_2)}\right]\\ &+2[1-e^{-2(t_1+t_2)}] - \frac{1}{54}[1-e^{-6(t_1+t_2)}]\\ &-\left\{(1-e^{-2t_1})\left[\frac{5}{3}t_2 + t_2e^{-2t_2} - \frac{3}{2}(1-e^{-2t_2}) + \frac{1}{18}(1-e^{-6t_2})\right]\right.\\ &\left.+(1-e^{-2t_2})\left[\frac{5}{3}t_1 + t_1e^{-2t_1} - \frac{3}{2}(1-e^{-2t_1}) + \frac{1}{18}(1-e^{-6t_1})\right]\right\}(1+\cos\theta)\\ &-\frac{1}{4}\left[(1-e^{-2t_1}) - \frac{1}{3}(1-e^{-6t_1})\right]\left[(1-e^{-2t_2}) - \frac{1}{3}(1-e^{-6t_2})\right](1-\cos^2\theta)\end{aligned} \tag{3.20}$$

We note that $f_{\mathrm{D}\epsilon}(t,0,\theta)$ given by eq 3.17 with $t_1 = t$ and $t_2 = 0$ [or $f_{\epsilon\mathrm{D}}(0,t,\theta)$] is identical with the second Daniels approximate expression for the mean reciprocal of the end-to-end distance of the KP linear chain of total contour length t obtained by Yamakawa and

Fujii,[11] up to $\mathcal{O}(t^{-2})$, and also note that the expression for $\langle R^2(t_1, t_2, \theta)\rangle$ given by eq 3.19 was first derived by Mansfield and Stockmayer.[18] In the rod limit, eqs 3.15 (strictly the fourth equation) reduces to

$$\langle R^{-1}(t_1, t_2, \theta)\rangle = [R_{\rm rod}(t_1, t_2, \theta)]^{-1} \qquad \text{(rod limit)} \tag{3.21}$$

where $R_{\rm rod}(t_1, t_2, \theta)$ is the end-to-end distance of the once-broken rod composed of the two straight rods of lengths t_1 and t_2 with the bending angle θ and is given by

$$R_{\rm rod}(t_1, t_2, \theta) = ({t_1}^2 + {t_2}^2 - 2t_1 t_2 \cos\theta)^{1/2} \tag{3.22}$$

Figures 3.3, 3.4, and 3.5 show plots of $R_{\rm rod}(t_1, t_2, 120^\circ)\langle R^{-1}(t_1, t_2, 120^\circ)\rangle$ against t_1 for the once-broken KP chain with $\theta = 120^\circ$ and with $t_2 = 0.1$, 1, and 2, respectively. The dashed (DD), two dot-dashed (Dϵ and ϵD), and dotted ($\epsilon\epsilon$) curves represent the theoretical asymptotic values calculated from eqs 3.15 with eqs 3.16, 3.17, and 3.18, respectively, with $\theta = 120^\circ$. In the figures, the unfilled circles and the solid curves represent the MC values and those calculated from an interpolation formula, which are obtained in the following two subsections.

3.4.2 MC Simulation

As seen from Figures 3.3, 3.4, and 3.5, it is difficult to construct an interpolation formula on the basis only of the theoretical asymptotic values because they cannot cover the whole range of t_1. In order to obtain additional reference values of $\langle R^{-1}(t_1, t_2, 120^\circ)\rangle$, we carry out MC simulation by the use of the ideal once-broken freely rotating chain such that two freely rotating subchains 1 and 2 are connected with a bending angle 120°, the subchain i (i = 1, 2) being composed of n_i bonds of length a (in units of λ^{-1}) joined with a complementary bond angle α. We note that the subchain i becomes identical with the KP chain of total contour length t_i in the limit of $n_i \to \infty$ and $a \to 0$ under the conditions $t_i = n_i a$ and $1 - \cos\alpha = 2a$. As done by Yamakawa and Fujii,[11] we replace the KP subchains approximately by the freely rotating ones having very small but finite α satisfying the above two conditions, i.e., $a = 0.01$ and $\cos\alpha = 0.98$.

By the use of the once-broken freely rotating chain so defined, we evaluate $\langle R^{-1}(t_1, t_2, 120^\circ)\rangle$ as follows. Let $\mathbf{a}_k^{(i)}$ (i = 1, 2; k = 1, 2, $\cdots$, n_i) be the kth bond vector on the subchain i, the bond vectors being numbered 1, 2, $\cdots$, n_i from the broken point to the end of the subchain i, and let $\mathbf{a}_1^{(1)} = (0, 0, a)^T$ and $\mathbf{a}_1^{(2)} = (\sqrt{3}a/2, 0, -a/2)^T$ in an external Cartesian coordinate system with the superscript T indicating the transpose. In the external system, $\mathbf{a}_k^{(i)}$ may then be written in the form,

$$\mathbf{a}_k^{(i)} = [\mathbf{A}(120^\circ, 180^\circ)]^{i-1} \cdot \mathbf{A}(\alpha, \phi_1^{(i)}) \cdot \mathbf{A}(\alpha, \phi_2^{(i)}) \cdots \mathbf{A}(\alpha, \phi_{k-1}^{(i)}) \cdot (0, 0, a)^T \tag{3.23}$$

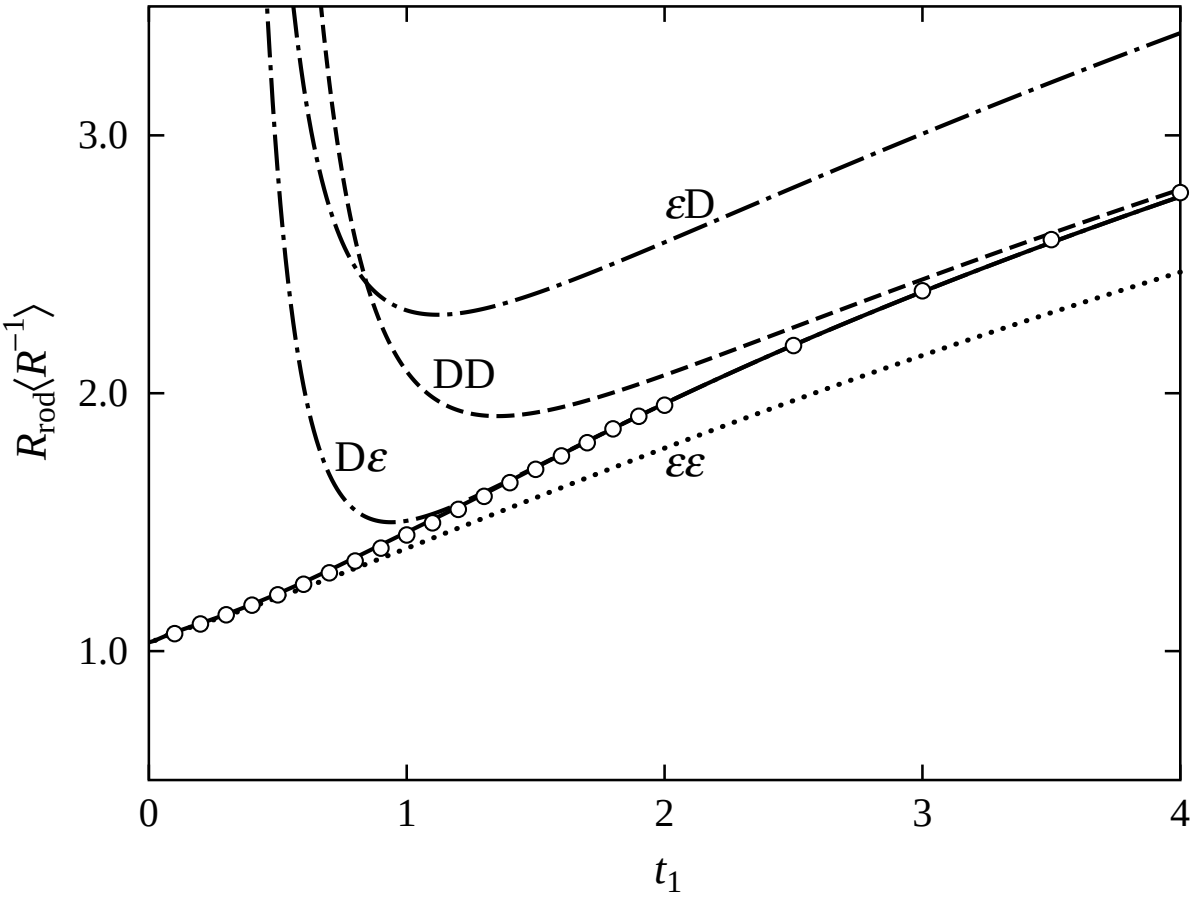

Figure 3.3. Plots of $R_{\rm rod}(t_1, t_2, 120^\circ)\langle R^{-1}(t_1, t_2, 120^\circ)\rangle$ against t_1 for the once-broken KP chain with $\theta = 120^\circ$ and $t_2 = 0.1$. The unfilled circles represent the MC values. The solid curve represents the values of the interpolation formula and the dashed (DD), two dot-dashed (Dϵ and ϵD), and dotted ($\epsilon\epsilon$) curves represent the theoretical asymptotic values for $t_1 \gg 1$ and $t_2 \gg 1$, $t_1 \gg 1$ and $t_2 \ll 1$, $t_1 \ll 1$ and $t_2 \gg 1$, and $t_1 \ll 1$ and $t_2 \ll 1$, respectively (see the text).

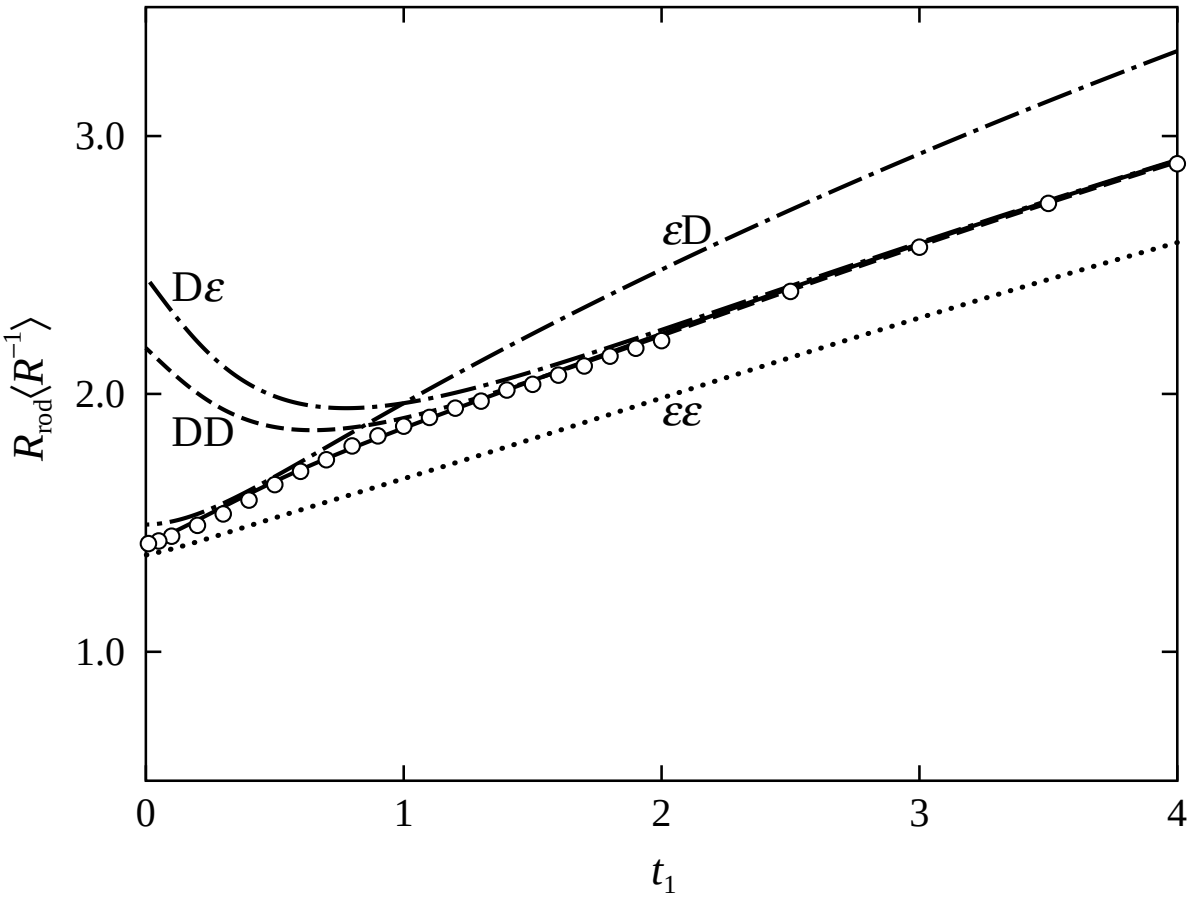

Figure 3.4. Plots of $R_{\rm rod}(t_1, t_2, 120^\circ)\langle R^{-1}(t_1, t_2, 120^\circ)\rangle$ against t_1 for the once-broken KP chain with $\theta = 120^\circ$ and $t_2 = 1$. All the symbols and curves have the same meaning as those in Figure 3.3.

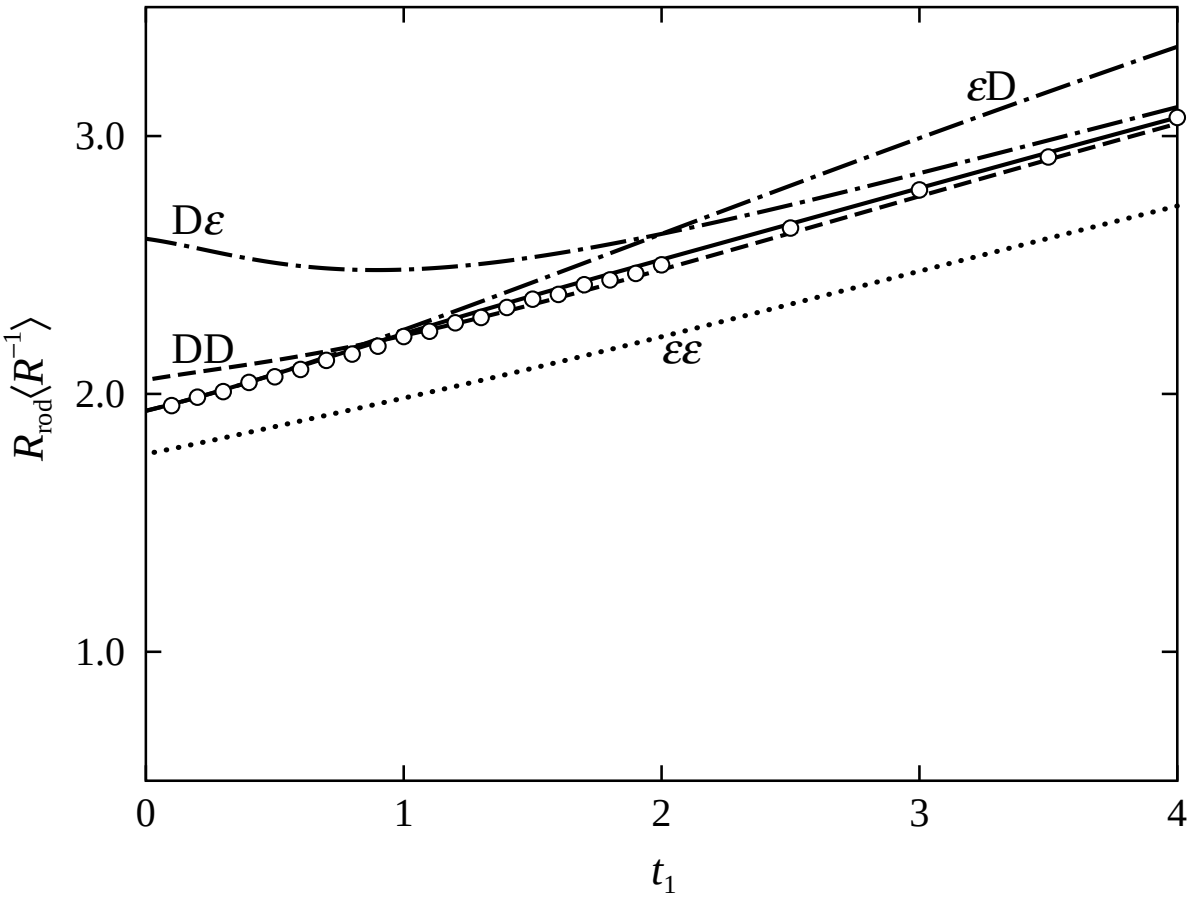

Figure 3.5. Plots of $R_{\rm rod}(t_1, t_2, 120^\circ)\langle R^{-1}(t_1, t_2, 120^\circ)\rangle$ against t_1 for the once-broken KP chain with $\theta = 120^\circ$ and $t_2 = 2$. All the symbols and curves have the same meaning as those in Figure 3.3.

where $\phi_k^{(i)}$ is the internal rotation angle around $\mathbf{a}_k^{(i)}$ and $\mathbf{A}(\alpha,\phi)$ is the orthogonal transformation matrix defined by

$$\mathbf{A}(\alpha,\phi)=\begin{pmatrix} -\cos\alpha\,\cos\phi & \sin\phi & -\sin\alpha\,\cos\phi \\ -\cos\alpha\,\sin\phi & -\cos\phi & -\sin\alpha\,\sin\phi \\ -\sin\alpha & 0 & \cos\alpha \end{pmatrix} \tag{3.24}$$

The configuration of the once-broken freely rotating chain may therefore be specified by the set of n_1+n_2-2 internal rotation angles $\{\phi_{n_1+n_2-2}\}=(\phi_1^{(1)},\,\phi_2^{(1)},\,\cdots,\,\phi_{n_1-1}^{(1)},\,\phi_1^{(2)},\,\phi_2^{(2)},\,\cdots,\,\phi_{n_2-1}^{(2)})$. On the basis of N sample configurations, i.e., N sets of n_1+n_2-2 internal rotation angles randomly chosen in the interval $[-\pi,\pi]$, $\langle R^{-1}(t_1,t_2,120^\circ)\rangle$ may be evaluated from

$$\langle R^{-1}(t_1,t_2,120^\circ)\rangle = N^{-1}\sum_{\{\phi_{n_1+n_2-2}\}}\left|\sum_{i=1}^{n_1}\mathbf{a}_i^{(1)}-\sum_{j=1}^{n_2}\mathbf{a}_j^{(2)}\right|^{-1} \tag{3.25}$$

where the first sum is taken over the N sample configurations.

In practice, we have adopted $N=10^5$. All the numerical work has been done by the use of a personal computer with an Intel Pentium4 CPU with a clock rate of 3.00 GHz. A source program coded in C has been compiled by the GNU C compiler version 3.3.3 with real variables of double precision.

The MC values of $R_{\rm rod}(t_1,t_2,120^\circ)\langle R^{-1}(t_1,t_2,120^\circ)\rangle$ so obtained for $t_2=0.1$, 1, and 2 are also shown in Figures 3.3, 3.4, and 3.5, respectively (unfilled circles). It is seen from Figure 3.3 for the case of small t_2 (= 0.1) that the MC values connect smoothly the $\epsilon\epsilon$ values which are valid for $t_1\ll 1$ and $t_2\ll 1$ and the Dϵ ones which are valid for $t_1\gg 1$ and $t_2\ll 1$. In the case of large t_2 (= 2), on the other hand, it is seen from Figure 3.5 that the MC values connect smoothly the ϵD values which are valid for $t_1\ll 1$ and $t_2\gg 1$ and the DD ones which are valid for $t_1\gg 1$ and $t_2\gg 1$. In the case of intermediate t_2 (= 1) shown in Figure 3.4, The MC values lie between the $\epsilon\epsilon$ and ϵD values for $t_1\lesssim 1$ and follow the DD values for $t_1\gtrsim 1$.

3.4.3 Interpolation Formula

Now we are in a position to construct an interpolation formula for $\langle R^{-1}(t_1,t_2,120^\circ)\rangle$ on the basis of the theoretical asymptotic forms given by eqs 3.15 with eqs 3.16—3.18 along with the MC ones for the once-broken KP chain.

The asymptotic form $f_{\rm D\epsilon}$ (or $f_{\epsilon\rm D}$) is not symmetric with respect to the pair of variables t_1 and t_2 and is not convenient for further developments as it stands. We therefore construct a hybrid $f_{\rm DD\epsilon}(t_1,t_2,120^\circ)$ between $f_{\rm DD}(t_1,t_2,120^\circ)$ and $f_{\rm D\epsilon}(t_1,t_2,120^\circ)$ given by eqs 3.16 and 3.17, respectively, both with $\theta=120^\circ$, prior to the construction of the

interpolation formula, which may be written in the form,

$$f_{\mathrm{DD}\epsilon}(t_1,t_2,120^\circ)=\left(\frac{6}{\pi}\right)^{1/2}\left[1-\frac{11}{40\langle R^2\rangle}+\frac{431}{4480\langle R^2\rangle^2}+\frac{C(t_1,t_2)}{\langle R^2\rangle^2}\right] \tag{3.26}$$

where $C(t_1,t_2)$ is given by

$$C(t_1,t_2)=\frac{108\bar{t}^2+77\bar{t}^4}{640(1+\bar{t}^4)} \tag{3.27}$$

with

$$\bar{t}^2=({t_1}^{-2}+{t_2}^{-2})^{-1} \tag{3.28}$$

We note that $f_{\mathrm{DD}\epsilon}$ so defined has the symmetry relation $f_{\mathrm{DD}\epsilon}(t_1,t_2,120^\circ)=f_{\mathrm{DD}\epsilon}(t_2,t_1,120^\circ)$ and recovers f_{DD} given by eq 3.16 up to $\mathcal{O}({t_2}^{-2})$ in the case of $t_2\gg 1$ and $f_{\mathrm{D}\epsilon}$ given by eq 3.17 up to $\mathcal{O}({t_2}^2)$ in the case of $t_2\ll 1$.

By combining $f_{\epsilon\epsilon}$ and $f_{\mathrm{DD}\epsilon}$ given by eqs 3.18 and 3.26, respectively, we then assume that $\langle R^{-1}(t_1,t_2,120^\circ)\rangle$ may be well represented by the following interpolation formula,

$$\begin{aligned}\langle R^{-1}(t_1,t_2,120^\circ)\rangle=\langle R^2\rangle^{-1/2}\big[1+A_1\langle R^2\rangle^{A_2}\big]^{-1}\big[f_{\epsilon\epsilon}(t_1,t_2,120^\circ)+A_3\langle R^2\rangle^{3/2}\\ +A_4t_1t_2(t_1+t_2)e^{-A_5t_1t_2}+A_1\langle R^2\rangle^{A_2}f_{\mathrm{DD}\epsilon}(t_1,t_2,120^\circ)\big]\end{aligned} \tag{3.29}$$

where $\langle R^2\rangle=\langle R^2(t_1,t_2,120^\circ)\rangle$ is given by eq 3.19 with $\theta=120^\circ$. In eq 3.29, A_1, A_2, $\cdots$, A_5 are numerical constants which must be determined so that the interpolation formula may well reproduce the MC values evaluated in the last subsection, their optimum values being given by

$$A_1=5,\quad A_2=\tfrac{11}{2},\quad A_3=0.045,\quad A_4=0.40,\quad A_5=1 \tag{3.30}$$

In Figures 3.3—3.5, the solid curves represent the approximate values calculated from eq 3.29 with eqs 3.18—3.20, 3.26—3.28, and 3.30 with $\theta=120^\circ$. It is seen that the interpolation formula so constructed may be well reproduced the MC values.

Finally, the necessary $\langle {R_{[(i-1)m+k][(j-1)m+l]}}^{-1}\rangle$ may be given by eq 3.14 with $\langle R^{-1}(t_k^{(i)},t_l^{(j)})\rangle$ given by

$$\begin{aligned}\langle R^{-1}(t_k^{(i)},t_l^{(j)})\rangle&=\langle R^{-1}(t_k^{(i)},t_l^{(j)},120^\circ)\rangle &&\text{for } i\neq j\\ &=\langle R^{-1}(|t_k^{(i)}-t_l^{(i)}|,0,120^\circ)\rangle &&\text{for } i=j\end{aligned} \tag{3.31}$$

We note that $\langle R^{-1}(t,0,120^\circ)\rangle$ and/or $\langle R^{-1}(0,t,120^\circ)\rangle$ represent the mean reciprocal of the end-to-end distance of the KP linear chain of total contour length t and its approximate value calculated from eq 3.29 with eqs 3.18—3.20, 3.26—3.28, and 3.30 and with $t_1=t$ and $t_2=0$ agrees with that calculated from the Yamakawa–Fujii[11] interpolation formula for the KP linear cylinder (with the cylinder diameter $d=0$) within 0.7% over the whole range of t.

3.5 Results for g_η Factor

We have calculated the KR contribution $[\eta]_{\mathrm{KR}}$ to the intrinsic viscosity $[\eta]$ from eq 3.2 with the numerical solutions ϕ_{ii} of the linear simultaneous equations 3.4 for both the KP regular three-arm star and linear touched-bead models, in the ranges of the total number $n+1$ of beads from 4 to 1501 and of the bead diameter d_{b} from 0.001 to 0.4. Note that the total contour length L of the chain is equal to $(n+1)d_{\mathrm{b}}$, as already mentioned. In eq 3.4, $\langle R^{-1}(t_k^{(i)}, t_l^{(j)})\rangle$ is given by eq 3.31 with eqs 3.18—3.20 and 3.26—3.30 for the star chain and by the second of eq 3.31 for the linear one and $\langle \mathbf{S}_i \cdot \mathbf{S}_j \rangle$ is given by eq 3.7 with eq 3.8 for the former and by eq 3.12 for the latter. We then have calculated $[\eta]$ from eq 3.1 with the values of $[\eta]_{\mathrm{KR}}$ so obtained along with $[\eta]_{\mathrm{E}}$ calculated from eq 3.3, for both the star and linear chains. Finally we have evaluated g_η as a function of L and d_{b} from the defining equation,

$$g_\eta(L, d_{\mathrm{b}}) = \frac{[\eta](\mathrm{star})}{[\eta](\mathrm{linear})} \tag{3.32}$$

with the values of $[\eta]$ so obtained for the star and linear chains having the same L and d_{b}.

Figure 3.6 shows plots of g_η against the logarithm of L. The unfilled circles represent the theoretical values of g_η, various directions of pips indicating different values of d_{b} indicated, and the dashed curves connect smoothly the theoretical values at constant d_{b}. The solid curves represent the values calculated from an interpolation formula, which are obtained and discussed in a later subsection. The horizontal line segment indicates the value 0.90 obtained by Irurzun[19] for the Gaussian regular three-arm star chain without excluded volume in the KR approximation. As L is decreased, g_η first decreases and then increases after passing through a minimum, in the range of d_{b} investigated. It should be noted that the behavior of g_η remarkably depends on d_{b}.

In the following subsections, we examine the behavior of g_η in the random-coil and rod limits and then propose an interpolation formula for g_η.

3.5.1 Random-Coil Limit

The value of g_η becomes a constant independent of d_{b} in the random-coil limit, i.e., the limit of L (in units of λ^{-1}) $\to \infty$. Figure 3.7 shows plots of $g_\eta(L, d_{\mathrm{b}})$ against $L^{-1/2}$ for $d_{\mathrm{b}} = 0.1$, 0.2, 0.3, and 0.4. All the symbols have the same meaning as those in Figure 3.6. The dashed curves connect smoothly the theoretical values at constant d_{b} and the solid straight lines indicate the respective initial tangents. It is seen that as $L^{-1/2}$ is decreased to 0 ($L \to \infty$), g_η approaches the above-mentioned value[19] 0.90 irrespective of the value

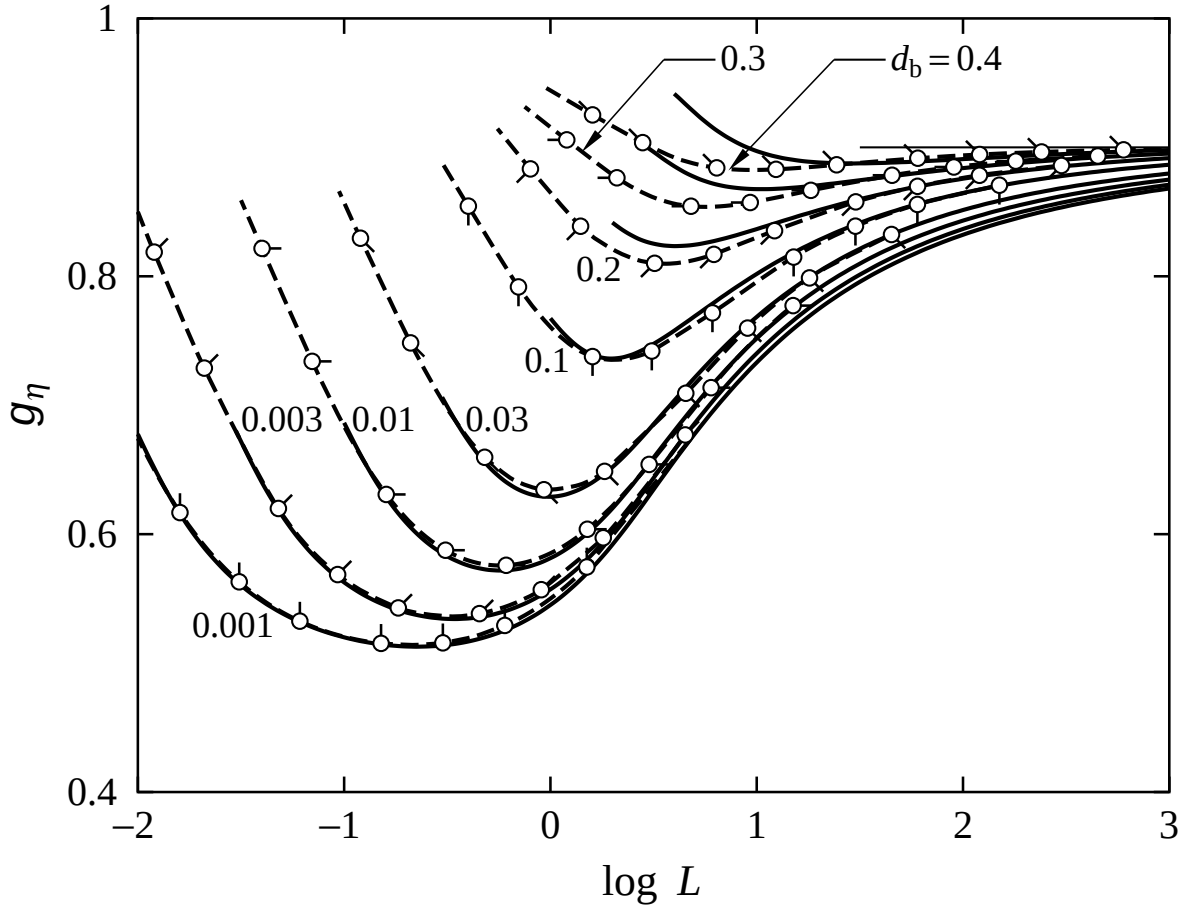

Figure 3.6. Plots of $g_\eta(L, d_\mathrm{b})$ against $\log L$. The unfilled circles represent the theoretical values, various directions of pips indicating different values of d_b indicated. The dashed curves connect smoothly the theoretical values at constant d_b. The horizontal line segment indicates the value 0.90 obtained by Irurzun[19] for the Gaussian regular three-arm star chain. The solid curves represent the values calculated from the interpolation formula (see the text).

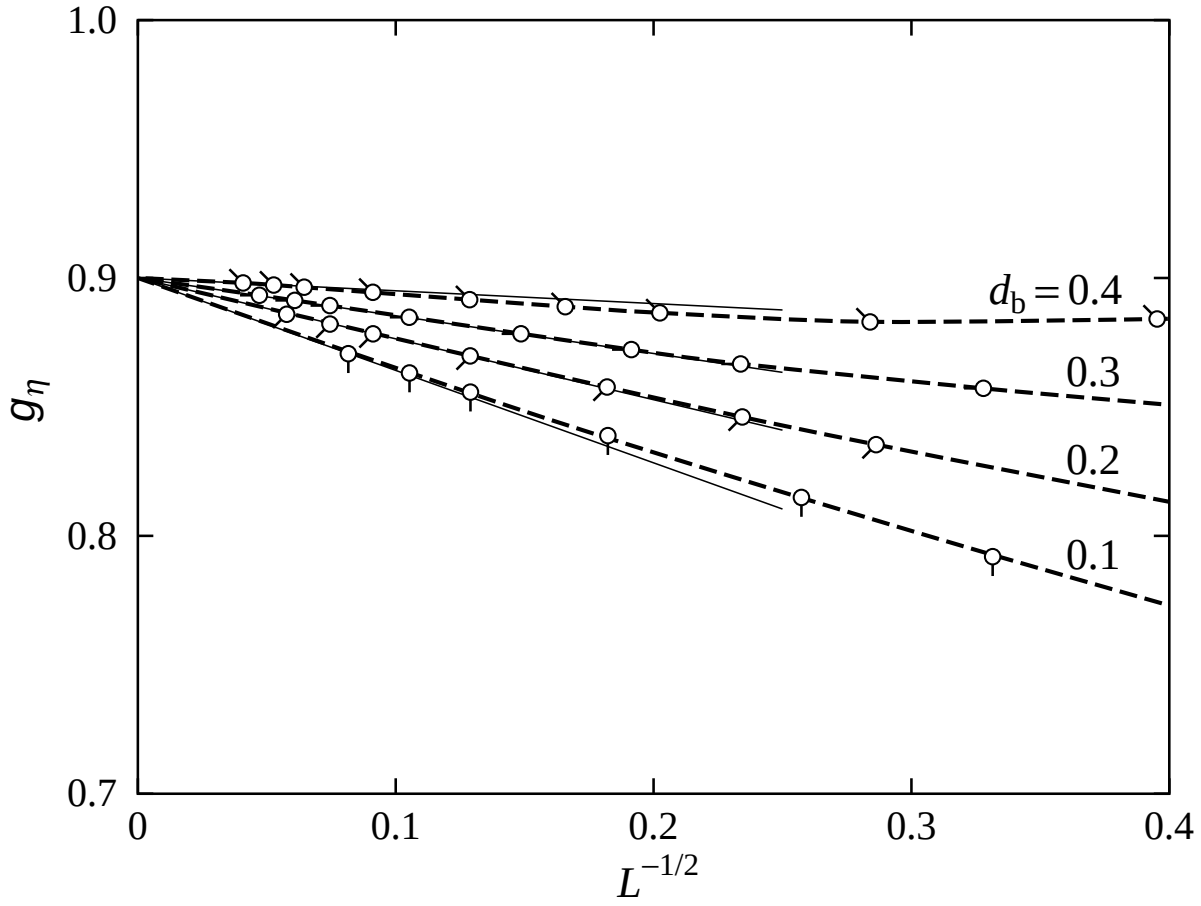

Figure 3.7. Plots of $g_\eta(L, d_\mathrm{b})$ against $L^{-1/2}$. All the symbols have the same meaning as those in Figure 3.6. The dashed curves connect smoothly the theoretical values at constant d_b and the solid straight lines indicate the respective initial tangents.

of d_b. On the basis of such numerical results, it may be concluded that

$$\lim_{L\to\infty} g_\eta(L, d_b) = 0.90_0 \qquad \text{(random coil)} \tag{3.33}$$

We note that the values of g_η for smaller d_b have been omitted in Figure 3.7, since we cannot make $L^{-1/2}$ $(= [(n+1)d_b]^{-1/2})$ small enough to evaluate g_η at $L^{-1/2} = 0$. We also note that the g_η value so obtained in the random-coil limit is somewhat smaller than the value 0.90_7 obtained by Zimm and Kilb[20] for the (dynamic) Gaussian spring–bead model[21,22] without excluded volume and with the preaveraged Oseen tensor.

The coil-limiting value in the KR approximation requires some comments. Khasat *et al.*[23] obtained the g_η value 0.87 for regular three-arm star polystyrene in cyclohexane at 34.5 °C (Θ), which is somewhat smaller than Irurzun's value 0.90. Further, the g_η values 0.75 and 0.63 obtained for regular four- and six-arm star polystyrenes, respectively, in cyclohexane at 34.5 °C (Θ)[24,25] are ca. 10% smaller than the respective theoretical values 0.82 and 0.70 obtained by Irurzun[19] for the Gaussian regular four- and six-arm star chains in the KR approximation. The KR approximation therefore seems to overestimate g_η because of the preaveraging of the Oseen tensor. It is interesting to refer the previous MC result[1] (Chapter 2) that the g_η values for the regular three-arm star freely rotating chain of bond angle 109° without the preaveraging approximation are ca. 5% smaller than the corresponding KR one.

3.5.2 Rod Limit

In the rod limit, i.e., the limit of $L \to 0$, $[\eta]$ in the limit of $L/d_b \to \infty$ (thin rod limit) may be written in the form (see Appendix 3.C),

$$\lim_{\substack{L\to 0 \\ L/d_b\to\infty}} [\eta] = \frac{\pi N_A L^3}{54M \ln(L/d_b)} \qquad \text{(thin rod limit, star)} \tag{3.34}$$

As for the linear chain, we have

$$\lim_{\substack{L\to 0 \\ L/d_b\to\infty}} [\eta] = \frac{\pi N_A L^3}{24M \ln(L/d_b)} \qquad \text{(thin rod limit, linear)} \tag{3.35}$$

which has been obtained from the result[17] for the cylinder model of diameter d along with the relation[8] $d = 0.74 d_b$.

In the rod limit, g_η should be a function only of L/d_b, i.e.,

$$\lim_{L\to 0} g_\eta(L, d_b) = g_\eta^0(L/d_b) \qquad \text{(rod limit)} \tag{3.36}$$

From eq 3.32 with eqs 3.34, 3.35, and 3.36, we have

$$\lim_{L/d_b\to\infty} g_\eta^0(L/d_b) = \frac{4}{9} \qquad \text{(thin rod limit)} \tag{3.37}$$

It is interesting to note that the ratio g_S of the mean-square radius of gyration of the KP regular three-arm star chain to that of the linear one,[18] both having the same L, also becomes 4/9 in the rod limit.

We have also evaluated $g_\eta^0(L/d_\mathrm{b})$ numerically in the same manner as in the evaluation of $g_\eta(L, d_\mathrm{b})$ mentioned above using the expressions for $\langle R_{ij}^{-1}\rangle$ given by eq 3.21 and $\langle \mathbf{S}_i \cdot \mathbf{S}_j\rangle$ given by eqs 3.9 and 3.13 in place of those for the KP chain. Figure 3.8 shows plots of g_η^0 against $[\ln(L/d_\mathrm{b})]^{-1}$. The unfilled circles represent the values so obtained and the horizontal line segment indicates the asymptotic value 4/9 in the limit of $[\ln(L/d_\mathrm{b})]^{-1} \to 0$ ($L/d_\mathrm{b} \to \infty$). As $[\ln(L/d_\mathrm{b})]^{-1}$ is decreased (L/d_b is increased), g_η^0 monotonically decreases to 4/9. For later convenience, we have constructed an interpolation formula for $g_\eta^0(L/d_\mathrm{b})$ in the range of $L/d_\mathrm{b} \gtrsim 10$, which is given by

$$g_\eta^0(x) = \frac{4}{9}\,\frac{1 - 2.551(\ln x)^{-1} + 2.946(\ln x)^{-2}}{1 - 2.913(\ln x)^{-1} + 2.965(\ln x)^{-2}} \qquad \text{for } x \gtrsim 10 \tag{3.38}$$

In Figure 3.8, the curve represents the values calculated from eq 3.38 with $x = L/d_\mathrm{b}$. The error in the value of $g_\eta^0(L/d_\mathrm{b})$ in the range of $L/d_\mathrm{b} \gtrsim 10$ (solid part) does not exceed 0.2%.

3.5.3 Interpolation Formula

A simple interpolation formula, if it is available, seems to be useful for practical purposes. Figure 3.9 shows plots of the ratio $g_\eta(L, d_\mathrm{b})/g_\eta^0(L/d_\mathrm{b})$ against the logarithm of L, where g_η/g_η^0 has been evaluated by dividing the g_η values shown in Figure 3.6 by the g_η^0 values calculated from eq 3.38 with $x = L/d_\mathrm{b}$. All the symbols have the same meaning as those in Figure 3.6. It is seen that the circles form a single composite curve almost independently of d_b for $d_\mathrm{b} \lesssim 0.2$ and the curve monotonically increases from 1 to 2.03 [$= 0.90_0/(4/9)$] with increasing L. We have therefore assumed that g_η/g_η^0 for $d_\mathrm{b} \lesssim 0.2$ may be represented by a function $f(L)$ of L irrespective of the value of d_b, and have constructed an empirical interpolation formula for $f(L)$, which may be written in the form,

$$\begin{aligned} f(L) &= 1 + 0.1466L - 0.01233L^2 && \text{for } L \le 3 \\ &= 2.03\,\frac{1 + 0.7106(\ln L)^{-1} + 3.219(\ln L)^{-2}}{1 + 0.9402(\ln L)^{-1} + 5.713(\ln L)^{-2}} && \text{for } L > 3 \end{aligned} \tag{3.39}$$

The function $f(L)$ given by eq 3.39 satisfies the asymptotic conditions $\lim_{L\to 0} f(L) = 1$ and $\lim_{L\to\infty} f(L) = 2.03$, which hold in the limit of $L/d_\mathrm{b} \to \infty$. In Figure 3.9, the solid curve represents the values calculated from eq 3.39. The factor $g_\eta(L, d_\mathrm{b})$ may then be approximately expressed as

$$g_\eta(L, d_\mathrm{b}) = g_\eta^0(L/d_\mathrm{b})\, f(L) \tag{3.40}$$

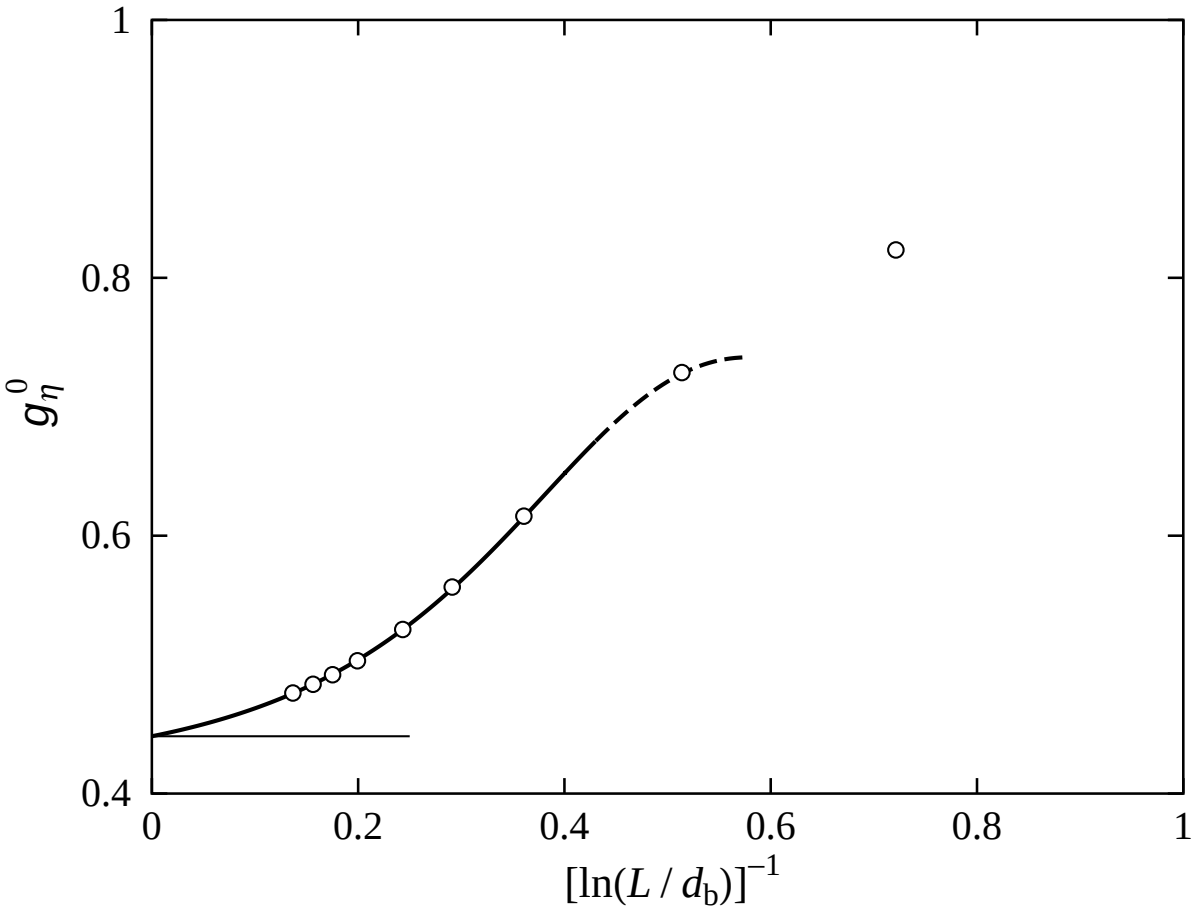

Figure 3.8. Plots of $g_\eta^0(L/d_\mathrm{b})$ against $[\ln(L/d_\mathrm{b})]^{-1}$. The unfilled circles represent the theoretical values. The horizontal line segment indicates the asymptotic value 4/9 in the limit of $[\ln(L/d_\mathrm{b})]^{-1} \to 0$ $(L/d_\mathrm{b} \to \infty)$. The curve represents the values of interpolation formula, the solid part indicating the range of $L/d_\mathrm{b} \gtrsim 10$ (see the text).

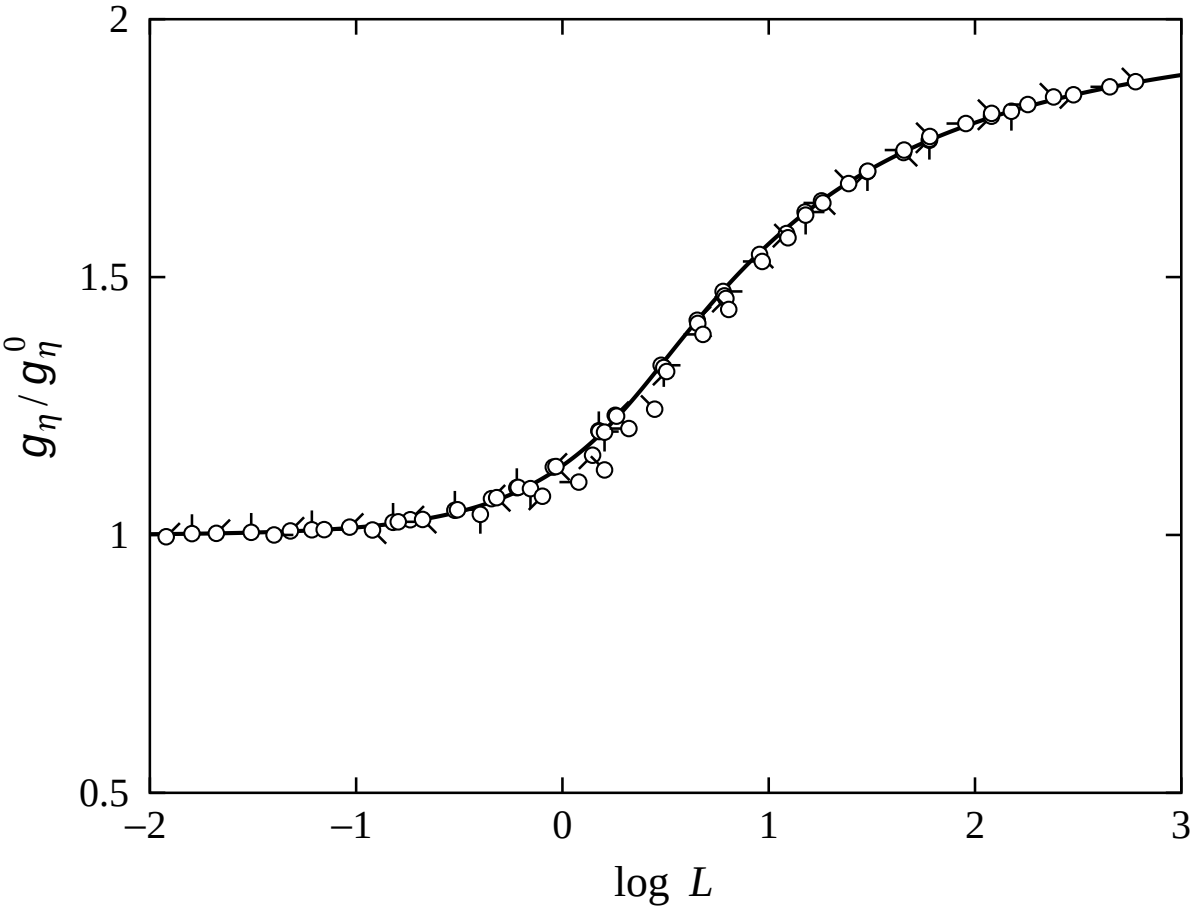

Figure 3.9. Plots of $g_\eta(L, d_\mathrm{b})/g_\eta^0(L/d_\mathrm{b})$ against $\log L$. All the symbols have the same meaning as those in Figure 3.6. The solid curve represents the values of the interpolation formula (see the text).

where $g_\eta^0(L/d_\mathrm{b})$ and $f(L)$ are given by eqs 3.38 and 3.39, respectively.

In Figure 3.6, the solid curves represent the approximate values calculated from eq 3.40 with eqs 3.38 and 3.39. It is seen that the interpolation formula for $g_\eta(L, d_\mathrm{b})$ so proposed may well reproduce the numerical theoretical values in the ranges of $d_\mathrm{b} \lesssim 0.2$ and $L/d_\mathrm{b} \gtrsim 10$. The error in the value of g_η in those ranges of d_b and L/d_b does not exceed 2%.

3.6 Conclusion

We have evaluated the ratio g_η of $[\eta]$ of the KP regular three-arm star touched-bead model to that of the KP linear one, both having the same (reduced) total contour length L and (reduced) bead diameter d_b, in the KR approximation, and then examined its behavior as a function of L and d_b. It is found that the ratio g_η/g_η^0 of g_η to the rod-limiting value g_η^0 of g_η monotonically increases from 1 to 2.03 with increasing L and is almost independent of d_b for $d_\mathrm{b} \lesssim 0.2$, although the behavior of g_η itself as a function of L remarkably depends on d_b. Thus we have constructed the empirical interpolation formula for $f(L) = g_\eta/g_\eta^0$ as a function of L. By the use of the expression for $f(L)$ along with that for g_η^0, which has also been constructed, the value of g_η may then be easily calculated for given L and d_b in the ranges of $d_\mathrm{b} \lesssim 0.2$ and $L/d_\mathrm{b} \gtrsim 10$.

Appendix 3.A Average $\langle \mathbf{S}(t^{(i)}) \cdot \mathbf{S}(t'^{(j)}) \rangle$

In this appendix, we consider the equilibrium configurational average $\langle \mathbf{S}(t^{(i)}) \cdot \mathbf{S}(t'^{(j)}) \rangle$ with $\mathbf{S}(t^{(i)})$ the vector distance from the center of mass of the KP regular f-arm star chain to the contour point on the ith arm ($i = 1, 2, \cdots, f$) with the contour distance $t^{(i)}$ from the branch point. Let L_a be the contour length of the arms and θ_{ij} the angle between the unit vectors tangent to the ith and jth arms at the branch point, so that the total contour length L of the chain becomes fL_a and $0 \le t^{(i)},\ t'^{(j)} \le L_\mathrm{a}$.

The average may be written in the form,

$$\begin{aligned}\langle \mathbf{S}(t^{(i)}) \cdot \mathbf{S}(t'^{(j)}) \rangle = \frac{1}{2L} \sum_{k=1}^{f} \int_0^{L_\mathrm{a}} \left[\langle R^2(t^{(i)}, s^{(k)}) \rangle + \langle R^2(t'^{(j)}, s^{(k)}) \rangle \right] ds^{(k)} \\ - \frac{1}{2} \langle R^2(t^{(i)}, t'^{(j)}) \rangle - \langle S^2 \rangle \end{aligned} \tag{3.A.1}$$

where $\langle R^2(t^{(i)}, t'^{(j)}) \rangle$ is the mean-square distance between the two contour points $t^{(i)}$ and $t'^{(j)}$ and is given by

$$\begin{aligned} \langle R^2(t^{(i)}, t'^{(j)}) \rangle &= \langle R^2(t^{(i)}, t'^{(j)}, \theta_{ij}) \rangle && \text{for } i \ne j \\ &= |t^{(i)} - t'^{(j)}| - \frac{1}{2}(1 - e^{-2|t^{(i)} - t'^{(j)}|}) && \text{for } i = j \end{aligned} \tag{3.A.2}$$

with $\langle R^2(t^{(i)}, t'^{(j)}, \theta_{ij})\rangle$ being given by eq 3.19. In eq 3.A.1, $\langle S^2\rangle$ is the mean-square radius of gyration of the KP regular f-arm star chain and is given by[18]

$$\begin{aligned}\langle S^2\rangle = {} & \frac{3f-2}{6f^2}L - \frac{2f-1}{4f} + \frac{1}{4L} + \left(\frac{f-1}{4L} - \frac{f}{8L^2}\right)(1-e^{-2L/f}) \\ & -\frac{1}{2f^2}\left[1 - \left(\frac{f}{L} - \frac{f^2}{2L^2}\right)(1-e^{-2L/f}) - \frac{f^2}{4L^2}(1-e^{-4L/f})\right] \\ & \times \sum_{i=1}^{f-1}\sum_{j=i+1}^{f}\cos\theta_{ij} \end{aligned} \tag{3.A.3}$$

Carrying out the integration over $s^{(k)}$, we obtain for the sum in eq 3.A.1

$$\begin{aligned}\sum_{k=1}^{f}\int_0^{L_a}\left[\langle R^2(t^{(i)}, s^{(k)})\rangle + \langle R^2(t'^{(j)}, s^{(k)})\rangle\right]ds^{(k)} = {} & fL_a{}^2 - (2f-1)L_a + \frac{1}{2}(f+1) \\ & +(t^{(i)})^2 + (t'^{(j)})^2 + (f-2)L_a(t^{(i)} + t'^{(j)}) + \frac{1}{2}(f-1)L_a(e^{-2t^{(i)}} + e^{-2t'^{(j)}}) \\ & -\frac{1}{2}(f-1)e^{-2L_a} - \frac{1}{4}(e^{-2t^{(i)}} + e^{-2t'^{(j)}}) - \frac{1}{4}e^{-2L_a}(e^{2t^{(i)}} + e^{2t'^{(j)}}) \\ & -\frac{1}{2}\left[L_a - \frac{1}{2}(1-e^{-2L_a})\right]\left[(1-e^{-2t^{(i)}})\sum_{\substack{k=1\\ \neq i}}^{f}\cos\theta_{ik} + (1-e^{-2t'^{(j)}})\sum_{\substack{k=1\\ \neq j}}^{f}\cos\theta_{jk}\right]\end{aligned} \tag{3.A.4}$$

Eq 3.A.1 with eqs 3.A.2—3.A.4 and also with eq 3.19 gives $\langle \mathbf{S}(t^{(i)})\cdot\mathbf{S}(t'^{(j)})\rangle$. For the special case of $f = 3$ and $\theta_{ij} = 120^\circ$ for all i and j, it reduces to eq 3.7 with $t^{(i)}$ and $t'^{(j)}$ in place of $t_k^{(i)}$ and $t_l^{(j)}$, respectively.

Appendix 3.B Asymptotic Forms for $\langle R^{-1}\rangle$ of the Once-Broken KP Chain

In this appendix, we derive asymptotic forms for the mean reciprocal $\langle R^{-1}(t_1, t_2, \theta)\rangle$ of the end-to-end distance R of the once-broken KP chain of total contour length $t_1 + t_2$ such that two KP subchains 1 and 2 of contour lengths t_1 and t_2, respectively, are connected with a bending angle θ (see Figure 3.2).

Considering the characteristic function $I(k; t_1, t_2, \theta)$, i.e., the Fourier transform of the distribution function $P(R; t_1, t_2, \theta)$ of R, defined by

$$I(k; t_1, t_2, \theta) = \int P(R; t_1, t_2, \theta)e^{i\mathbf{k}\cdot\mathbf{R}}d\mathbf{R} \tag{3.B.1}$$

and then integrating both sides of eq 3.B.1 over $\mathbf{k}$, we obtain the following expression for $\langle R^{-1}(t_1, t_2, \theta)\rangle$,

$$\langle R^{-1}(t_1, t_2, \theta)\rangle = \frac{2}{\pi}\int_0^\infty I(k; t_1, t_2, \theta)dk \tag{3.B.2}$$

Then the problem is to obtain asymptotic forms for $I(k; t_1, t_2, \theta)$.

The distribution function $P(R; t_1, t_2, \theta)$ may be written in the form,

$$P(R; t_1, t_2, \theta) = \frac{1}{8\pi^2} \int' \Bigg[\int G(\mathbf{R}_1|\mathbf{u}_1; t_1)\, G(\mathbf{R}_2|\mathbf{u}_2; t_2) \times \delta(\mathbf{R} - \mathbf{R}_1 + \mathbf{R}_2)\, d\mathbf{R}_1\, d\mathbf{R}_2 \Bigg] d\mathbf{u}_1\, d\mathbf{u}_2 \tag{3.B.3}$$

where $G(\mathbf{R}_p|\mathbf{u}_p; t_p)$ ($p = 1, 2$) is the conditional distribution function (or the Green's function) of the vector distance $\mathbf{R}_p$ from the broken point to the terminal end of the pth subchain of contour length t_p with the unit vector $\mathbf{u}_p$ tangent to the pth contour at the broken point (see Figure 3.2) being fixed,[7] and $\delta(\mathbf{R})$ is the three-dimensional Dirac delta function. In eq 3.B.3, $\int' \cdots d\mathbf{u}_1 d\mathbf{u}_2$ means the integrations over $\mathbf{u}_1$ and $\mathbf{u}_2$ with θ being fixed. From eq 3.B.1 with eq 3.B.3, we have for $I(k; t_1, t_2, \theta)$,

$$I(k; t_1, t_2, \theta) = \frac{1}{8\pi^2} \int' I^*(\mathbf{k}|\mathbf{u}_1; t_1) I(\mathbf{k}|\mathbf{u}_2; t_2) d\mathbf{u}_1\, d\mathbf{u}_2 \tag{3.B.4}$$

where $I(\mathbf{k}|\mathbf{u}_p; t_p)$ is the characteristic function of $G(\mathbf{R}_p|\mathbf{u}_p; t_p)$ and the asterisk indicates the complex conjugate.

The characteristic function $I(\mathbf{k}|\mathbf{u}_p; t_p)$ may be expanded in terms of the (normalized) spherical harmonics Y_l^m as follows,

$$I(\mathbf{k}|\mathbf{u}_p; t_p) = (4\pi)^{1/2} \sum_{l=0}^{\infty} \mathcal{I}_l(k; t_p) \sum_{m=-l}^{l} Y_l^{m*}(\theta_p, \phi_p) Y_l^m(\chi, \omega) \tag{3.B.5}$$

where $\mathcal{I}_l(k; t_p)$ is the expansion coefficient and $\mathbf{u}_p = (1, \theta_p, \phi_p)$ and $\mathbf{k} = (k, \chi, \omega)$ in spherical polar coordinates in an external Cartesian coordinate system. We note that the above expression for $I(\mathbf{k}|\mathbf{u}; t)$ is essentially identical with eq 5 of ref 15 and the coefficient $\mathcal{I}_l(k; t)$ in eq 3.B.5 is identical with $\mathcal{I}_{0ll}^{00,00}(k; t)$ in eq 5 of ref 15, although the direction of $\mathbf{u}_p$ was chosen to coincide with the z-axis of the external system in ref 15. In order to perform the integrations on the right-hand side of eq 3.B.4 over $\mathbf{u}_1$ and $\mathbf{u}_2$ with θ being fixed, we introduce a Cartesian coordinate system associated with $\mathbf{u}_1$ and $\mathbf{u}_2$ such that $\mathbf{u}_p$ becomes equal to $(1, \tilde{\theta}_p, 0)$ in spherical polar coordinates in it with $\tilde{\theta}_1 = 0$ and $\tilde{\theta}_2 = \theta$. Let $\Omega = (\theta', \phi', \psi')$ be the Euler angles defining the orientation of the Cartesian coordinate system with respect to the external one. Then the integration $\int' \cdots d\mathbf{u}_1 d\mathbf{u}_2$ may be replaced by $\int \cdots d\Omega$ ($d\Omega = \sin\theta' d\theta' d\phi' d\psi'$) and $Y_l^m(\theta_p, \phi_p)$ may be written in terms of Ω as

$$Y_l^m(\theta_p, \phi_p) = (-1)^{(m+|m|)/2} \left(\frac{8\pi^2}{2l+1} \right)^{1/2} \sum_{j=-l}^{l} (-1)^{(j+|j|)/2} \mathcal{D}_l^{mj}(\Omega) Y_l^j(\tilde{\theta}_p, 0) \tag{3.B.6}$$

where $\mathcal{D}_l^{mj}(\Omega)$ is the (normalized) Wigner function of Ω.[26] Substituting eq 3.B.5 with eq 3.B.6 into eq 3.B.4 and performing the integration over Ω, we obtain

$$I(k;t_1,t_2,\theta) = (4\pi)^{-1}\sum_{l=0}^{\infty}(2l+1)\mathcal{I}_l^*(k;t_1)\,\mathcal{I}_l(k;t_2)\,P_l(\cos\theta) \tag{3.B.7}$$

where we have used the relations,

$$\int \mathcal{D}_l^{mj*}(\Omega)\,\mathcal{D}_{l'}^{m'j'}(\Omega)\,d\Omega = \delta_{ll'}\delta_{mm'}\delta_{jj'} \tag{3.B.8}$$

$$\sum_{m=-l}^{l} Y_l^{m*}(\chi,\omega)\,Y_l^m(\chi,\omega) = \frac{2l+1}{4\pi} \tag{3.B.9}$$

$$Y_l^m(0,0) = \delta_{m0}\left(\frac{2l+1}{4\pi}\right)^{1/2} \tag{3.B.10}$$

$$Y_l^0(\theta,0) = \left(\frac{2l+1}{4\pi}\right)^{1/2} P_l(\cos\theta) \tag{3.B.11}$$

and $P_l(x)$ is the Legendre polynomial.

The asymptotic form for $\mathcal{I}_l(k;t_p)$ in the case of $t_p \gg 1$ may be obtained in the Daniels approximation,[7,12–14] and its general expression [for the helical wormlike (HW) chain[7]] is given by eq 44 of ref 14 with $l_1 = 0$, $l_2 = l_3 = l$, $m_1 = m_2 = 0$, and $j_1 = j_2 = 0$. On retaining terms up to $\mathcal{O}({t_p}^{-2})$ (i.e., the second Daniels approximation), the necessary $\mathcal{I}_l(k;t_p)$'s with $l = 0, 1, \cdots, 4$ can be straightforwardly evaluated to be

$$\mathcal{I}_l(k;t_p) = \frac{(4\pi)^{1/2}}{2l+1}\exp\left(-\frac{1}{6}t_p k^2\right)(ik)^l g_l(k;t_p) \tag{3.B.12}$$

with i the imaginary unit and

$$\begin{aligned}
g_0(k;t_p) &= 1 + \frac{1}{12}k^2 + \left(\frac{107}{6480} - \frac{11}{1080}t_p\right)k^4 - \frac{607}{272160}t_p k^6 + \frac{121}{2332800}{t_p}^2 k^8\\
g_1(k;t_p) &= \frac{1}{2} + \frac{13}{180}k^2 - \frac{11}{2160}t_p k^4\\
g_2(k;t_p) &= \frac{1}{18} + \frac{85}{9072}k^2 - \frac{11}{19440}t_p k^4\\
g_3(k;t_p) &= \frac{1}{360}\\
g_4(k;t_p) &= \frac{1}{12600}
\end{aligned} \tag{3.B.13}$$

The asymptotic form for $\mathcal{I}_l(k;t_p)$ in the case of $t_p \ll 1$, on the other hand, may be obtained by the ϵ method,[7,15,16] and its general expression (for the HW chain) is given

by eq 10 of ref 16. On retaining terms up to $\mathcal{O}({t_p}^2)$, the necessary $\mathcal{I}_l(k;t_p)$'s with $l = 0$, $1, \cdots, 4$ may be explicitly written in the form,

$$\mathcal{I}_l(k;t_p) = (4\pi)^{1/2} i^l \left[(1 + \langle \delta_l \rangle)\, j_l(kt_p) - \frac{1}{2} kt_p (\langle \epsilon \rangle + \langle \delta_l \epsilon \rangle)\, j_{l+1}(kt_p) + \frac{1}{8} (kt_p)^2 \langle \epsilon^2 \rangle\, j_{l+2}(kt_p) \right] \tag{3.B.14}$$

where $j_l(x)$ is the spherical Bessel function of the first kind and ϵ and δ_l are relative deviations of the square end-to-end distance ${R_p}^2$ and of the quantity ${R_p}^l Y_l^0(\theta_p, \phi_p) Y_l^0(\Theta_p, \Phi_p)$ with $\mathbf{R}_p = (R_p, \Theta_p, \Phi_p)$ in spherical polar coordinates in the external system, respectively, of the KP subchain p, from the respective rod-limiting values. We note that δ_l is identical with $\delta_{0ll}^{00,00}$ defined for the HW chain by eq 4 of ref 16. The equilibrium averages $\langle \epsilon \rangle$, $\langle \epsilon^2 \rangle$, $\langle \delta_l \rangle$, and $\langle \delta_l \epsilon \rangle$ in eq 3.B.14 are given by eqs 5, 6, and 7 of ref 16 and are explicitly given by

$$\begin{aligned}
\langle \epsilon \rangle &= -\frac{2}{3} t_p + \frac{1}{3} {t_p}^2 \\
\langle \epsilon^2 \rangle &= \frac{28}{45} {t_p}^2 \\
\langle \delta_l \rangle &= 4\pi \langle {R_p}^l Y_l^0(\theta_p, \phi_p) Y_l^0(\Theta_p, \Phi_p) \rangle {t_p}^{-l} - 1 \\
\langle \delta_l \epsilon \rangle &= 4\pi \langle {R_p}^{l+2} Y_l^0(\theta_p, \phi_p) Y_l^0(\Theta_p, \Phi_p) \rangle {t_p}^{-l-2} - (1 + \langle \epsilon \rangle + \langle \delta_l \rangle)
\end{aligned} \tag{3.B.15}$$

The moments $\langle {R_p}^l Y_l^0 Y_l^0 \rangle$ and $\langle R_p^{l+2} Y_l^0 Y_l^0 \rangle$ in eqs 3.B.15 may be evaluated analytically by the use of the operational method,[7,27] and then we have

$$\begin{aligned}
\langle {R_p}^l Y_l^0 Y_l^0 \rangle = (4\pi)^{-1} &\frac{(2l+1)!}{2^l (2l+1)^{1/2} l!} \\
&\times \int \left\{ Y_0^{0*} \left[\prod_{j=1}^{l} \int_0^{s_{j-1}} ds_j e^{\mathcal{L}_0 (s_{j-1} - s_j)} \delta \bar{\mathcal{L}} \right] e^{-l(l+1) s_l} Y_l^0 \right\} d\mathbf{u}_p'
\end{aligned} \tag{3.B.16}$$

$$\begin{aligned}
\langle {R_p}^{l+2} Y_l^0 Y_l^0 \rangle = (4\pi)^{-1} &\frac{(2l+3)!}{2^l (2l+1)^{1/2} (l+1)!} \\
&\times \int \left\{ Y_0^{0*} \left[\prod_{j=1}^{l+2} \int_0^{s_{j-1}} ds_j e^{\mathcal{L}_0 (s_{j-1} - s_j)} \delta \bar{\mathcal{L}} \right] e^{-l(l+1) s_{l+2}} Y_l^0 \right\} d\mathbf{u}_p'
\end{aligned} \tag{3.B.17}$$

where $s_0 = t_p$, $\mathbf{u}_p' = (1, \theta_p', \phi_p')$ is the unit venctor tangent to the terminal end of the pth contour in spherical polar coordinates in the external system, $\mathcal{L}_0$ is the Laplacian operator given by

$$\mathcal{L}_0 = \nabla_{\mathbf{u}_p'}^2 = \frac{1}{\sin \theta_p'} \frac{\partial}{\partial \theta_p'} \sin \theta_p' \frac{\partial}{\partial \theta_p'} + \frac{1}{\sin^2 \theta_p'} \frac{\partial^2}{\partial {\phi_p'}^2} \tag{3.B.18}$$

and $\delta \bar{\mathcal{L}}$ is given by

$$\delta \bar{\mathcal{L}} = a_1^0 + a_{-1}^0 \tag{3.B.19}$$

with a_μ^0 ($\mu = 1, 2$) the creation and annihilation operator which operate on Y_l^m as

$$a_\mu^0 Y_l^m = A_{l+(1/2)(\mu-1)}^{|m|} Y_{l+\mu}^m \tag{3.B.20}$$

In eq 3.B.20, the eigenvalue A_l^m is given by

$$A_l^m = \left[\frac{(l+m+1)(l-m+1)}{(2l+1)(2l+3)}\right]^{1/2} \tag{3.B.21}$$

Performing the integration over $\mathbf{u}'_p$ in eqs 3.B.16 and 3.B.17 using with eqs 3.B.18–3.B.21, we have the necessary expressions for $\langle {R_p}^l Y_l^0 Y_l^0\rangle$ and $\langle R_p^{l+2} Y_l^0 Y_l^0\rangle$ as follows,

$$\begin{aligned}
\langle R_p Y_1^0 Y_1^0\rangle &= \frac{1}{8\pi}(1-e^{-2t_p}) \\
\langle {R_p}^2 Y_2^0 Y_2^0\rangle &= \frac{1}{16\pi}(1-e^{-2t_p}) - \frac{1}{48\pi}(1-e^{-6t_p}) \\
\langle {R_p}^3 Y_3^0 Y_3^0\rangle &= \frac{3}{160\pi}(1-e^{-2t_p}) - \frac{1}{96\pi}(1-e^{-6t_p}) + \frac{1}{480\pi}(1-e^{-12t_p}) \\
\langle {R_p}^4 Y_4^0 Y_4^0\rangle &= \frac{1}{240\pi}(1-e^{-2t_p}) - \frac{1}{336\pi}(1-e^{-6t_p}) + \frac{1}{960\pi}(1-e^{-12t_p}) - \frac{1}{6720\pi}(1-e^{-20t_p})
\end{aligned} \tag{3.B.22}$$

$$\begin{aligned}
\langle {R_p}^3 Y_1^0 Y_1^0\rangle &= \frac{5}{24\pi}t_p - \frac{3}{16\pi}(1-e^{-2t_p}) + \frac{1}{144\pi}(1-e^{-6t_p}) + \frac{1}{8\pi}t_p e^{-2t_p} \\
\langle {R_p}^4 Y_2^0 Y_2^0\rangle &= \frac{7}{72\pi}t_p - \frac{83}{800\pi}(1-e^{-2t_p}) + \frac{5}{864\pi}(1-e^{-6t_p}) - \frac{7}{2400\pi}(1-e^{-12t_p}) \\
&\quad + \frac{7}{80\pi}t_p e^{-2t_p} - \frac{1}{144\pi}t_p e^{-6t_p} \\
\langle {R_p}^5 Y_3^0 Y_3^0\rangle &= \frac{1}{32\pi}t_p - \frac{217}{6000\pi}(1-e^{-2t_p}) + \frac{17}{7056\pi}(1-e^{-6t_p}) - \frac{7}{24000\pi}(1-e^{-12t_p}) \\
&\quad + \frac{1}{47040\pi}(1-e^{-20t_p}) + \frac{27}{800\pi}t_p e^{-2t_p} - \frac{1}{224\pi}t_p e^{-6t_p} + \frac{1}{600}t_p e^{-12t_p} \\
\langle {R_p}^6 Y_4^0 Y_4^0\rangle &= \frac{11}{1440\pi}t_p - \frac{519}{56000\pi}(1-e^{-2t_p}) + \frac{269}{395136\pi}(1-e^{-6t_p}) \\
&\quad - \frac{413}{3888000\pi}(1-e^{-12t_p}) + \frac{3}{219520\pi}(1-e^{-20t_p}) - \frac{1}{1088640\pi}(1-e^{-30t_p}) \\
&\quad + \frac{11}{1200\pi}t_p e^{-2t_p} - \frac{11}{7056\pi}t_p e^{-6t_p} + \frac{11}{43200\pi}t_p e^{-12t_p} - \frac{1}{47040\pi}t_p e^{-20t_p}
\end{aligned} \tag{3.B.23}$$

Substituting eqs 3.B.15 with eqs 3.B.22 and 3.B.23 into eq 3.B.14, we can finally

obtain

$$\begin{aligned}
\mathcal{I}_0(k;t_p) &= (4\pi)^{1/2}\left[j_0(kt_p) - \frac{1}{6}{t_p}^2(t_p-2)kj_1(kt_p) + \frac{7}{90}{t_p}^4k^2j_2(kt_p)\right] \\
\mathcal{I}_1(k;t_p) &= (4\pi)^{1/2}i\left[\left(\frac{2}{3}{t_p}^2 - t_p + 1\right)j_1(kt_p) - \frac{1}{30}{t_p}^2(19t_p-10)kj_2(kt_p)\right. \\
&\qquad \left. + \frac{7}{90}{t_p}^4k^2j_3(kt_p)\right] \\
\mathcal{I}_2(k;t_p) &= (4\pi)^{1/2}\left[-\left(\frac{13}{3}{t_p}^2 - \frac{8}{3}t_p + 1\right)j_2(kt_p) + \frac{1}{90}{t_p}^2(127t_p-30)kj_3(kt_p)\right. \\
&\qquad \left. - \frac{7}{90}{t_p}^4k^2j_4(kt_p)\right] \\
\mathcal{I}_3(k;t_p) &= (4\pi)^{1/2}i\left[-\left(\frac{73}{5}{t_p}^2 - 5t_p + 1\right)j_3(kt_p) + \frac{1}{6}{t_p}^2(15t_p-2)kj_4(kt_p)\right. \\
&\qquad \left. - \frac{7}{90}{t_p}^4k^2j_5(kt_p)\right] \\
\mathcal{I}_4(k;t_p) &= (4\pi)^{1/2}\left[\left(\frac{221}{5}{t_p}^2 - 8t_p + 1\right)j_4(kt_p) - \frac{1}{30}{t_p}^2(117t_p-10)kj_5(kt_p)\right. \\
&\qquad \left. + \frac{7}{90}{t_p}^4k^2j_6(kt_p)\right]
\end{aligned} \tag{3.B.24}$$

Substituting eqs 3.B.7 with $\mathcal{I}_l(k;t_1)$ and $\mathcal{I}_l(k;t_2)$, both given by eq 3.B.12 with eqs 3.B.13, into eq 3.B.2 and performing the integration over k, we have for the asymptotic form for $\langle R^{-1}(t_1,t_2,\theta)\rangle$ in the case of $t_1 \gg 1$ and $t_2 \gg 1$

$$\begin{aligned}
\langle R^{-1}(t_1,t_2,\theta)\rangle = \left[\frac{6}{\pi(t_1+t_2)}\right]^{1/2}\Bigg\{1 - \frac{1}{40(t_1+t_2)} - \frac{73}{4480(t_1+t_2)^2} \\
+\left[\frac{1}{4(t_1+t_2)} + \frac{49}{160(t_1+t_2)^2}\right](1+\cos\theta) - \frac{1}{40(t_1+t_2)^2}(1-\cos^2\theta)\Bigg\} \\
(t_1 \gg 1,\ t_2 \gg 1)
\end{aligned} \tag{3.B.25}$$

If we use $\mathcal{I}_l(k;t_2)$ given by eqs 3.B.24 in the above calculation, we have the asymptotic form in the case of $t_1 \gg 1$ and $t_2 \ll 1$

$$\begin{aligned}
\langle R^{-1}(t_1,t_2,\theta)\rangle = \left(\frac{6}{\pi t_1}\right)^{1/2}\Bigg[1 - \frac{1}{40t_1} - \frac{t_2}{2t_1} - \frac{73}{4480{t_1}^2} + \frac{3t_2}{80{t_1}^2} + \frac{3{t_2}^2}{8{t_1}^2} \\
+\left(\frac{1}{2t_1} - \frac{3}{80{t_1}^2}\right)(t_2 - {t_2}^2)(1+\cos\theta) - \frac{3{t_2}^2}{20{t_1}^2}(1-\cos^2\theta)\Bigg] \\
(t_1 \gg 1,\ t_2 \ll 1)
\end{aligned} \tag{3.B.26}$$

Considering the fact that $\langle R^2(t_1,t_2,\theta)\rangle$ given by eq 3.19 may be expanded in the above

two cases as follows,

$$\begin{aligned}\langle R^2(t_1,t_2,\theta)\rangle &= t_1+t_2-\frac{1}{2}-\frac{1}{2}(1+\cos\theta) && (t_1\gg 1,\ t_2\gg 1)\\ &= t_1+t_2-\frac{1}{2}-({t_2}-{t_2}^2)(1+\cos\theta) && (t_1\gg 1,\ t_2\ll 1)\end{aligned} \quad \text{(3.B.27)}$$

the expressions for $\langle R^2(t_1,t_2,\theta)\rangle$ in the two cases given by eqs 3.B.25 and 3.B.26 may be rewritten as those given by eqs 3.16 and 3.17, respectively.

As for the asymptotic form in the case of $t_1 \ll 1$ and $t_2 \ll 1$, we have applied the ϵ method directly to $\langle R^{-1}(t_1,t_2,\theta)\rangle$ and derived the expression given by eq 3.18, which is valid up to $\mathcal{O}({t_1}^2)$, $\mathcal{O}({t_2}^2)$, and $\mathcal{O}(t_1t_2)$. We note that in the derivation ϵ has been chosen to be the relative deviation of R^2 from $\langle R^2\rangle$ given by eq 3.19.

Appendix 3.C Intrinsic Viscosity of the Three-Arm Star in the Rod Limit

In this appendix, we derive the asymptotic solution in the limit of $L/d_\mathrm{b} \to \infty$ (thin or long rod limit) for $[\eta]$ of the KP regular three-arm star in the rod limit. In the thin rod limit, $[\eta]_\mathrm{E}$ may be ignored, so that we only consider $[\eta]_\mathrm{KR}$ given by eq 3.2. Further, the distance between the adjacent beads, i.e., d_b for the touched-bead model, becomes very small compared to L, so that we may convert the sums in eqs 3.2 and 3.4 to integrals. Eq 3.2 with eq 3.4 may then be rewritten in the form,

$$[\eta] = \frac{3N_\mathrm{A}L}{M}\int_0^1 \psi_0(x,x)dx \quad \text{(3.C.1)}$$

where $\psi_0(x,y)$ is the solution of the set of integral equations,

$$\begin{aligned}\int_0^1 [K_0(x,\xi)\psi_0(\xi,y)+2K_1(x,\xi)\psi_1(\xi,y)]d\xi &= g_0(x,y)\\ \int_0^1 [K_0(x,\xi)\psi_1(\xi,y)+K_1(x,\xi)\psi_0(\xi,y)+K_1(x,\xi)\psi_1(\xi,y)]d\xi &= g_1(x,y)\end{aligned} \quad \text{(3.C.2)}$$

In eq 3.C.2, $K_0(x,y)$ and $K_1(x,y)$ are the continuous versions of the mean reciprocal of the distance between the centers of two beads on the same arm and on different ones, respectively, and $g_0(x,y)$ and $g_1(x,y)$ are those of $\pi\langle \mathbf{S}_i\cdot\mathbf{S}_j\rangle$ for the centers of two beads on the same arm and on different ones, respectively. They are explicitly given by

$$\begin{aligned}K_0(x,y) &= \frac{3}{L}|x-y|^{-1} && \text{for } |x-y|\ge 3d_\mathrm{b}/L\\ &= 0 && \text{for } |x-y|< 3d_\mathrm{b}/L\end{aligned} \quad \text{(3.C.3)}$$

$$K_1(x,y) = \frac{3}{L}(x^2+y^2+xy)^{-1/2} \quad \text{(3.C.4)}$$

$$g_0(x,y) = \frac{\pi L}{9}xy \tag{3.C.5}$$

$$g_1(x,y) = -\frac{\pi L}{18}xy \tag{3.C.6}$$

Now we expand $\psi_0(x,y)$, $\psi_1(x,y)$, $g_0(x,y)$, and $g_1(x,y)$ in terms of the shifted Legendre polynomial $\tilde{P}_l(x)$ as, for example,

$$\psi_0(x,y) = \sum_{i=0}^{\infty}\sum_{j=0}^{\infty}\psi_{0,ij}\tilde{P}_i(x)\tilde{P}_j(y) \tag{3.C.7}$$

where $\tilde{P}_l(x)$ ($l = 0, 1, 2, \cdots$) is defined by

$$\tilde{P}_l(x) = (-1)^l P_l(2x-1) \tag{3.C.8}$$

We note that $\tilde{P}_l(x)$ satisfies the following orthogonality relation,

$$\int_0^1 \tilde{P}_l(x)\tilde{P}_{l'}(x)dx = \frac{\delta_{ll'}}{2l+1} \tag{3.C.9}$$

Then eq 3.C.1 may be written in terms of the expansion coefficients $\psi_{0,ij}$ as

$$[\eta] = \frac{3N_{\mathrm{A}}L}{M}\sum_{i=0}^{\infty}\frac{\psi_{0,ii}}{2i+1} \tag{3.C.10}$$

and the integral equations 3.C.2 may be converted to a set of linear simultaneous equations, which may be written in the following matrix form,

$$\mathbf{K}\cdot\boldsymbol{\psi} = \mathbf{g} \tag{3.C.11}$$

The three matrices $\mathbf{K}$, $\boldsymbol{\psi}$, and $\mathbf{g}$ in eq 3.C.11 have the same structure composed of 9 submatrices and may be explicitly written as, for example,

$$\mathbf{K} = \begin{pmatrix} \mathbf{K}_0 & \mathbf{K}_1 & \mathbf{K}_1 \\ \mathbf{K}_1 & \mathbf{K}_0 & \mathbf{K}_1 \\ \mathbf{K}_1 & \mathbf{K}_1 & \mathbf{K}_0 \end{pmatrix} \tag{3.C.12}$$

where $\mathbf{K}_0$ and $\mathbf{K}_1$ are the symmetric matrices whose ij elements are given by

$$K_{k,ij} = \int_0^1\int_0^1 K_k(x,y)\tilde{P}_i(x)\tilde{P}_j(y)dxdy \qquad (k = 0, 1) \tag{3.C.13}$$

Similarly, $\boldsymbol{\psi}$ ($\mathbf{g}$) is composed of $\boldsymbol{\psi}_0$ and $\boldsymbol{\psi}_1$ ($\mathbf{g}_0$ and $\mathbf{g}_1$) whose ij elements are the expansion coefficients $\psi_{0,ij}$ and $\psi_{1,ij}$ ($g_{0,ij}$ and $g_{1,ij}$), respectively.

It can be shown in the limit of $L/d_{\mathrm{b}} \to \infty$ that the diagonal elements $K_{0,ii}$ of $\mathbf{K}$ are proportional to $L^{-1}\ln(L/d_{\mathrm{b}})$ while the off-diagonal ones $K_{0,ij}$ ($i \neq j$) and $K_{1,ij}$ are of

$\mathcal{O}(L^{-1}[\ln(L/d_\mathrm{b})]^0)$ at most. Further the elements $g_{0,ij}$ and $g_{1,ij}$ of $\mathbf{g}_0$ and $\mathbf{g}_1$, respectively, may be calculated to be

$$g_{0,ij} = \frac{\pi L}{36}(2i+1)(2j+1)\left(\delta_{i0} - \frac{1}{3}\delta_{i1}\right)\left(\delta_{j0} - \frac{1}{3}\delta_{j1}\right) \tag{3.C.14}$$

$$g_{1,ij} = -\frac{\pi L}{72}(2i+1)(2j+1)\left(\delta_{i0} - \frac{1}{3}\delta_{i1}\right)\left(\delta_{j0} - \frac{1}{3}\delta_{j1}\right) \tag{3.C.15}$$

Then we have

$$\psi_{ii} = \frac{\pi L}{36(2i+1)}[\delta_{i0}K_{0,00}^{-1} + \delta_{i1}K_{0,11}^{-1} + \mathcal{O}(L[\ln(L/d_\mathrm{b})]^{-2})] \tag{3.C.16}$$

and $[\eta]$ may be written in the form

$$\lim_{L/d_\mathrm{b}\to\infty}[\eta] = \frac{\pi N_\mathrm{A} L^2}{12M}\left(K_{0,00}^{-1} + \frac{1}{9}K_{0,11}^{-1}\right) \tag{3.C.17}$$

The necessary elements $K_{0,00}$ and $K_{0,11}$ of $\mathbf{K}$ are calculated to be

$$\begin{aligned} K_{0,00} &= 6\ln(L/d_\mathrm{b})/L \\ K_{0,11} &= 2\ln(L/d_\mathrm{b})/L \end{aligned} \tag{3.C.18}$$

Substitution of eqs 3.C.18 into eq 3.C.17 leads to eq 3.34.

References

1. D. Ida and T. Yoshizaki, *Polym. J.*, **39**, 1373 (2007).
2. J. G. Kirkwood and J. Riseman, *J. Chem. Phys.*, **16**, 565 (1948).
3. H. Yamakawa, "Modern Theory of Polymer Solutions," Harper & Row, New York, 1971. Its electronic edition is available on-line at the URL: `http://www.molsci.polym.kyoto-u.ac.jp/archives/redbook.pdf`
4. B. H. Zimm, *Macromolecules*, **13**, 592 (1980).
5. M. Fixman, *J. Chem. Phys.*, **78**, 1588 (1983).
6. M. Fixman, *J. Chem. Phys.*, **78**, 1594 (1983).
7. H. Yamakawa, "Helical Wormlike Chains in Polymer Solutions," Springer, Berlin, 1997.
8. T. Yoshizaki, I. Nitta, and H. Yamakawa, *Macromolecules*, **21**, 165 (1988).
9. O. Kratky and G. Porod, *Recl. Trav. Chim. Pay-Bas.*, **68**, 1106 (1949).
10. J. E. Hearst and W. H. Stockmayer, *J. Chem. Phys.*, **37**, 1425 (1962).
11. H. Yamakawa and M. Fujii, *Macromolecules*, **6**, 407 (1973).
12. H. E. Daniels, *Proc. Roy. Soc., Ser. A*, **63**, 290 (1952).

13. W. Gobush, H. Yamakawa, W. H. Stockmayer, and W. S. Magee, *J. Chem. Phys.*, **57**, 2839 (1972).
14. J. Shimada and H. Yamakawa, *J. Chem. Phys.*, **67**, 344 (1977).
15. H. Yamakawa, J. Shimada, and M. Fujii, *J. Chem. Phys.*, **68**, 2140 (1978).
16. M. Fujii and H. Yamakawa, *J. Chem. Phys.*, **72**, 6005 (1980).
17. H. Yamakawa and M. Fujii, *Macromolecules*, **7**, 128 (1974).
18. M. L. Mansfield and W. H. Stockmayer, *Macromolecules*, **13**, 1713 (1980).
19. I. M. Irurzun, *J. Polym. Sci., Part B: Polym. Phys.*, **35**, 563 (1997).
20. B. H. Zimm and R. W. Kilb, *J. Polym. Sci.*, **37**, 19 (1959).
21. P. E. Rouse, Jr., *J. Chem. Phys.*, **21**, 1272 (1953).
22. B. H. Zimm, *J. Chem. Phys.*, **24**, 269 (1956).
23. N. Khasat, R. W. Pennisi, N. Hadjichristidis, and L. J. Fetters, *Macromolecules*, **21**, 1100 (1988).
24. M. Okumoto, K. Terao, Y. Nakamura, T. Norisuye, and A. Teramoto, *Macromolecules*, **30**, 7493 (1997).
25. M. Okumoto, Y. Tasaka, Y. Nakamura, and T. Norisuye, *Macromolecules*, **32**, 7430 (1999).
26. A. R. Edmonds, "Angular Momentum in Quantum Mechanics," Princeton Univ., Princeton, 1974.
27. H. Yamakawa, *J. Chem. Phys.*, **59**, 3811 (1973).

4 Second Virial Coefficient of Semiflexible Three-Arm Stars

4.1 Introduction

In Chapters 2 and 3, we have examined effects of chain stiffness on the intrinsic viscosity $[\eta]$ of unperturbed regular three-arm star polymer chains by Monte Carlo (MC) simulations[1] or on the basis of the Kirkwood–Riseman theory.[2–4] The ratio g_η of $[\eta]$ of an unperturbed regular three-arm star chain to that of an unperturbed linear one, both having the same molecular weight and chain stiffness, has been shown to become remarkably smaller than the value *ca.* 0.9 in the random-coil limit[5,6] as the chains become stiffer, as in the case of the ratio g_S of the mean-square radius of gyration $\langle S^2 \rangle$ of the former chain to that of the latter.[7] We note that g_S becomes 7/9 in the random-coil limit.[8] Since $[\eta]$ and $\langle S^2 \rangle$ are measures of the average chain dimension, the above-mentioned results for g_η and g_S indicate that the average dimension of the unperturbed regular three-arm star chain becomes much smaller than that of the corresponding linear one as the chains become stiffer.

As already mentioned in Chapter 1, short-ranged repulsive interactions work between segments constituting the polymer chains in good solvents (perturbed state), expanding the individual chains and yielding an effective volume V_E excluded to one chain by the presence of another. The volume V_E is another measure of the average chain dimension, although well-defined only in a good solvent system or in the perturbed state. The quantity V_E may be defined from the second virial coefficient A_2 as follows,[4]

$$A_2 = 4N_\mathrm{A}V_\mathrm{E}/M^2 \tag{4.1}$$

where N_A is the Avogadro constant and M is the molecular weight. It is then interesting to examine the effects of chain stiffness on the ratio g_{A_2} of A_2 of a regular three-arm star chain to that of the corresponding linear one. In this chapter, we make an MC study of g_{A_2} as a necessary continuation of the previous studies[1,2] (Chapters 2 and 3).

An available theoretical value of g_{A_2} for the regular three-arm star chain is 0.968 in the random-coil limit obtained by Douglas and Freed[9] on the basis of the polymer renormalization group (RG) theory, being nearly equal to unity. Then the main question

we must answer in this chapter is whether or not g_{A_2} becomes remarkably smaller than unity as the chains become stiffer, as in the cases of g_η and g_S.

4.2 Models and Methods

The MC models used in this study are the same as those used in the previous one[1] (Chapter 2) except for the value of a parameter of interactions between segments (beads).

The star chain model is the regular three-arm star freely rotating chain, each arm composed of m successive bonds of length unity, so that it is composed of $3m$ $(= n)$ bonds, in total, and $3m + 1$ beads whose centers are located at $3m - 3$ junctions of two successive bonds on the arms, at the three terminal ends, and at the branch point (center) (see Figure 2.1 in Chapter 2). The angle between each pair of the bonds connected to the center is fixed to be 120°, so that those bonds are on the same plane. For convenience, the three arms are designated the first, second, and third ones and the beads on the ith arm ($i = 1, 2, 3$) are numbered $(i-1)m+1$, $(i-1)m+2$, $\cdots$, im from the center to the end, with the center bead numbered 0. The ith bond vector ($1 \le i \le 3m$; $i \ne m+1$, $2m+1$) connects the centers of the $(i-1)$th and ith beads with its direction from the $(i-1)$th to ith bead, and the $(m+1)$th and $(2m+1)$th bond vectors are from the 0th to the $(m+1)$th and $(2m+1)$th beads, respectively. All the $3m-3$ bond angles θ (not supplement) except for those around the center are fixed, so that the configuration of the entire chain may be specified by the set of $3m-3$ rotation angles $\{\phi_{3m-3}\} = (\phi_1, \cdots, \phi_{m-1}, \phi_{m+1}, \cdots, \phi_{2m-1}, \phi_{2m+1}, \cdots, \phi_{3m-1})$ apart from its position and orientation in an external Cartesian coordinate system, where ϕ_i is the internal rotation angle around the ith bond vector.

The linear chain model, the counterpart of the above star one, is the freely rotating chain composed of n bonds of length unity and $n+1$ beads, whose centers are located at the $n-1$ junctions of two successive bonds and at the two terminal ends. We set n equal to $3m$. The beads are numbered $0, 1, 2, \cdots, n$ from one end to the other, and the ith bond vector ($i = 1, 2, \cdots, n$) connects the centers of the $(i-1)$th and ith beads with its direction from the $(i-1)$th to the ith bead. All the $n-1$ bond angles are fixed at θ, so that the configuration of the linear chain may be specified by the set of $n-2$ internal rotation angles $\{\phi_{n-2}\} = (\phi_2, \phi_3, \cdots, \phi_{n-1})$ apart from its position and orientation in the external Cartesian coordinate system.

The total potential energy U of the regular three-arm star chain as a function of

$\{\phi_{3m-3}\}$ may be given by

$$U(\{\phi_{3m-3}\}) = \sum_{i=0}^{1}\sum_{j=i+1}^{2}\sum_{k,l=1}^{m} h(k+l-4)\,u(R_{(im+k)(jm+l)}) + \sum_{i=0}^{2}\sum_{j=1}^{m-4}\sum_{k=j+4}^{m} u(R_{(im+j)(im+k)}) + \sum_{i=0}^{2}\sum_{j=4}^{m} u(R_{0(im+j)}) \qquad \text{(regular three-arm star)} \tag{4.2}$$

and that of the linear one as a function of $\{\phi_{n-2}\}$ by

$$U(\{\phi_{n-2}\}) = \sum_{i=0}^{n-4}\sum_{j=i+4}^{n} u(R_{ij}) \qquad \text{(linear)} \tag{4.3}$$

where $h(x)$ is a unit step function such that $h(x) = 1$ for $x \geq 0$ and $h(x) = 0$ for $x < 0$ and R_{ij} is the distance between the centers of the ith and jth beads. We note that in eqs 4.2 and 4.3 the interactions between the third-neighbor beads along the chain have been neglected, since they seem to make the chain locally take the *cis* conformation to excess.

Similarly, the total intermolecular (excluded-volume) potential energy $U_{12}(1,2)$ between two chains 1 and 2 as a function of all the coordinates of chains 1 and 2 may be given by

$$U_{12}(1,2) = \sum_{i_1=0}^{n}\sum_{i_2=0}^{n} u(R_{i_1 i_2}) \tag{4.4}$$

where $R_{i_1 i_2}$ is the distance between the centers of the i_1th bead of chain 1 and of the i_2th one of chain 2. We note that we use the McMillan–Mayer symbolism[4,10] to formulate A_2, here and hereafter. Then the ith bead ($i = 0, 1, 2, \cdots, n$) of chain α ($\alpha = 1, 2$) is labeled as i_α, and the symbol (α) ($\alpha = 1, 2$) denotes all the coordinates (external and internal) of chain α.

We adopt as the pair potential $u(R)$ (of mean force) the cutoff version of the Lennard–Jones (LJ) 6-12 potential given by

$$\begin{aligned} u(R) &= \infty && \text{for } 0 \leq R < c\sigma \\ &= u^{\mathrm{LJ}}(R) && \text{for } c\sigma \leq R < 3\sigma \\ &= 0 && \text{for } 3\sigma \leq R \end{aligned} \tag{4.5}$$

where $u^{\mathrm{LJ}}(R)$ is the LJ potential[11] given by

$$u^{\mathrm{LJ}}(R) = 4\epsilon\left[\left(\frac{\sigma}{R}\right)^{12} - \left(\frac{\sigma}{R}\right)^{6}\right] \tag{4.6}$$

with σ and ϵ the collision diameter and the depth of the potential well at the minimum of $u^{\mathrm{LJ}}(R)$, respectively. We note that $u(R)$ given by eqs 4.5 is the LJ potential cut off at the upper bound 3σ. The lower bound $c\sigma$ in eqs 4.5 has been introduced for numerical convenience; the factor c is properly chosen so that the Boltzmann factor $e^{-u^{\mathrm{LJ}}/k_{\mathrm{B}}T}$ may be regarded as numerically vanishing compared to unity, where k_{B} is the Boltzmann constant and T is the absolute temperature. In practice, in double-precision computation, we put

$$c = \left[2/\left(1+\sqrt{1+36T^*}\right)\right]^{1/6} \tag{4.7}$$

so that $e^{-u^{\mathrm{LJ}}/k_{\mathrm{B}}T} \lesssim 2\times 10^{-16}$ for $0 \le R < c\sigma$, where T^* is the reduced temperature defined by $T^* = k_{\mathrm{B}}T/\epsilon$. Further, we put $\sigma = 1$ for simplicity, as previously[1] (Chapter 2) done. We note that the value 3.72 of T^* corresponds to the Θ temperature and 8.0 to a good solvent system.[12,13]

The mean-square radius of gyration $\langle S^2\rangle$, i.e., the ensemble average of the square radius of gyration S^2 may be evaluated from

$$\langle S^2\rangle = N_{\mathrm{s}}^{-1}\sum_{\{\phi_k\}} S^2(\{\phi_k\}) \tag{4.8}$$

where the sum is taken over N_{s} sample configurations $\{\phi_k\}$ with k being equal to $3m-3$ for the star chain and $n-2$ for the linear one, $\{\phi_k\}$ generated in an MC run by an application of the pivot algorithm[14,15] and the Metropolis method of importance sampling[16] as done in the previous MC studies.[1,12] For each sample configuration, S^2 as a function of $\{\phi_k\}$ may be calculated from

$$S^2 = \frac{1}{n+1}\sum_{i=0}^{n} |\mathbf{r}_i - \mathbf{r}_{\mathrm{c.m.}}|^2 \tag{4.9}$$

with $\mathbf{r}_i$ the vector position of the center of the ith bead and $\mathbf{r}_{\mathrm{c.m.}}$ the vector position of the center of mass of the chain given by

$$\mathbf{r}_{\mathrm{c.m.}} = \frac{1}{n+1}\sum_{i=0}^{n}\mathbf{r}_i \tag{4.10}$$

In every MC run, an initial configuration is generated by trial and error so that all the distances between the centers of beads are greater than or equal to c. (Note that $\sigma = 1$.) One configuration is sampled at every M_{nom} (nominal) pivot steps, so that $N_{\mathrm{s}}\times M_{\mathrm{nom}}$ pivot steps are required to obtain a set of N_{s} sample configurations. The number of M_{nom} has been chosen to be ca. $10n$ for the regular three-arm star chains and ca. $2n$ for the linear ones.

As for the second virial coefficient A_2, it may be evaluated from

$$A_2 = \frac{2\pi N_{\mathrm{A}}}{M^2}\int_0^\infty \left\{1-\exp\left[-\frac{\overline{U}_{12}(r)}{k_{\mathrm{B}}T}\right]\right\} r^2 dr \tag{4.11}$$

where $\overline{U}_{12}(r)$ is the averaged intermolecular potential as a function of the distance $r = |\mathbf{r}|$ between the centers of mass of chains 1 and 2 defined by

$$\overline{U}_{12}(r) = -k_{\mathrm{B}}T \ln\left\langle \exp\left[-\frac{U_{12}(1,2)}{k_{\mathrm{B}}T}\right]\right\rangle_r \tag{4.12}$$

In eq 4.12, $\langle\cdots\rangle_r$ indicates the conditional equilibrium average taken over the configurations of the two chains with $\mathbf{r}$ fixed by the use of the single-chain distribution function for each with the intramolecular excluded-volume potential for the star and linear chains given by eqs 4.2 and 4.3, respectively. In practice, the conditional average may be calculated by the use of a set of N_{s} sample configurations $\{\phi_k\}$ generated above, as follows. First, we randomly sample a pair of sample configurations (chains 1 and 2) from the set and calculate the intermolecular potential U_{12} from eq 4.4 at given r after randomizing the orientations of the two configurations in the external coordinate system. Numerical evaluation of U_{12} may be carried out following the procedure used in the previous study[13] of A_2 with the use of the "zippering" method.[17,18] Then the average on the right-hand side of eq 4.12 may be evaluated from

$$\left\langle \exp\left[-\frac{U_{12}(1,2)}{k_{\mathrm{B}}T}\right]\right\rangle_r = {N_{\mathrm{p}}}^{-1} {\sum_{(1,2)}}' \exp\left[-\frac{U_{12}(1,2)}{k_{\mathrm{B}}T}\right] \tag{4.13}$$

where ${\sum}'_{(1,2)}$ indicates summation over N_{p} pairs of sample configurations (1,2) at given r. With the values of $\overline{U}_{12}(r)$ so evaluated for various values of r at given T^*, the quantity A_2M^2 for given n may then be calculated from eq 4.11 by numerical integration with the use of the trapezoidal rule formula.

In the practical evaluation of $\langle S^2\rangle$ and A_2 for the regular three-arm star and linear freely rotating chains at $T^* = 8.0$ (good solvent system), we have generated 10 sets of 10^5 $(= N_{\mathrm{s}})$ sample configurations for $n = 30$, 60, 90, 150, and 300, 5 sets of those for $n = 600$, and 2 sets of those for $n = 900$. In the evaluation of $\overline{U}_{12}$ (and A_2), 10^6 or 10^7 $(= N_{\mathrm{p}})$ sample pairs have been taken from each set. Then the total number of sample pairs is equal to the number N_{p} of sample pairs in each set multiplied by the number of sets.

All the numerical work has been done by the use of a personal computer with an Intel Core2 Duo E6600 CPU. A source program coded in C has been compiled by the GNU C compiler version 3.4.6 with real variables of double precision. For a generation of pseudorandom numbers, the subroutine package MT19937 supplied by Matsumoto and Nishimura[19] has been used instead of the subroutine RAND included in the standard C library.

4.3 Results and Discussion

4.3.1 Mean-Square Radius of Gyration

We have carried out MC runs to generate sample configurations for the regular three-arm star and linear freely rotating chains with n $(= 3m) = 30$, 60, 90, 150, 300, 600, and 900 and $\theta = 109°$, 120°, 135°, 165°, and 175° at $T^* = 8.0$ (good solvent system). The chain of $\theta = 109°$ corresponds to a typical flexible chain, and the chain becomes stiffer with increasing θ from 109° to 175°.

The MC values of $\langle S^2 \rangle / n$ for the star and linear chains are given in the second and fourth columns, respectively, of Table 4.1, the number in the parentheses attached to each value indicating its statistical error. The $\langle S^2 \rangle / n$ value and its error for each chain are the mean and the standard deviation, respectively, of independent MC results.

Figure 4.1 shows double-logarithmic plots of $\langle S^2 \rangle / n$ against n at $T^* = 8.0$ (good solvent system). The open and closed symbols represent the MC values for the star and linear chains, respectively, of $\theta = 109°$ ($\bigcirc$, $\bullet$), 120° ($\square$, $\blacksquare$), 135° ($\diamond$, $\blacklozenge$), 165° ($\triangle$, $\blacktriangle$), and 175° ($\triangledown$, $\blacktriangledown$). The solid and dashed curves represent the theoretical values of $\langle S^2 \rangle / n$ for the ideal regular three-arm star and linear freely rotating chains, respectively, without interactions between beads, which have been calculated from

$$\begin{aligned}
\langle S^2 \rangle = {} & \frac{7}{54}\frac{1-\cos\theta}{1+\cos\theta}n + \frac{1}{54}\frac{31+90\cos\theta-13\cos^2\theta}{(1+\cos\theta)^2} \\
& + \frac{1}{18}\frac{19+49\cos\theta+71\cos^2\theta+5\cos^3\theta}{(1+\cos\theta)^3}\frac{1}{n+1} \\
& - \frac{2(1+2\cos\theta)}{(1+\cos\theta)^3}\frac{1-(-\cos\theta)^{n/3+1}}{n+1} \\
& + \frac{1}{27}\frac{(1-\cos\theta)(37-16\cos\theta+\cos^2\theta)}{(1+\cos\theta)^3}\frac{1}{(n+1)^2} \\
& - \frac{2(2+\cos^2\theta)}{(1+\cos\theta)^4}\frac{1-(-\cos\theta)^{n/3+1}}{(n+1)^2} \\
& + \frac{3}{(1+\cos\theta)^4}\frac{\left[1-(-\cos\theta)^{n/3+1}\right]^2}{(n+1)^2} \\
& \qquad \text{(regular three-arm star)}
\end{aligned} \tag{4.14}$$

and

$$\begin{aligned}
\langle S^2 \rangle = {} & \frac{1}{6}\frac{1-\cos\theta}{1+\cos\theta}n + \frac{1}{6}\frac{1+6\cos\theta-\cos^2\theta}{(1+\cos\theta)^2} \\
& + \frac{1}{6}\frac{-1-7\cos\theta+7\cos^2\theta+\cos^3\theta}{(1+\cos\theta)^3}\frac{1}{n+1} \\
& - \frac{2\cos^2\theta}{(1+\cos\theta)^4}\frac{1-(-\cos\theta)^{n+1}}{(n+1)^2} \qquad \text{(linear)}
\end{aligned} \tag{4.15}$$

Table 4.1. MC results at $T^* = 8.0$ (good solvent system)

	three-arm star		linear	
	$\langle S^2\rangle/n$	$A_2{M_\mathrm{b}}^2/N_\mathrm{A}$	$\langle S^2\rangle/n$	$A_2{M_\mathrm{b}}^2/N_\mathrm{A}$
n	(error %)	(error %)	(error %)	(error %)
		$\theta = 109°$		
30	0.302_0 (0.1)	0.251_5 (0.1)	0.389_3 (0.1)	0.261_5 (0.2)
60	0.340_7 (0.1)	0.203_4 (0.1)	0.443_3 (0.1)	0.213_4 (0.2)
90	0.366_1 (0.1)	0.181_8 (0.1)	0.477_3 (0.1)	0.191_5 (0.1)
150	0.400_4 (0.1)	0.159_0 (0.1)	0.523_4 (0.1)	0.168_4 (0.1)
300	0.451_5 (0.1)	0.133_6 (0.1)	0.591_5 (0.1)	0.142_1 (0.1)
600	0.508_8 (0.1)	0.113_1 (0.1)	0.667_7 (0.1)	0.120_3 (0.2)
900	0.545_8 (0.1)	0.102_5 (0.0)	0.716_9 (0.1)	0.109_5 (0.1)
		$\theta = 120°$		
30	0.379_4 (0.1)	0.285_9 (0.1)	0.500_9 (0.1)	0.301_1 (0.2)
60	0.431_1 (0.1)	0.241_4 (0.1)	0.565_9 (0.1)	0.252_9 (0.2)
90	0.462_2 (0.1)	0.218_9 (0.1)	0.604_8 (0.1)	0.229_8 (0.1)
150	0.502_6 (0.1)	0.194_2 (0.1)	0.656_0 (0.1)	0.205_0 (0.1)
300	0.561_3 (0.1)	0.165_9 (0.2)	0.732_6 (0.1)	0.175_7 (0.1)
600	0.626_0 (0.1)	0.141_8 (0.1)	0.817_3 (0.1)	0.150_5 (0.2)
900	0.667_5 (0.0)	0.129_3 (0.1)	0.872_3 (0.0)	0.137_5 (0.0)
		$\theta = 135°$		
30	0.553_7 (0.1)	0.327_4 (0.2)	0.790_1 (0.1)	0.336_2 (0.2)
60	0.663_5 (0.1)	0.287_3 (0.3)	0.907_9 (0.2)	0.297_3 (0.1)
90	0.720_1 (0.1)	0.268_4 (0.1)	0.966_6 (0.2)	0.278_8 (0.2)
150	0.782_9 (0.1)	0.246_3 (0.2)	1.03_6 (0.1)	0.256_9 (0.2)
300	0.862_6 (0.1)	0.219_0 (0.1)	1.12_7 (0.1)	0.229_4 (0.1)
600	0.941_4 (0.1)	0.193_5 (0.1)	1.22_4 (0.1)	0.203_1 (0.1)
900	0.990_4 (0.0)	0.179_7 (0.0)	1.28_5 (0.1)	0.188_7 (0.0)
		$\theta = 165°$		
30	1.10_9 (0.0)	0.355_6 (0.4)	2.18_5 (0.0)	0.352_4 (0.4)
60	1.88_6 (0.0)	0.330_7 (0.3)	3.57_1 (0.0)	0.331_4 (0.4)
90	2.51_6 (0.0)	0.323_3 (0.4)	4.56_1 (0.1)	0.323_6 (0.6)
150	3.46_1 (0.0)	0.316_1 (0.3)	5.85_1 (0.1)	0.317_7 (0.2)
300	4.82_3 (0.1)	0.310_0 (0.3)	7.37_8 (0.1)	0.311_6 (0.3)
600	5.95_1 (0.1)	0.304_4 (0.1)	8.42_8 (0.1)	0.307_5 (0.1)
900	6.44_4 (0.1)	0.303_0 (0.1)	8.82_9 (0.0)	0.305_2 (0.3)

(continued)

			$\theta = 175^\circ$				
30	1.22_6	(0.0)	0.354_3	(0.3)	2.60_5	(0.0)	0.343_8 (0.6)
60	2.29_2	(0.0)	0.327_9	(0.4)	4.93_6	(0.0)	0.320_1 (0.8)
90	3.33_0	(0.0)	0.319_1	(0.5)	7.16_4	(0.0)	0.311_8 (0.5)
150	5.32_8	(0.0)	0.310_9	(0.3)	11.3_4	(0.0)	0.307_3 (0.8)
300	9.90_0	(0.0)	0.304_1	(0.5)	20.3_4	(0.0)	0.302_9 (0.5)
600	17.5_3	(0.1)	0.301_8	(0.3)	33.7_4	(0.1)	0.299_9 (0.9)
900	23.5_9	(0.1)	0.299_7	(0.5)	43.0_3	(0.1)	0.297_0 (0.6)

respectively, with the indicated values of θ. We note that eq 4.14 is a special case of the theoretical expression obtained by Guenza *et al.*[20] for the regular f-arm star freely rotating chain.

In the cases of $\theta = 109°$, 120° and 135°, the MC values for both the star and linear chains deviate upward from the corresponding ideal-chain ones because of the intramolecular excluded-volume effect and also of the effect of the interactions between beads on the unperturbed chain dimension through the short-range interference.[12,21,22] In the cases of $\theta = 165°$ and 175°, on the other hand, the MC values for both the star and linear chains are almost identical with the corresponding ideal-chain values, because the effects of the intramolecular interactions between beads become negligibly small for a typical stiff chain if its total contour length is not very long. We note that the ring-closure or intramolecular-contact probability approaches zero in the rigid-rod limit and therefore the intramolecular excluded-volume effect vanishes in the limit.

Figure 4.2 shows plots of g_S against $\log n$ at $T^* = 8.0$ (good solvent system), where g_S is the ratio of $\langle S^2 \rangle$ of the regular three-arm star chain to that of the corresponding linear one. The symbols represent the MC values of g_S calculated from the values of $\langle S^2 \rangle / n$ given in the second and fourth columns in Table 4.1 for $\theta = 109°$ ($\bigcirc$), 120° ($\square$), 135° ($\diamondsuit$), 165° ($\triangle$), and 175° ($\triangledown$). The solid curves represent the theoretical values for the ideal chains calculated from eqs 4.14 and 4.15. The upper and lower dotted horizontal lines represent the asymptotic values 7/9 in the ideal (unperturbed) random-coil limit[8] and 4/9 in the rigid-rod limit,[7] respectively.

In the case of $\theta = 109°$ (typical flexible chain), the MC value 0.76 of g_S for $n = 900$ is somewhat (*ca.* 2%) smaller than the value 7/9 (= 0.778) in the ideal random-coil limit. The available experimental values of g_S for regular f-arm star polystyrenes (PS) in good solvents obtained by Khasat *et al.*[23] for $f = 3$ and by Okumoto *et al.*[24,25] for $f = 4$ and 6 are 0.79, 0.61, and 0.45, respectively, and are in good agreement with the respective ideal random-coil limiting values 7/9 (= 0.778), 5/8 (= 0.625), and 4/9 (= 0.444), which have been calculated from $g_S = (3f - 2)/f^2$.[8] The available theoretical values of g_S obtained by Douglas and Freed[9] on the bases of the polymer RG theory for the regular three-, four-, and six-arm stars in the perturbed random-coil limit are 0.778, 0.631, and 0.453, respectively, and are consistent with the experimental ones. Then the present MC result for long flexible chains is consistent with the above-mentioned experimental and theoretical results.

As a natural consequence of the results shown in Figure 4.1, the MC value of g_S becomes almost identical with the ideal chain value as the chain becomes stiffer. The ratio g_S, on the whole, remarkably depends on the chain stiffness but scarcely on the intramolecular excluded volume.

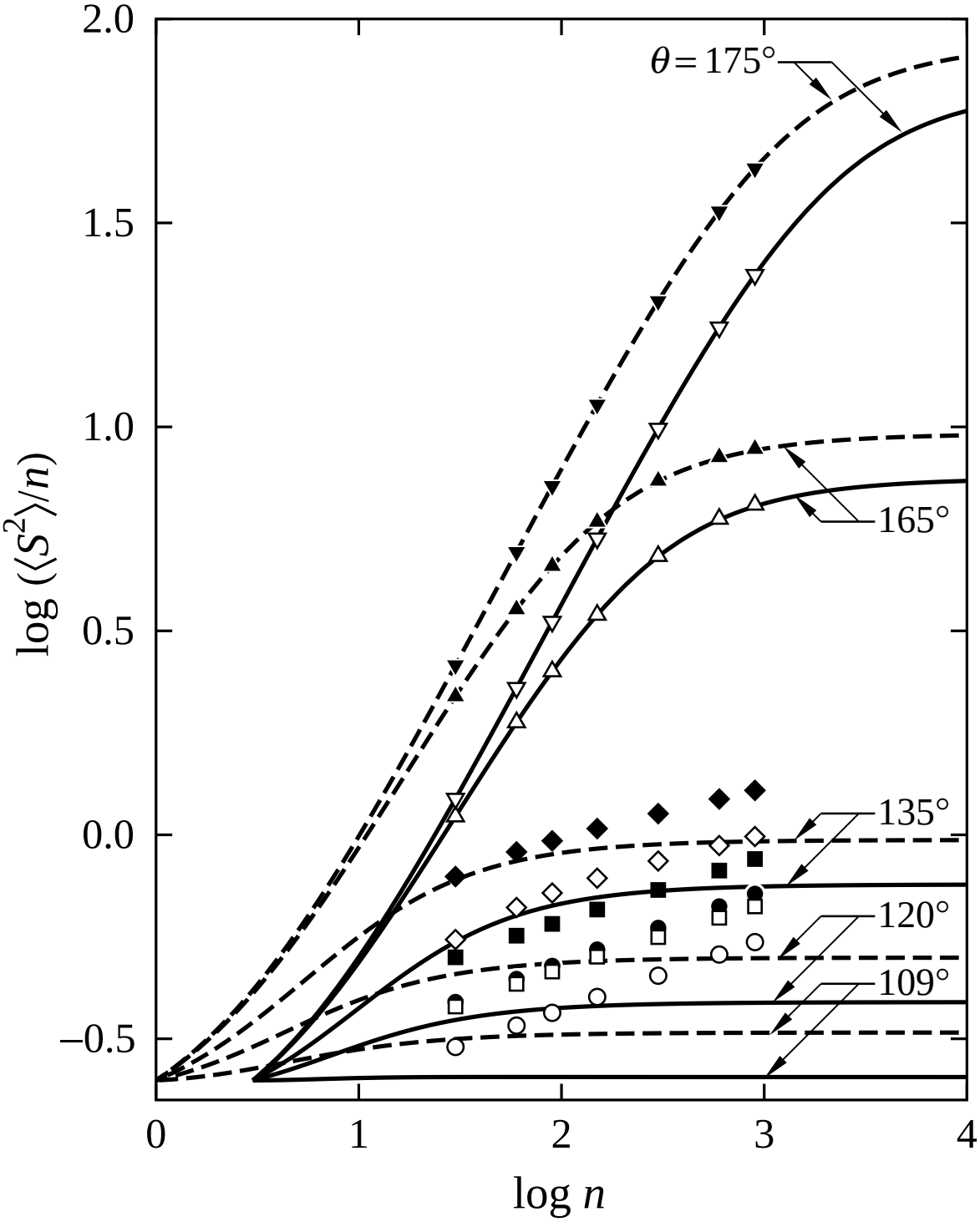

Figure 4.1. Double-logarithmic plots of $\langle S^2 \rangle / n$ against n at $T^* = 8.0$ (good solvent system). The open and closed symbols represent the MC values for the regular three-arm star and linear freely rotating chains, respectively, of $\theta = 109°$ ($\circ$, $\bullet$), $120°$ ($\square$, $\blacksquare$), $135°$ ($\diamond$, $\blacklozenge$), $165°$ ($\triangle$, $\blacktriangle$), and $175°$ ($\triangledown$, $\blacktriangledown$). The solid and dashed curves represent the theoretical values for the ideal regular three-arm star and linear freely rotating chains, respectively, with the indicated values of θ.

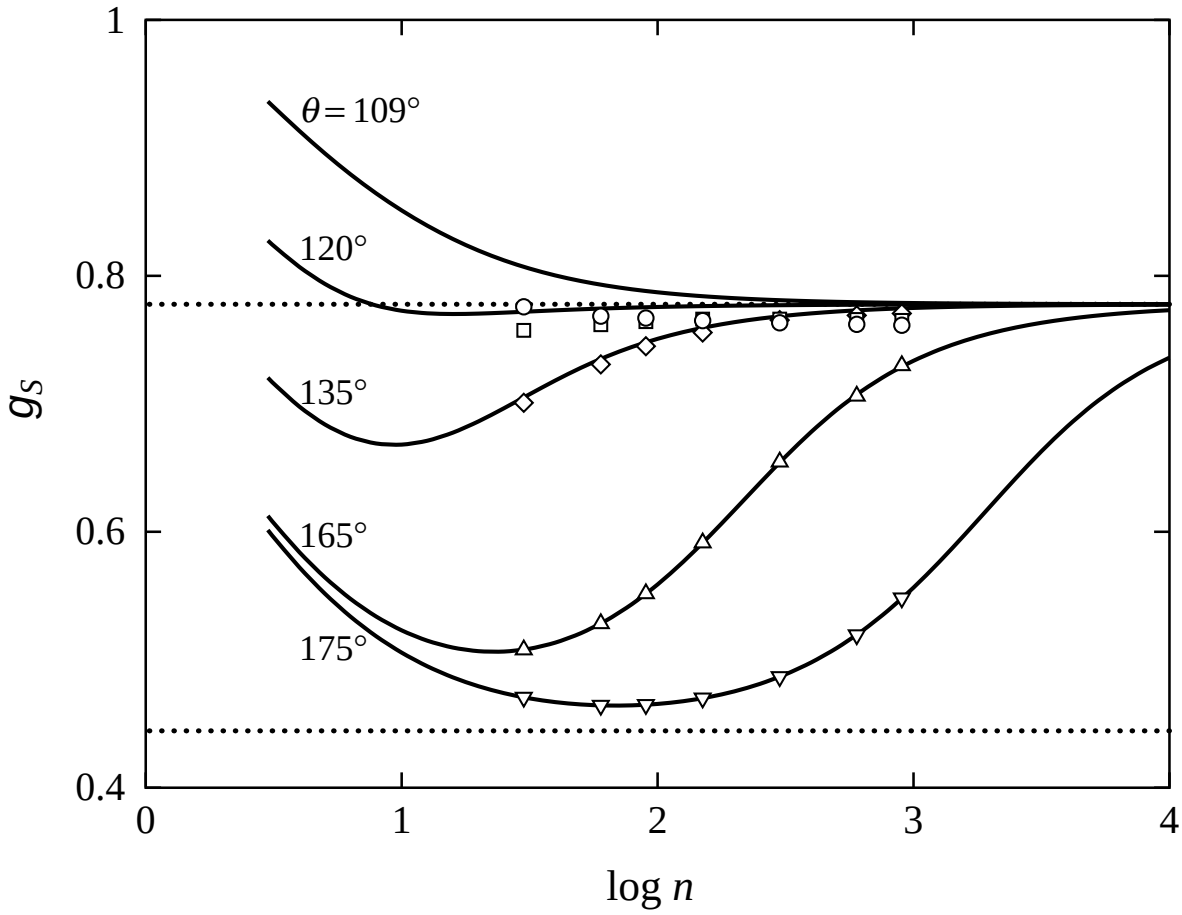

Figure 4.2. Plots of g_S against $\log n$ at $T^* = 8.0$ (good solvent system) for the freely rotating chains of $\theta = 109°$ ($\bigcirc$), 120° ($\square$), 135° ($\diamond$), 165° ($\triangle$), and 175° ($\triangledown$). The solid curves represent the theoretical values for the ideal freely rotating chains with the indicated values of θ. The upper and lower dotted horizontal lines represent the asymptotic values 7/9 in the ideal random-coil limit and 4/9 in the rigid-rod limit, respectively.

4.3.2 Second Virial Coefficient

We have numerically evaluated A_2M^2/N_A from eqs 4.11—4.13 on the basis of the sets of sample configurations generated in the above-mentioned MC evaluation of $\langle S^2 \rangle$. The MC values of $A_2{M_b}^2/N_A$ with $M_b = M/n$ so obtained for the star and linear chains are given in the third and fifth columns, respectively, of Table 4.1, the number in the parentheses attached to each value indicating its statistical error. The $A_2{M_b}^2/N_A$ value and its error for each chain are the mean and the standard deviation, respectively, of independent MC results.

Figure 4.3 shows double-logarithmic plots of $A_2{M_b}^2/N_A$ against n at $T^* = 8.0$ (good solvent system), where all the open and closed symbols have the same meaning as those in Figure 4.1. In the case of $\theta = 109°$ (typical flexible chain), the value for the regular three-arm star is somewhat (6% at most) smaller than the corresponding value for the linear chain. For both the star and linear chains, A_2 decreases with increasing n and the slopes of the plots become almost identical with the asymptotic value -0.2 for very large n. The difference in the value of A_2 between the two chains becomes small and the slopes become gentle, as θ (chain stiffness) is increased. In the case of $\theta = 175°$ (typical semiflexible or stiff chain), A_2 becomes almost independent of n for $n \geq 100$, as in the case of the rigid rod.

It is interesting to note that the value of A_2 for the chain of $\theta = 175°$ is smaller than that of $\theta = 165°$ over the whole range of n examined. It may be regarded as arising from the fact that two chains with the LJ potential (having the attractive interaction), which are close to each other, prefer to be parallel rather than perpendicular to each other when their stiffness becomes large and their A_2 may therefore be suppressed (see the next Chapter), as discussed by Schoot and Odijk[26] in the case of long rigid rods with a van der Waals-type potential.

Figure 4.4 shows plots of g_{A_2} against $\log n$ at $T^* = 8.0$ (good solvent system). The symbols, which have the same meaning as those in Figure 4.2, represent the MC values of g_{A_2} calculated from the values of $A_2{M_b}^2/N_A$ given in the third and fifth columns in Table 4.1. We note that from the defining equation 4.1 for the effective intermolecular excluded volume V_E, g_{A_2} may be written in terms of V_E as follows,

$$g_{A_2} = \frac{A_2(\text{star})}{A_2(\text{linear})} = \frac{V_E(\text{star})}{V_E(\text{linear})} \tag{4.16}$$

In the case of $\theta = 109°$ (typical flexible chain), g_{A_2} slightly decreases with increasing n and then seems to approach a constant independent of n. The asymptotic value of g_{A_2} in the limit of $n \to \infty$ may be estimated to be 0.94 which is the mean of the three MC values 0.94_0, 0.94_0, and 0.93_6 for $n = 300$, 600, and 900, respectively. The g_{A_2} value so

obtained is rather in good agreement with the RG theory value[9] 0.968 represented by the dotted horizontal line segment in Figure 4.4. In this connection, we refer to literature experimental and theoretical values of g_{A_2} for regular stars. The former values are 0.89 and 0.79 for the regular four- and six-arm star PSs,[24,25] respectively, and they are rather in good agreement with the corresponding RG theory values[9] 0.923 and 0.808. Strictly speaking, the RG theory values are somewhat (ca. 3%) larger than the corresponding experimental and present MC values.

It is more important to see in Figure 4.4 that g_{A_2} slightly increases with increasing θ (chain stiffness) in the range of θ from 109° to 165° and it becomes almost identical with unity for $\theta = 165°$ and 175° in the range of $n \gtrsim 100$. We note that g_{A_2} in the cases of $\theta = 165°$ and 175° approaches, of course, the above-mentioned asymptotic value in the limit of $n \to \infty$. In contrast to the cases of g_S and g_η, g_{A_2} is rather insensitive to change in θ (chain stiffness). Such characteristic behavior of g_{A_2} may be regarded as arising from the fact that in terms of the (classical) perturbation theory,[4] effects of the multiple intermolecular contact become negligibly small, if any, in the rigid-rod limit. The decreases in A_2 of the star and linear chains due to the attractive interaction in the LJ potential may be considered to cancel out with each other in g_{A_2}.

Finally, we consider the *apparent* interpenetration function $\Psi_{\rm ap}$ defined by[27]

$$A_2 = 4\pi^{3/2} N_{\rm A} \frac{\langle S^2 \rangle^{3/2}}{M^2} \Psi_{\rm ap} \tag{4.17}$$

from the *whole* A_2 including effects of chain ends.[28,29] Figure 4.5 shows double-logarithmic plots of $\Psi_{\rm ap}$ against n at $T^* = 8.0$ (good solvent system). The open and closed symbols, which have the same meaning as those in Figures 4.1 and 4.3, represent the MC values for the star and linear chains, respectively, calculated from eq 4.17 with the values of $\langle S^2 \rangle / n$ and $A_2 {M_{\rm b}}^2 / N_{\rm A}$ given in Table 4.1.

In the case of $\theta = 109°$ (typical flexible chain), $\Psi_{\rm ap}$ for both the star and linear chains slightly decreases with increasing n and then seems to approach the asymptotic values 0.34 and 0.24, respectively, which are the means of the three $\Psi_{\rm ap}$ values for $n = 300$, 600, and 900, although $\Psi_{\rm ap}$ is appreciably larger for the star chain than for the linear one. The two asymptotic values are in good agreement with the literature MC values 0.35 for the star chain and 0.235 for the linear one obtained by Ohno *et al.*[30] and Barrett,[31] respectively, by the use of self-avoiding chains on the simple cubic lattice. In Figure 4.5, the two literature values for the star and linear chains are represented by the solid and dashed horizontal line segments, respectively. We note that the RG theory values[9] 0.384 and 0.269 of $\Psi_{\rm ap}$ for the perturbed flexible regular three-arm star and linear chains, respectively, are somewhat (ca. 10%) larger than the above-mentioned present and literature MC values. As θ (chain stiffness) is increased from 109° to 175°, $\Psi_{\rm ap}$ decreases monotonically.

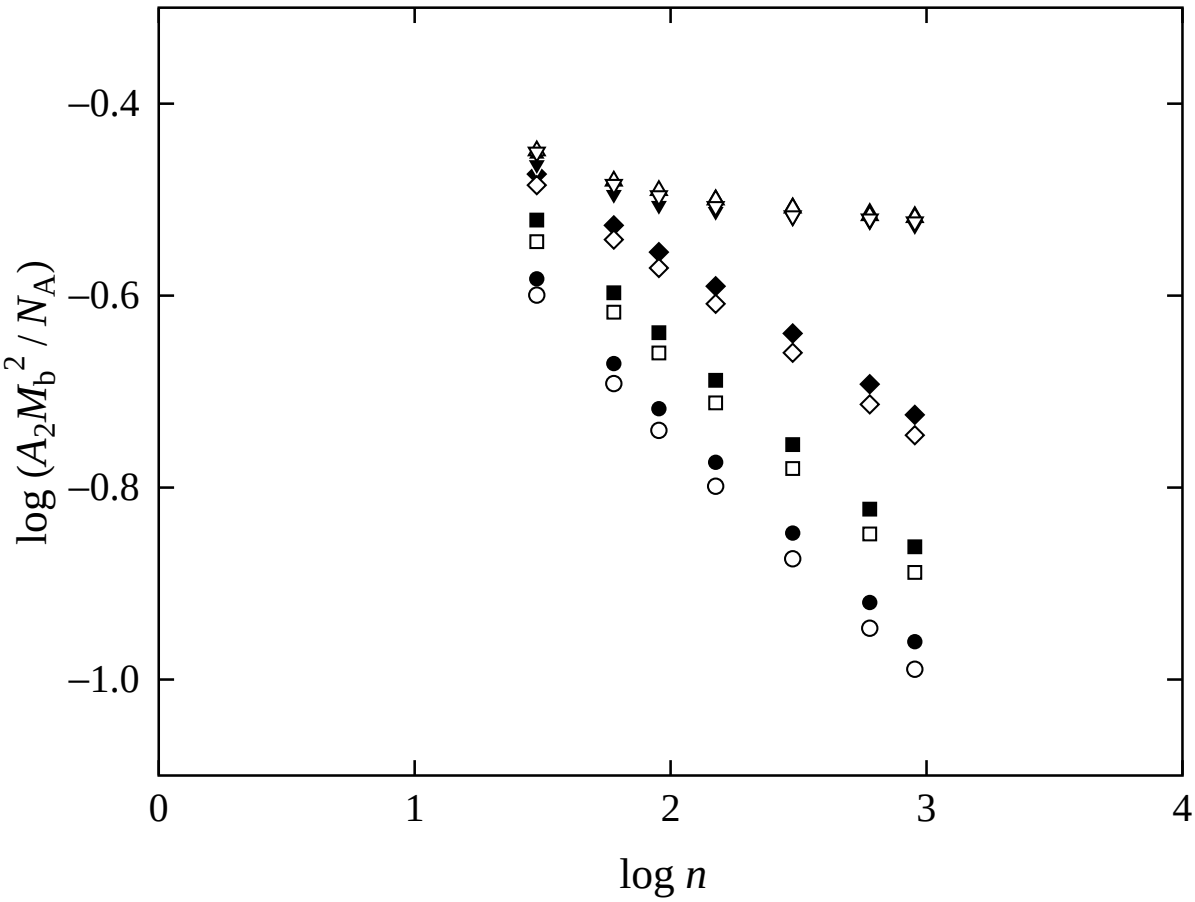

Figure 4.3. Double-logarithmic plots of $A_2{M_\mathrm{b}}^2/N_\mathrm{A}$ against n at $T^* = 8.0$ (good solvent system). All the symbols have the same meaning as those in Figure 4.1.

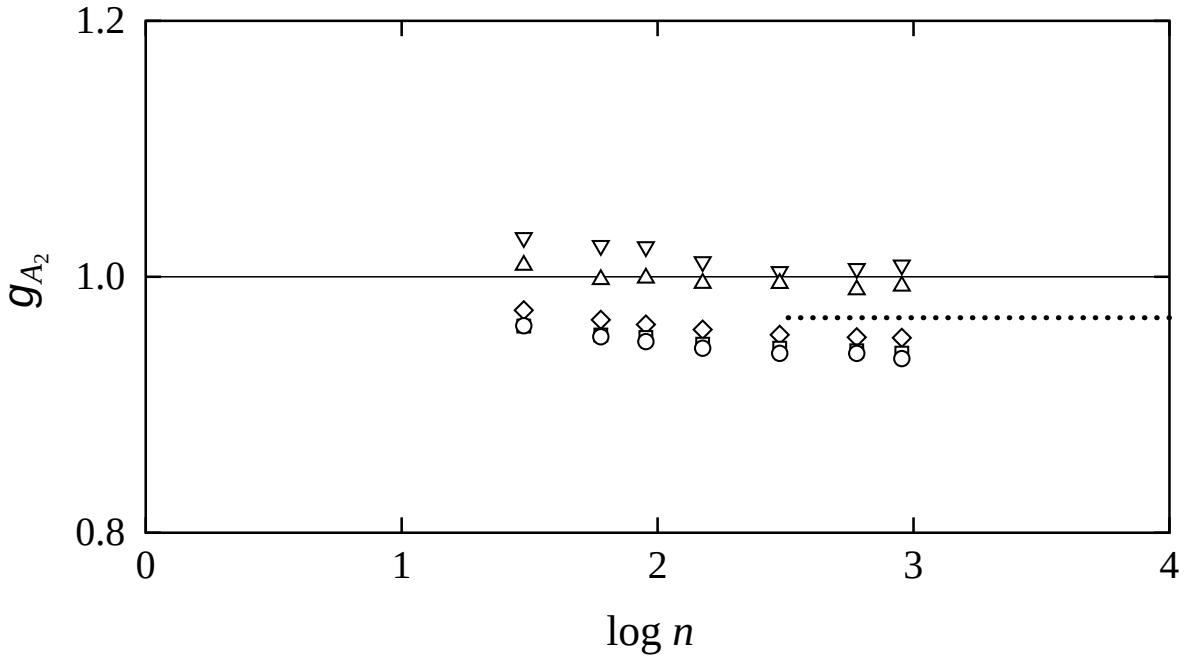

Figure 4.4. Plots of g_{A_2} against $\log n$ at $T^* = 8.0$ (good solvent system). All the symbols have the same meaning as those in Figure 4.2. The dotted horizontal line segment represents the RG theory value[9] 0.968.

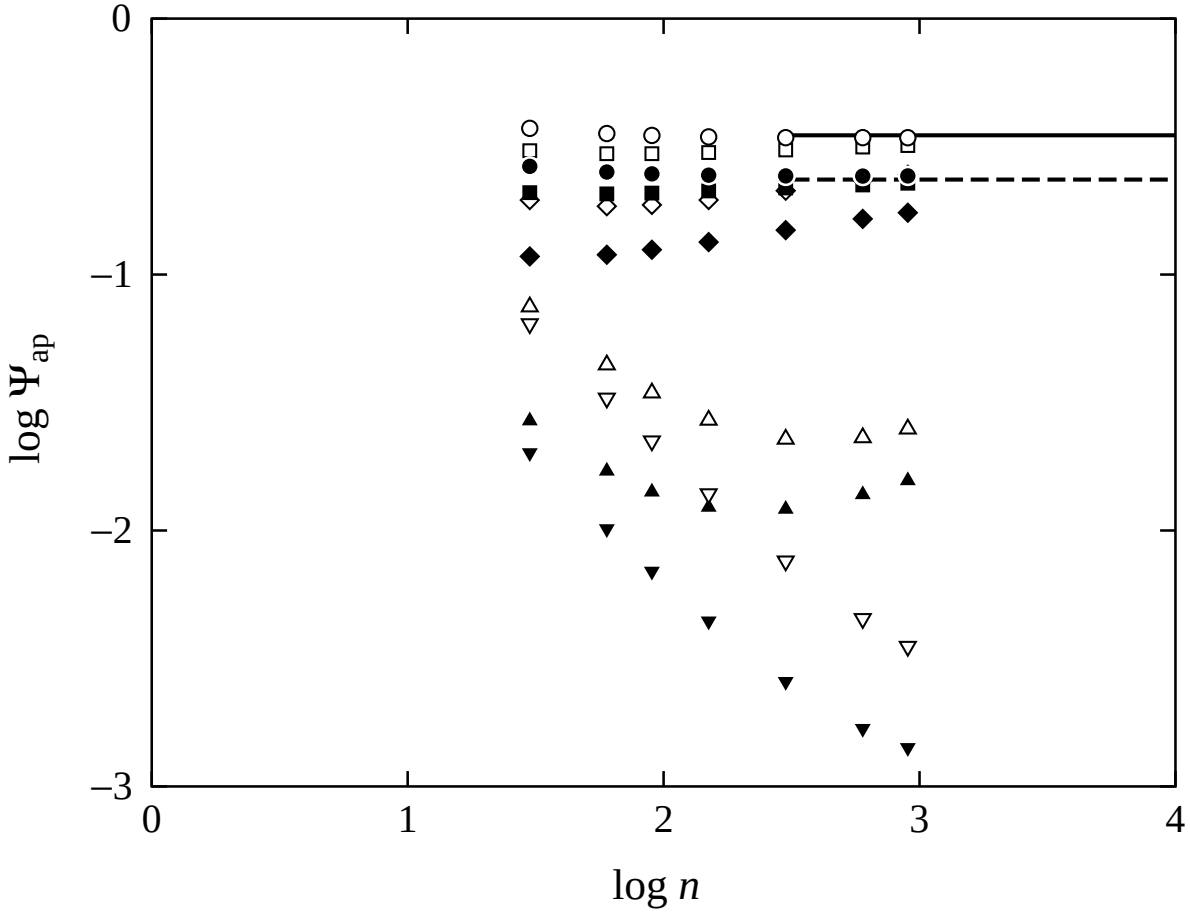

Figure 4.5. Double-logarithmic plots of $\Psi_{\rm ap}$ against n at $T^* = 8.0$ (good solvent system). All the symbols have the same meaning as those in Figure 4.1. The solid horizontal line segment represents the asymptotic value 0.35 in the random-coil limit obtained by Ohno *et al.*[30] for the self-avoiding regular three-arm star chain on the simple cubic lattice and the dashed one the corresponding value 0.235 obtained by Barrett[31] for the self-avoiding linear chain on the same lattice.

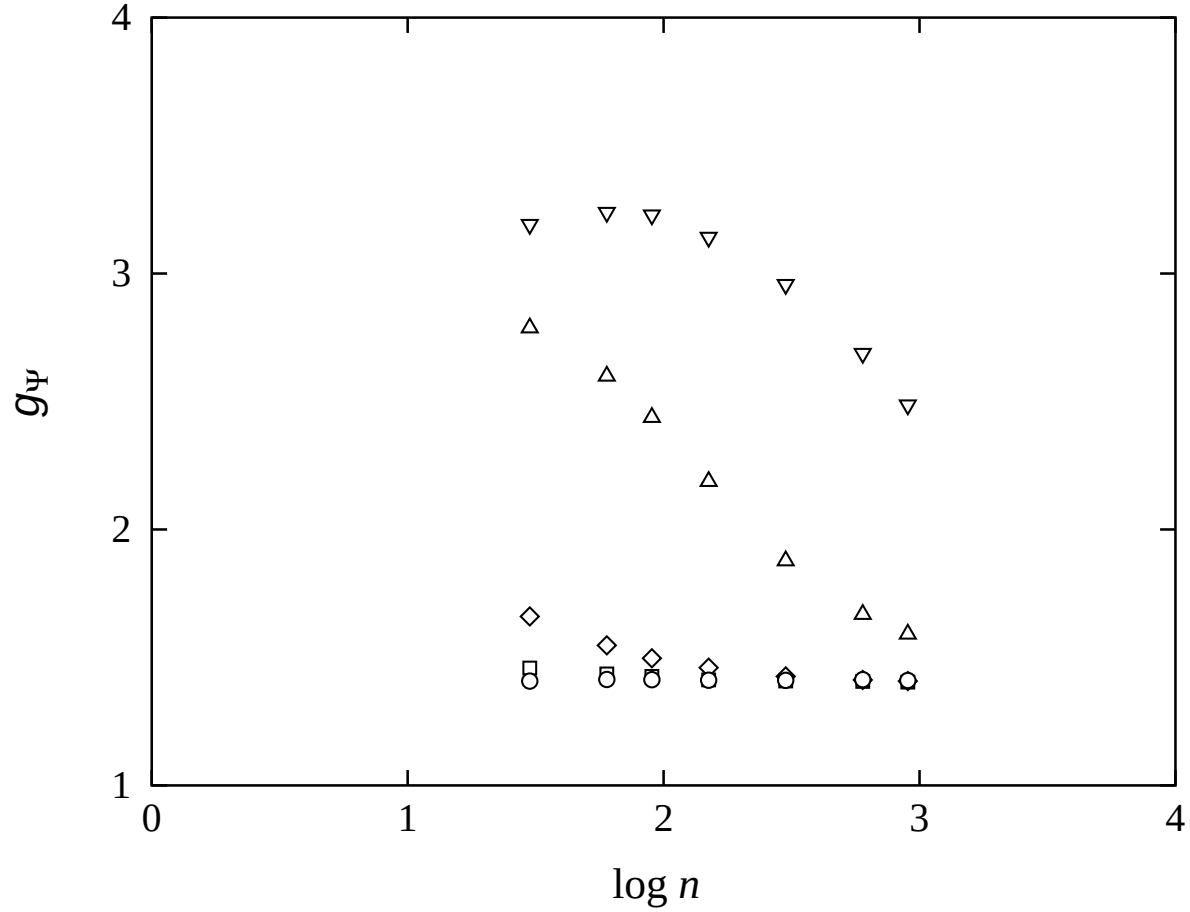

Figure 4.6. Plots of g_Ψ against $\log n$ at $T^* = 8.0$ (good solvent system). All the symbols have the same meaning as those in Figure 4.2.

From eqs 4.16 and 4.17, g_{A_2} may be written in the form,

$$g_{A_2} = g_S^{3/2} g_\Psi \tag{4.18}$$

where g_Ψ is the ratio of $\Psi_{\rm ap}$ of the regular three-arm star chain to that of the corresponding linear one. Figure 4.6 shows plots of g_Ψ against $\log n$ at $T^* = 8.0$ (good solvent system), where all the symbols have the same meaning as those in Figures 4.2 and 4.4. It is seen that g_Ψ remarkably increases with increasing θ (chain stiffness). From eq 4.18 with the results shown in Figures 4.2, 4.4, and 4.6, it may be said that the increase in g_Ψ compensates the decrease in $g_S^{3/2}$ and therefore g_{A_2} is insensitive to change in θ (chain stiffness).

4.4 Conclusion

We have examined the effects of chain stiffness on the ratio g_{A_2} of A_2 of the regular three-arm star chain to that of the corresponding linear one on the basis of the MC results for A_2 and $\langle S^2 \rangle$ of the freely rotating chains with the LJ 6-12 potential corresponding to a good solvent system. It is found that g_{A_2} is rather insensitive to change in chain stiffness in contrast to the cases of the ratios g_S and g_η related to $\langle S^2 \rangle$ and $[\eta]$, respectively, which remarkably decrease with increasing chain stiffness. Such characteristic behavior of g_{A_2} may be regarded as arising from the fact that in terms of the (classical) perturbation theory,[4] the effects of the multiple intermolecular contact become negligibly small, if any, in the rigid-rod limit, or in other words, the increase in the ratio g_Ψ related to $\Psi_{\rm ap}$ compensates the decrease in $g_S^{3/2}$.

References

1. D. Ida and T. Yoshizaki, *Polym. J.*, **39**, 1373 (2007).
2. D. Ida, Y. Nakamura, and T. Yoshizaki, *Polym. J.*, **40**, 256 (2008).
3. J. G. Kirkwood and J. Riseman, *J. Chem. Phys.*, **16**, 565 (1948).
4. H. Yamakawa, "Modern Theory of Polymer Solutions," Harper & Row, New York, 1971. Its electronic edition is available on-line at the URL: `http://www.molsci.polym. kyoto-u.ac.jp/archives/redbook.pdf`
5. B. H. Zimm and R. W. Kilb, *J. Polym. Sci.*, **37**, 19 (1959).
6. I. M. Irurzun, *J. Polym. Sci., Part B: Polym. Phys.*, **35**, 563 (1997).
7. M. L. Mansfield and W. H. Stockmayer, *Macromolecules*, **13**, 1713 (1980).
8. B. H. Zimm and W. H. Stockmayer, *J. Chem. Phys.*, **17**, 1301 (1949).
9. J. F. Douglas and K. F. Freed, *Macromolecules*, **17**, 1854 (1984).

10. W. G. McMillan and J. E. Mayer, *J. Chem. Phys.*, **13**, 276 (1945).
11. J. P. Hansen and I. R. McDonald, "Theory of Simple Liquids," 3rd ed., Academic, London, 2006.
12. H. Yamakawa and T. Yoshizaki, *J. Chem. Phys.*, **118**, 2911 (2003).
13. H. Yamakawa and T. Yoshizaki, *J. Chem. Phys.*, **119**, 1257 (2003).
14. M. Lal, *Mol. Phys.*, **17**, 57 (1969).
15. N. Madras and A. D. Sokal, *J. Stat. Phys.*, **50**, 109 (1988).
16. N. Metropolis, A. W. Rosenbluth, M. N. Rosenbluth, A. H. Teller, and E. Teller, *J. Chem. Phys.*, **21**, 1087 (1953).
17. S. D. Stellman and P. J. Gans, *Macromolecules*, **5**, 516 (1972).
18. S. D. Stellman, M. Froimowitz, and P. J. Gans, *J. Comput. Phys.*, **7**, 178 (1971).
19. M. Matsumoto and T. Nishimura, *ACM Trans. Model. Comput. Simul.*, **8**, 3 (1998), see also the URL: `http://www.math.keio.ac.jp/matsumoto/emt.html`
20. M. Guenza, M. Mormino, and P. Perico, *Macromolecules*, **24**, 6168 (1991).
21. W. Bruns, *Macromolecules*, **17**, 2826 (1984).
22. H. Yamakawa and T. Yoshizaki, *J. Chem. Phys.*, **121**, 3295 (2004).
23. N. Khasat, R. W. Pennisi, N. Hadjichristidis, and L. J. Fetters, *Macromolecules*, **21**, 1100 (1988).
24. M. Okumoto, Y. Nakamura, T. Norisuye, and A. Teramoto, *Macromolecules*, **31**. 1615 (1998).
25. M. Okumoto, Y. Iwamoto, Y. Nakamura, and T. Norisuye, *Polym. J.*, **32**. 422 (2000).
26. P. van der Schoot and T. Odijk *J. Chem. Phys.*, **97**, 515 (1992).
27. Y. Einaga, F. Abe, and H. Yamakawa, *Macromolecules*, **26**, 6243 (1993).
28. H. Yamakawa, *Macromolecules*, **25**, 1912 (1992).
29. H. Yamakawa, "Helical Wormlike Chains in Polymer Solutions," Springer, Berlin, 1997.
30. K. Ohno, K. Shida, M. Kimura, and Y. Kawazoe, *Macromolecules*, **29**, 2269 (1996).
31. A. J. Barrett, *Macromolecules*, **18**, 196 (1985).

5 Some Comments on the Second Virial Coefficient of Semiflexible Polymers

5.1 Introduction

When we consider dilute solution behavior of nonionic flexible polymers in good solvents, interactions between segments constituting the polymer chains are all, without exception, treated in the binary cluster approximation, both in the frameworks of the (classical) perturbation theory[1] and of the polymer renormalization group theory.[2–4] The approximation assumes that the effect of the interactions, i.e., the excluded-volume effect, does not depend on a detailed form of the pair potential $u(R)$ of mean force between the segments as a function of their separation R but only on the binary-cluster integral β defined by

$$\beta = 4\pi \int_0^\infty [1 - e^{-u(R)/k_{\mathrm{B}}T}] R^2 \, dR \tag{5.1}$$

with k_{B} the Boltzmann constant and T the absolute temperature. The quantity β so defined in the perturbation theory represents the effective volume excluded to one segment by the presence of another,[1] which, strictly speaking, might be distinguished from an analog defined in the polymer renormalization group theory. Since $u(R)$ is in general short-ranged for nonionic polymers, the approximation is considered to be valid and has actually been working well as far as nonionic flexible polymers are concerned. In this chapter, we consider the question of whether or not the approximation is still valid when the polymer chain becomes stiff. We note that such a question is, of course, outside the scope of the polymer renormalization group theory which completely discards information about local structures of polymer chains.

For the present purpose, we carry out a Monte Carlo (MC) simulation study of the mean-square radius of gyration $\langle S^2 \rangle$ and second virial coefficient A_2 for the freely rotating chain[1,5] of bond angle θ ranging from 109° to 175° and with the Lennard–Jones (LJ) 6-12 potential[6] or the hard-sphere (HS) one. The chain of $\theta = 109°$ ($\simeq$ tetrahedral bond angle) is usually used as a model for flexible polymer chains,[7–9] and the stiffness of the chain increases with increasing θ from 109° to 175°. Considering the fact that the binary cluster approximation works well for flexible chains, it is expected that we can find an appropriate diameter of the HS model so that both its $\langle S^2 \rangle$ and A_2 agree with the corresponding ones

of the LJ model with given energy parameters. In anticipation of results, we note that such a diameter really exists. Then the above question becomes more concrete, i.e., how the values of $\langle S^2 \rangle$ and A_2 for the two interaction potentials come to be, as θ is increased from 109° to 175°.

5.2 Models and Methods

The model chain and the simulation algorithm used in this study is the same as those in the previous studies[7,8] of $\langle S^2 \rangle$ and A_2, except for the inclusion of the HS potential. Here we give brief descriptions of the model and algorithm.

The model chain is the freely rotating chain[1,5] composed of n bonds, each of length unity, and of $n+1$ identical beads, whose centers are located at the $n-1$ junctions of two successive bonds and at the two terminal ends. The beads are numbered 0, 1, 2, $\cdots$, n from one end to the other, and the ith bond vector connects the centers of the $(i-1)$th and ith beads with its direction from the $(i-1)$th to the ith bead. All the $n-1$ bond angles (not supplements) are fixed at θ, so that the configuration of the entire chain may be specified by the set of $n-2$ internal rotation angles $\{\phi_{n-2}\} = (\phi_2, \phi_3, \cdots, \phi_{n-1})$ apart from its position and orientation in an external Cartesian coordinate system, where ϕ_i is the internal rotation angle around the ith bond vector.

The total intramolecular (excluded-volume) potential energy U of the chain as a function of $\{\phi_{n-2}\}$ may be given by

$$U(\{\phi_{n-2}\}) = \sum_{i=0}^{n-4} \sum_{j=i+4}^{n} u(R_{ij}) \tag{5.2}$$

where $u(R_{ij})$ is the pair potential as a function of the distance R_{ij} between the centers of the ith and jth beads. We must note here that the pairwise decomposability of the potential energy has been assumed, as is usually done in the field.[1] We also note that in eq 5.2 the interactions between the third-neighbor beads along the chain have been neglected, since they seem to make the chain locally take the *cis* conformation to excess in the case of the LJ 6-12 potential with an attractive interaction.

Similarly, the total intermolecular (excluded-volume) potential energy $U_{12}(1,2)$ between two chains 1 and 2 as a function of all the coordinates of chains 1 and 2 may be given by

$$U_{12}(1,2) = \sum_{i_1=0}^{n} \sum_{i_2=0}^{n} u(R_{i_1 i_2}) \tag{5.3}$$

where $R_{i_1 i_2}$ is the distance between the centers of the i_1th bead of chain 1 and of the i_2th one of chain 2. We note that we use the McMillan–Mayer symbolism[1,10] to formulate A_2,

here and hereafter. Then the ith bead ($i = 0, 1, 2, \cdots, n$) of chain α ($\alpha = 1, 2$) is labeled as i_α, and the symbol (α) ($\alpha = 1, 2$) denotes all the coordinates (external and internal) of chain α.

As mentioned in Section 5.1, we adopt as the pair potentials $u(R)$ the LJ 6-12 potential in a cutoff version and the HS one, the former being given by

$$\begin{aligned} u(R) &= \infty && \text{for } 0 \le R < c\sigma \\ &= u^{\mathrm{LJ}}(R) && \text{for } c\sigma \le R < 3\sigma \\ &= 0 && \text{for } 3\sigma \le R \end{aligned} \tag{5.4}$$

where $u^{\mathrm{LJ}}(R)$ is the LJ 6-12 potential given by[6]

$$u^{\mathrm{LJ}}(R) = 4\epsilon\left[\left(\frac{\sigma}{R}\right)^{12} - \left(\frac{\sigma}{R}\right)^{6}\right] \tag{5.5}$$

with σ and ϵ the collision diameter and the depth of the potential well at the minimum of $u^{\mathrm{LJ}}(R)$, respectively. We note that $u(R)$ given by eqs 5.4 is the LJ potential cut off at the upper bound 3σ. The lower bound $c\sigma$ in eqs 5.4 has been introduced for numerical convenience; the factor c is properly chosen so that the Boltzmann factor $e^{-u^{\mathrm{LJ}}(c\sigma)/k_{\mathrm{B}}T}$ may be regarded as numerically vanishing compared to unity. In practice, in double-precision numerical computation, we put

$$c = \left[2/\left(1 + \sqrt{1 + 36T^*}\right)\right]^{1/6} \tag{5.6}$$

so that $e^{-u^{\mathrm{LJ}}/k_{\mathrm{B}}T} \lesssim 2 \times 10^{-16}$ for $0 \le R < c\sigma$, where T^* is the reduced temperature defined by $T^* = k_{\mathrm{B}}T/\epsilon$. On the other hand, the HS potential is simply written in the form,[6]

$$\begin{aligned} u(R) &= \infty && \text{for } 0 \le R < \sigma_{\mathrm{c}} \\ &= 0 && \text{for } \sigma_{\mathrm{c}} \le R \end{aligned} \tag{5.7}$$

where σ_{c} is the collision diameter.

The mean-square radius of gyration $\langle S^2 \rangle$, i.e., the ensemble average of the square radius of gyration S^2 may be evaluated from

$$\langle S^2 \rangle = {N_{\mathrm{s}}}^{-1} \sum_{\{\phi_{n-2}\}} S^2(\{\phi_{n-2}\}) \tag{5.8}$$

where the sum is taken over N_{s} sample configurations $\{\phi_{n-2}\}$ generated in an MC run by an application of the pivot algorithm[11,12] and the Metropolis method of importance sampling,[13] as done in the previous MC study[7] of $\langle S^2 \rangle$. For each sample configuration, S^2 as a function of $\{\phi_{n-2}\}$ may be calculated from

$$S^2 = \frac{1}{n+1} \sum_{i=0}^{n} |\mathbf{r}_i - \mathbf{r}_{\mathrm{c.m.}}|^2 \tag{5.9}$$

with $\mathbf{r}_i$ the vector position of the center of the ith bead and $\mathbf{r}_{\mathrm{c.m.}}$ the vector position of the center of mass of the chain given by

$$\mathbf{r}_{\mathrm{c.m.}} = \frac{1}{n+1}\sum_{i=0}^{n}\mathbf{r}_i \tag{5.10}$$

In every MC run, an initial configuration is generated by trial and error so that all the distances between the centers of beads are greater than or equal to $c\sigma$ in the case of the LJ potential or σ_{c} in the case of the HS one. One configuration is sampled at every M_{nom} (nominal) pivot steps, so that $N_{\mathrm{s}} \times M_{\mathrm{nom}}$ pivot steps are required to obtain a set of N_{s} sample configurations.

As for the second virial coefficient A_2, it may be evaluated from[8]

$$A_2 = \frac{2\pi N_{\mathrm{A}}}{M^2}\int_0^\infty \left\{1 - \exp\left[-\frac{\overline{U}_{12}(r)}{k_{\mathrm{B}}T}\right]\right\} r^2 dr \tag{5.11}$$

where N_{A} is the Avogadro constant, M is the molecular weight, and $\overline{U}_{12}(r)$ is the averaged intermolecular potential as a function of the distance $r = |\mathbf{r}|$ between the centers of mass of chains 1 and 2 defined by

$$\overline{U}_{12}(r) = -k_{\mathrm{B}}T \ln\left\langle \exp\left[-\frac{U_{12}(1,2)}{k_{\mathrm{B}}T}\right]\right\rangle_r \tag{5.12}$$

In eq 5.12, $\langle\cdots\rangle_r$ indicates the conditional equilibrium average taken over the configurations of the two chains with $\mathbf{r}$ fixed by the use of the single-chain distribution function for each with the intramolecular excluded-volume potential given by eq 5.2. In practice, the conditional average may be calculated by the use of a set of N_{s} sample configurations generated above, as follows. First, we randomly sample a pair of sample configurations (chains 1 and 2) from the set and calculate the intermolecular potential U_{12} from eq 5.3 at given r after randomizing the orientations of the two configurations in the external coordinate system. Numerical evaluation of U_{12} may be carried out following the procedure used in the previous study of A_2 with the use of the "zippering" method.[14,15] Then the average on the right-hand side of eq 5.12 may be evaluated from

$$\left\langle \exp\left[-\frac{U_{12}(1,2)}{k_{\mathrm{B}}T}\right]\right\rangle_r = {N_{\mathrm{p}}}^{-1}\sum_{(1,2)}{}' \exp\left[-\frac{U_{12}(1,2)}{k_{\mathrm{B}}T}\right] \tag{5.13}$$

where $\sum'_{(1,2)}$ indicates summation over N_{p} pairs of sample configurations (1,2) at a given r. With the values of $\overline{U}_{12}(r)$ so evaluated for various values of r in the case of the LJ potential at a given T^* or of the HS potential with a given σ_{c}, the quantity A_2M^2 for a given n may then be calculated from eq 5.11 by numerical integration with the use of the trapezoidal rule formula.

In the practical evaluation of $\langle S^2 \rangle$, we have generated 10 sets of 10^5 ($= N_\mathrm{s}$) sample configurations for $n = 6$, 10, 20, 50, 100, and 200, 5 sets of those for $n = 500$, and 2 sets of those for $n = 1000$. In each case, M_nom has been chosen to be ca. $2n$. In the evaluation of $\overline{U}_{12}$ (and A_2), 10^6 or 10^7 ($= N_\mathrm{p}$) sample pairs have been taken from each set. Then the total number of sample pairs is equal to the number N_p of sample pairs in each set multiplied by the number of sets. In the both evaluations of $\langle S^2 \rangle$ and A_2, the parameter σ in the LJ potential is set equal to unity.

All the numerical work has been done by the use of a personal computer with an AMD Athlon XP 2200+ CPU. A source program coded in C has been compiled by the GNU C compiler version 2.95.4 with real variables of double precision. In the program, the subroutine package MT19937 supplied by Matsumoto and Nishimura[16] has been used instead of the subroutine RAND included in the standard C library.

5.3 Results and Discussion

5.3.1 Mean-Square Radius of Gyration

In the second column of Table 5.1 are given the MC values of $\langle S^2 \rangle / n$ for the freely rotating chains with the LJ potential at $T^* = 8.0$ (good solvent condition[7]) and with $\theta = 109°$, 120°, 135°, 165°, and 175° and $n = 6$, 10, 20, 50, 100, 200, 500, and 1000, the number in the parentheses attached to each value indicating its statistical error. The value and error for each chain are the mean and the standard deviation, respectively, of independent MC results. We note that the values for the chains with $\theta = 109°$ have been reproduced from Table I of Ref. 7 and Table III of Ref. 8

Figure 5.1 shows double-logarithmic plots of $\langle S^2 \rangle / n$ against n. The open symbols represent the above-mentioned MC values for the chains with the LJ potential for $\theta = 109°$ ($\bigcirc$), 120° ($\square$), 135° ($\diamond$), 165° ($\triangle$), and 175° ($\triangledown$). The solid curves represent the theoretical values of $\langle S^2 \rangle / n$ for the ideal freely rotating chain without interactions between beads, which have been calculated from

$$\begin{aligned} \langle S^2 \rangle = & \frac{1}{6}\frac{1-\cos\theta}{1+\cos\theta}n + \frac{1}{6}\frac{1+6\cos\theta-\cos^2\theta}{(1+\cos\theta)^2} \\ & + \frac{1}{6}\frac{-1-7\cos\theta+7\cos^2\theta+\cos^3\theta}{(1+\cos\theta)^3}\frac{1}{n+1} \\ & - \frac{2\cos^2\theta}{(1+\cos\theta)^4}\frac{1-(-\cos\theta)^{n+1}}{(n+1)^2} \end{aligned} \tag{5.14}$$

Table 5.1. Results of Monte Carlo simulation.

	$\langle S^2\rangle/n$ (error %)		$10A_2{M_\mathrm{b}}^2/N_\mathrm{A}$ (error %)	
n	LJ	HS	LJ	HS
		$\theta = 109°$		
6	0.289_2 (0.1)	0.288_6 (0.1)	5.12_2 (0.2)	4.98_5 (0.1)
10	0.315_8 (0.1)	0.313_4 (0.1)	3.94_2 (0.1)	3.99_1 (0.2)
20	0.359_9 (0.1)	0.354_9 (0.1)	2.98_8 (0.1)	3.10_8 (0.1)
50	0.428_7 (0.1)	0.421_9 (0.1)	2.24_5 (0.1)	2.36_3 (0.1)
100	0.486_7 (0.1)	0.480_7 (0.1)	1.86_6 (0.1)	1.96_0 (0.1)
200	0.551_1 (0.2)	0.546_2 (0.1)	1.56_7 (0.1)	1.64_3 (0.1)
500	0.647_2 (0.1)	0.645_8 (0.1)	1.25_8 (0.0)	1.31_0 (0.1)
1000	0.729_4 (0.1)	0.729_8 (0.1)	1.06_6 (0.1)	1.10_4 (0.1)
		$\theta = 120°$		
6	0.353_9 (0.1)	0.354_4 (0.1)	5.39_4 (0.2)	5.22_8 (0.1)
10	0.398_7 (0.1)	0.399_1 (0.1)	4.28_4 (0.2)	4.30_5 (0.1)
20	0.463_1 (0.1)	0.463_4 (0.1)	3.37_6 (0.1)	3.49_1 (0.1)
50	0.549_1 (0.1)	0.549_1 (0.1)	2.64_2 (0.2)	2.76_8 (0.1)
100	0.615_1 (0.1)	0.617_0 (0.1)	2.24_5 (0.2)	2.35_9 (0.1)
200	0.686_7 (0.1)	0.691_1 (0.2)	1.92_1 (0.1)	2.01_7 (0.1)
500	0.794_7 (0.1)	0.800_5 (0.1)	1.56_8 (0.1)	1.63_7 (0.1)
1000	0.886_8 (0.1)	0.899_4 (0.0)	1.34_0 (0.0)	1.39_7 (0.1)
		$\theta = 135°$		
6	0.458_8 (0.0)	0.459_0 (0.0)	5.43_6 (0.2)	5.41_2 (0.1)
10	0.562_3 (0.0)	0.562_5 (0.0)	4.43_0 (0.2)	4.59_7 (0.2)
20	0.710_7 (0.1)	0.711_8 (0.1)	3.65_7 (0.3)	3.92_0 (0.2)
50	0.880_0 (0.1)	0.883_4 (0.2)	3.06_7 (0.2)	3.34_2 (0.2)
100	0.982_0 (0.1)	0.989_8 (0.1)	2.73_6 (0.2)	2.98_8 (0.1)
200	1.07_4 (0.2)	1.08_6 (0.1)	2.45_3 (0.2)	2.66_7 (0.1)
500	1.19_8 (0.0)	1.21_8 (0.3)	2.10_1 (0.1)	2.27_5 (0.1)
1000	1.30_4 (0.1)	1.33_3 (0.2)	1.85_2 (0.1)	2.00_0 (0.1)
		$\theta = 165°$		
6	0.638_1 (0.0)	0.638_1 (0.0)	5.36_2 (0.4)	5.55_5 (0.3)
10	0.930_7 (0.0)	0.930_7 (0.0)	4.40_5 (0.4)	4.81_8 (0.2)
20	1.59_8 (0.0)	1.59_8 (0.0)	3.73_6 (0.5)	4.28_7 (0.2)
50	3.16_1 (0.0)	3.16_1 (0.0)	3.36_0 (0.5)	3.97_1 (0.3)
100	4.82_9 (0.0)	4.82_8 (0.1)	3.22_4 (0.2)	3.84_8 (0.4)
200	6.53_4 (0.1)	6.53_4 (0.1)	3.14_7 (0.2)	3.78_3 (0.2)
500	8.19_4 (0.1)	8.20_4 (0.0)	3.07_8 (0.4)	3.70_1 (0.2)
1000	8.92_4 (0.3)	8.95_2 (0.1)	3.03_2 (0.1)	3.64_4 (0.2)

(continued)

	$\theta = 175^\circ$			
6	0.663_4 (0.0)	0.663_4 (0.0)	5.31_9 (0.3)	5.57_0 (0.2)
10	0.991_9 (0.0)	0.991_9 (0.0)	4.35_0 (0.4)	4.83_3 (0.4)
20	1.80_5 (0.0)	1.80_4 (0.0)	3.64_9 (0.4)	4.31_2 (0.5)
50	4.17_1 (0.0)	4.17_1 (0.0)	3.24_8 (1.1)	4.02_2 (0.3)
100	7.88_5 (0.0)	7.88_5 (0.0)	3.10_7 (0.8)	3.92_8 (0.6)
200	14.5_5 (0.0)	14.5_5 (0.0)	3.02_9 (1.0)	3.85_9 (0.5)
500	29.8_2 (0.0)	29.8_3 (0.0)	2.98_6 (1.4)	3.83_6 (0.2)
1000	45.5_2 (0.0)	45.5_3 (0.0)	2.94_8 (0.7)	3.82_2 (0.1)

with the indicated values of θ. For the chain of $\theta = 109°$, which corresponds to a typical flexible chain, the MC data points deviate upward from the corresponding solid curves n is increased because of the intramolecular excluded-volume effect. For the chains of $\theta = 120°$ and 135°, the situations are the same as that in the case of $\theta = 109°$ but the deviation of the MC value from the ideal one becomes small as θ is increased. As for the chains of $\theta = 165°$ and 175°, which correspond to typical semiflexible or stiff chains, the MC values almost agree with the corresponding ideal ones over the whole range of n examined. We note that the intramolecular excluded-volume effect may be neglected for typical semiflexible or stiff chains of short chain lengths.

In the third column of Table 5.1 are also given the MC values of $\langle S^2\rangle/n$ for the freely rotating chains with the HS potential with $\sigma_c = 0.624$, the σ_c value being chosen so that the $\langle S^2\rangle/n$ values for the chains of $\theta = 109°$ are as close as possible to the corresponding values given in the second column for the chains with the LJ potential at $T^* = 8.0$. It is seen that the values of $\langle S^2\rangle/n$ for the two freely rotating chains of each θ and n agree with each other within ca. 2%. In Figure 5.1 are also shows the HS values by the closed symbols, although they are almost hidden by the open symbols (LJ values). We note that the agreement between the $\langle S^2\rangle/n$ values for the two chains of larger θ (165° and 175°) is rather natural since the intramolecular excluded-volume effect becomes immaterial for typical semiflexible or stiff chains with short chain lengths, as mentioned above. The results imply that we may assign a proper value to σ_c of the chain with the HS potential so that its $\langle S^2\rangle$ agree well with that for the chain with the LJ potential at a given T^* irrespective of the chain stiffness.

It is pertinent to make here a remark on the unperturbed value $\langle S^2\rangle_0$ of $\langle S^2\rangle$ without the excluded-volume effect. In a real polymer–solvent system, $\langle S^2\rangle_0$ means the $\langle S^2\rangle$ value in the Θ state which may be realized when repulsive and attractive interactions between repeat units (beads) cancel out each other but does not correspond to that of the ideal chain without any interactions between them. For the freely rotating chain with $\theta = 109°$, the Θ state may be reproduced by the use of the LJ potential at $T^* = 3.72$ (and with $\sigma = 1$) where $\langle S^2\rangle/n$ becomes a constant independent of n for very large n,[7] which is ca. 20% larger than the asymptotic value (ca. 1/3) of $\langle S^2\rangle/n$ calculated from eq 5.14 forthe ideal chain in the limit of $n \to \infty$. The implication is that the interactions between beads may appreciably affect $\langle S^2\rangle_0$ through the short-range interference.[7,9,17] The situation is somewhat different in the case of the HS potential only with a repulsive core, by the use of which we cannot reproduce the real unperturbed chain but only the ideal one with $\sigma_c = 0$. (Note that the chain with the LJ potential becomes the ideal one when

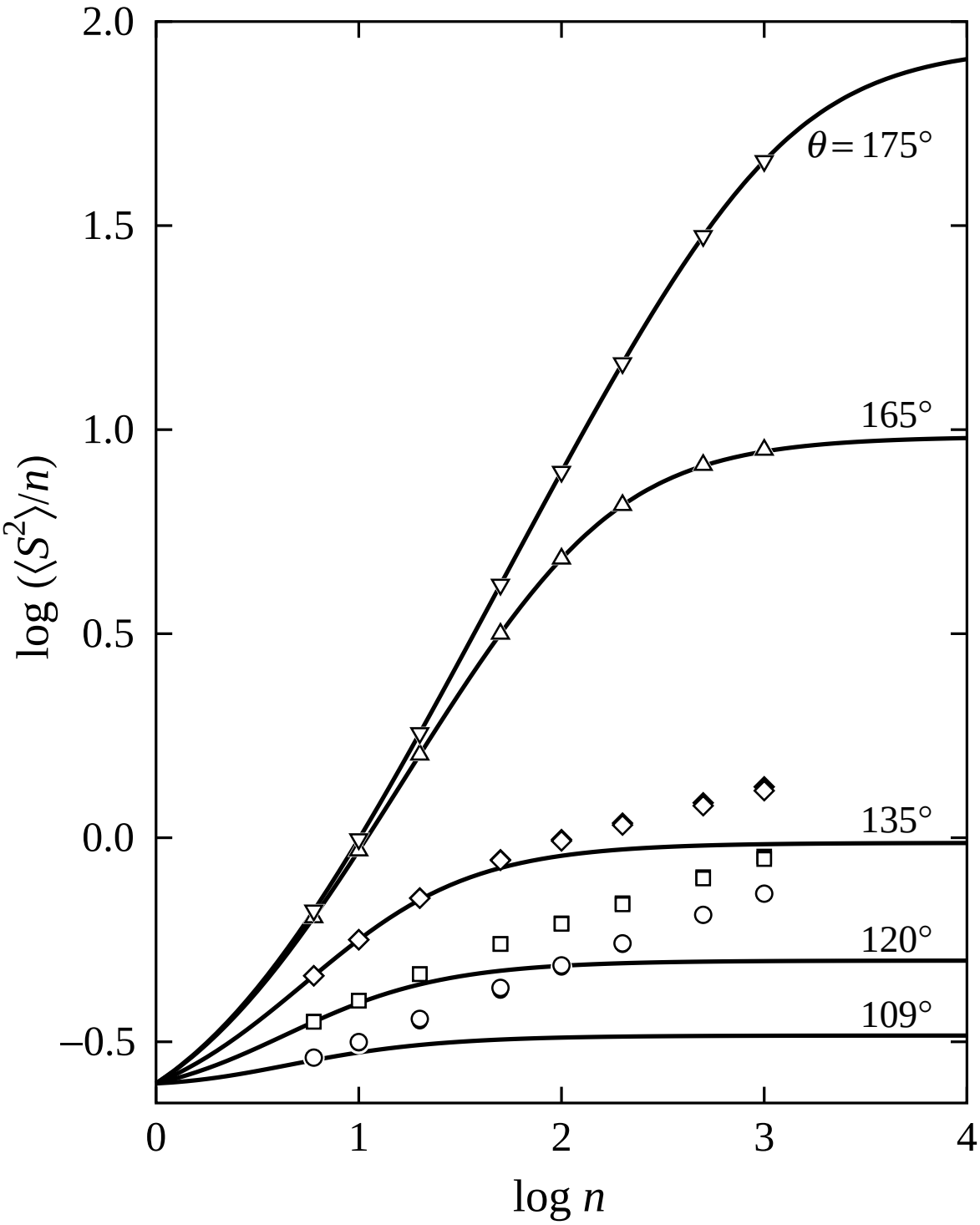

Figure 5.1. Double-logarithmic plots of $\langle S^2 \rangle / n$ against n. The open and closed symbols represent the MC values for the freely rotating chains with the LJ potential $T^* = 8.0$ and the HS one with $\sigma_c = 0.624$, respectively, for $\theta = 109°$ (○, ●), 120° (□, ■), 135° (◇, ◆), 165° (△, ▲), and 175° (▽, ▼). The solid curves represent the theoretical values for the ideal freely rotating chain without interactions between beads calculated from eq 5.14 with the indicated values of θ.

$\sigma = 0$.) Although the interaction between beads affects $\langle S^2 \rangle_0$ through the short-range interference also in the case of the HS potential, we cannot evaluate it separately from $\langle S^2 \rangle$ with the excluded-volume effect.

5.3.2 Second Virial Coefficient and Interpenetration Function

Now the problem is whether or not the values of A_2 for the two freely rotating chains considered above agree with each other irrespective of the chain stiffness. In the fourth and fifth columns of Table 5.1 are given the MC values of $A_2 {M_\mathrm{b}}^2 / N_\mathrm{A}$ for the chains with the LJ potential at $T^* = 8.0$ and with the HS one with $\sigma_\mathrm{c} = 0.624$, respectively, where M_b $(= M/n)$ is the molecular weight per bond, the number in the parentheses attached to each value indicating its statistical error.

Figure 5.2 shows double-logarithmic plots of $A_2 {M_\mathrm{b}}^2 / N_\mathrm{A}$ against n, all the symbols having the same meaning as those in Figure 5.1. In the case of $\theta = 109°$, which corresponds to a typical flexible chain, the values of A_2 for the chain with the LJ potential (○) are slightly (5% at most) smaller than the corresponding ones for the chain with the HS potential (●) for all n except $n = 6$. For both the chains, A_2 decreases with increasing n and the slopes of the plots become almost identical with the asymptotic value -0.2 for very large n. For a given n, A_2 increases with increasing θ in the range of large n. In the case of $\theta = 175°$, which corresponds to a typical semiflexible or stiff chain, A_2 becomes almost independent of n for $n \geq 100$, as in the case of the rigid rod.

It is more important to see in Figure 5.2 that as θ (chain stiffness) is increased, the value of A_2 for the chain with the LJ potential becomes remarkably smaller than the corresponding value for the chain with the HS one and that A_2 for the former chain with a given n has a maximum at $\theta = 165°$ while it increases monotonically with increasing θ for the latter. It may be regarded as arising from the fact that two chains with the LJ potential (having the attractive interaction) which are close to each other prefer to be parallel rather than perpendicular to each other when their stiffness becomes large and their A_2 may therefore be suppressed, as discussed by Schoot and Odijk[18] in the case of long rigid rods with a van der Waals-type potential.

Finally, we examine the behavior of the *apparent* interpenetration function Ψ_ap defined by[19]

$$A_2 = 4\pi^{3/2} N_\mathrm{A} \frac{\langle S^2 \rangle^{3/2}}{M^2} \Psi_\mathrm{ap} \tag{5.15}$$

from the *whole* A_2 including the effects of chain ends[20,21] as a function of n. Figure 5.3 shows double-logarithmic plots of Ψ_ap against n, where the values of Ψ_ap have been calculated from eq 5.15 with the MC values of $\langle S^2 \rangle / n$ and $A_2 {M_\mathrm{b}}^2 / N_\mathrm{A}$ given in Table 5.1.

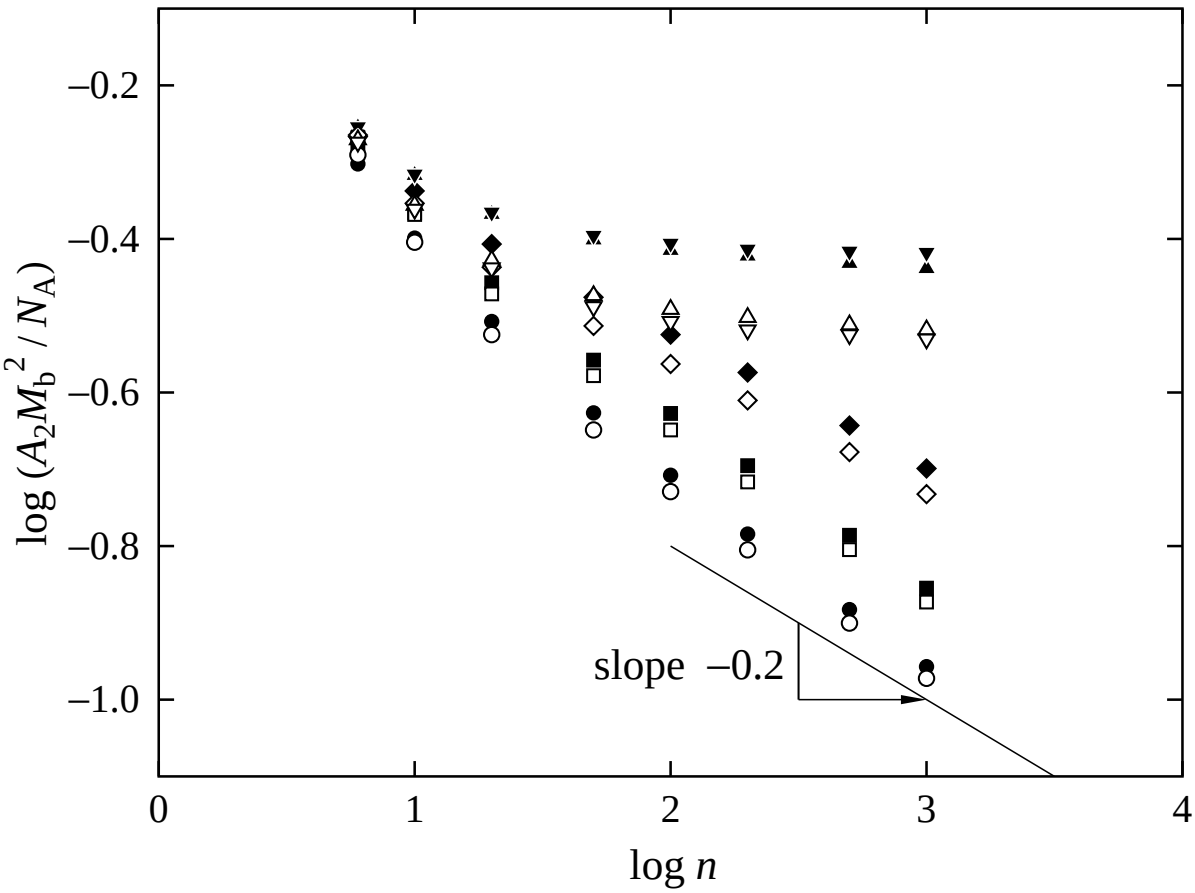

Figure 5.2. Double-logarithmic plots of $A_2{M_\mathrm{b}}^2/N_\mathrm{A}$ against n. All the symbols have the same meaning as those in Figure 5.1.

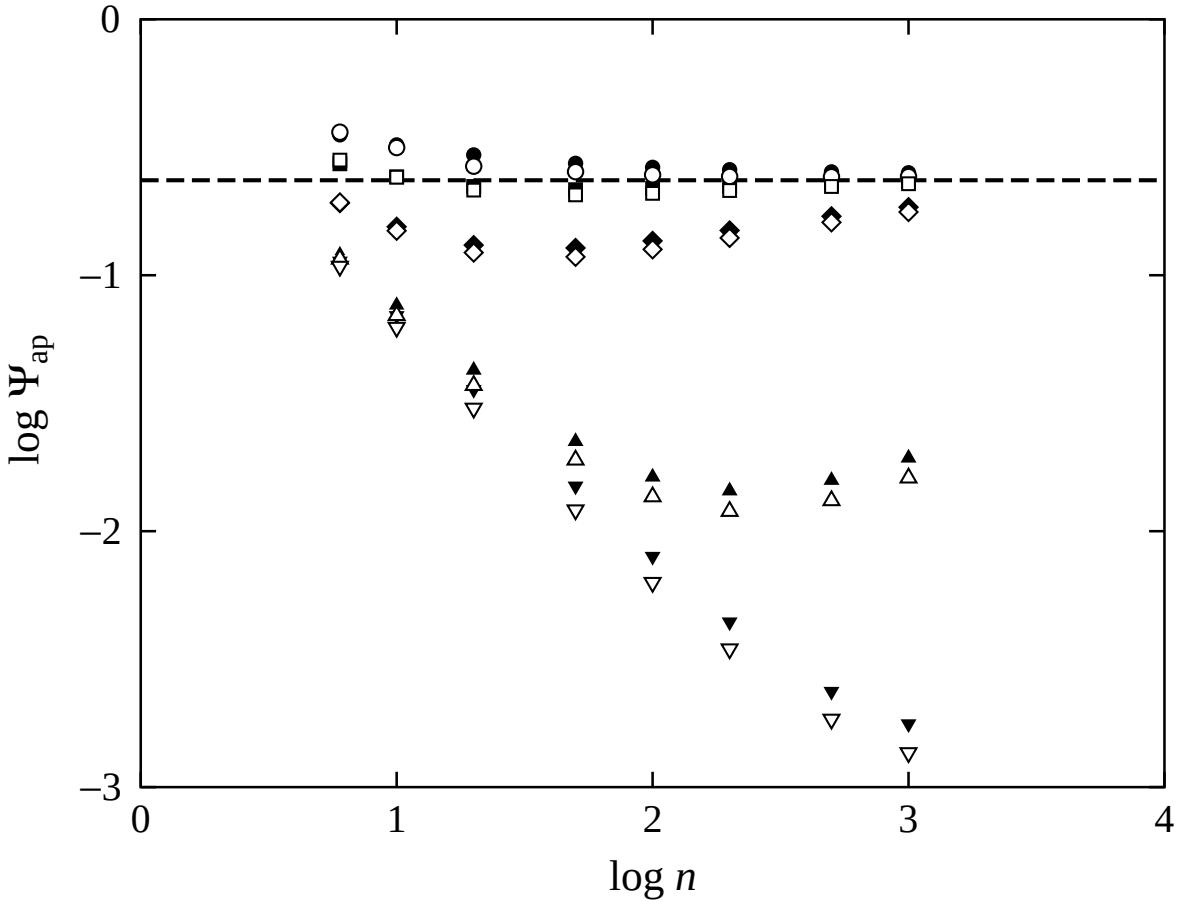

Figure 5.3. Double-logarithmic plots of Ψ_{ap} against n. All the symbols have the same meaning as those in Figure 5.1. The dashed horizontal line represents the asymptotic value 0.235 of Ψ obtained by Barrett.[22]

All the symbols have the same meaning as those in Figure 5.1 and the dashed horizontal line represents the asymptotic value 0.235 of $\Psi_{\rm ap}$ (or Ψ without the effects of chain ends) obtained by Barrett.[22]

In the case of $\theta = 109°$, the values of $\Psi_{\rm ap}$ for the chains with the LJ and HS potentials agree with each other within 7% at most, which is a natural consequence of the results for $\langle S^2 \rangle$ and A_2 for the two chains shown in Figures 5.1 and 5.2, respectively, and they decrease monotonically with increasing n and seem to approach the above asymptotic value. In the cases of $\theta = 120°$, 135°, and 165°, $\Psi_{\rm ap}$ for the chains with a given n decreases with increasing θ and $\Psi_{\rm ap}$ as a function of n exhibits a minimum and increases monotonically with increasing n after passing through the minimum. In the case of $\theta = 175°$, $\Psi_{\rm ap}$ does not exhibit a minimum and decreases monotonically with increasing n in the whole range of n examined. We note that even in this case, $\Psi_{\rm ap}$ approaches to the asymptotic value in the limit of $n \to \infty$ after passing through a minimum at some value of n larger than 1000. It is seen that the larger downward deviation from the asymptotic value is, the larger difference between the values of the two chains with the LJ and HS potentials is.

From the MC results shown in Figures 5.2 and 5.3, it may be concluded that the intermolecular excluded volume of the chain with the LJ potential becomes smaller than that of the corresponding chain with the HS one as the chain stiffness is increased even if $\sigma_{\rm c}$ properly determined so that the intramolecular excluded for the two chains agree well with each other. In other words, the binary cluster approximation does not seem to work well for typical semiflexible and stiff polymers.

5.4 Conclusion

We have examined the behavior of the mean-square radius of gyration $\langle S^2 \rangle$ and second virial coefficient A_2 for the two freely rotating chains with the LJ 6-12 and HS potentials under a good solvent condition by MC simulation, giving major attention to the effect of chain stiffness on the intra- and intermolecular excluded volumes. It is shown that we may satisfactorily assign the value 0.624 to the collision diameter $\sigma_{\rm c}$ of the HS potential so that $\langle S^2 \rangle$ of the chain with the HS potential agrees well with that of the chain with the LJ one at the reduced temperature $T^* = 8.0$ irrespective of the chain stiffness (i.e., the bond angle θ of the freely rotating chain in the range from 109° to 175°). It is then found that A_2 of the latter chain becomes remarkably smaller than that of the former as the chain stiffness (θ) is increased in contrast to the case of $\langle S^2 \rangle$. The result implies that the binary cluster approximation does not seem to work well for typical semiflexible and stiff polymers.

References

1. H. Yamakawa, "Modern Theory of Polymer Solutions," Harper & Row, New York, 1971. Its electronic edition is available on-line at the URL: `http://www.molsci.polym.kyoto-u.ac.jp/archives/redbook.pdf`
2. P.-G. de Gennes, "Scaling Concepts in Polymer Physics," Cornell Univ., Ithaca, New York, 1979.
3. K. F. Freed, "Renormalization Group Theory of Macromolecules," John Wiley & Sons, New York, 1987.
4. J. des Cloizeaux and G. Jannink, "Polymers in Solution. Their Modelling and Structure," Clarendon Press, Oxford, 1990.
5. P. J. Flory, "Statistical Mechanics of Chain Molecules," Interscience, New York, 1969.
6. J. P. Hansen and I. R. McDonald, "Theory of Simple Liquids," 3rd ed., Academic, London, 2006.
7. H. Yamakawa and T. Yoshizaki, *J. Chem. Phys.*, **118**, 2911 (2003).
8. H. Yamakawa and T. Yoshizaki, *J. Chem. Phys.*, **119**, 1257 (2003).
9. H. Yamakawa and T. Yoshizaki, *J. Chem. Phys.*, **121**, 3295 (2004).
10. W. G. McMillan and J. E. Mayer, *J. Chem. Phys.*, **13**, 276 (1945).
11. M. Lal, *Mol. Phys.*, **17**, 57 (1969).
12. N. Madras and A. D. Sokal, *J. Stat. Phys.*, **50**, 109 (1988).
13. N. Metropolis, A. W. Rosenbluth, M. N. Rosenbluth, A. H. Teller, and E. Teller, *J. Chem. Phys.*, **21**, 1087 (1953).
14. S. D. Stellman and P. J. Gans, *Macromolecules*, **5**, 516 (1972).
15. S. D. Stellman, M. Froimowitz, and P. J. Gans, *J. Comput. Phys.*, **7**, 178 (1971).
16. M. Matsumoto and T. Nishimura, *ACM Trans. Model. Comput. Simul.*, **8**, 3 (1998), see also the URL: `http://www.math.keio.ac.jp/matsumoto/emt.html`
17. W. Bruns, *Macromolecules*, **17**, 2826 (1984).
18. P. van der Schoot and T. Odijk, *J. Chem. Phys.*, **97**, 515 (1992).
19. Y. Einaga, F. Abe, and H. Yamakawa, *Macromolecules*, **26**, 6243 (1993).
20. H. Yamakawa, *Macromolecules*, **25**, 1912 (1992).
21. H. Yamakawa, "Helical Wormlike Chains in Polymer Solutions," Springer, Berlin, 1997.
22. A. J. Barrett, *Macromolecules*, **18**, 196 (1985).

List of Publications

CHAPTER 2

1. A Monte Carlo Study of the Intrinsic Viscosity of Semiflexible Three-Arm Star Polymers; D. Ida and T. Yoshizaki, *Polym. J.*, **39**, 1373—1382 (2007).

CHAPTER 3

2. Intrinsic Viscosity of Wormlike Regular Three-Arm Stars; D. Ida, Y. Nakamura and T. Yoshizaki, *Polym. J.*, **40**, 256—267 (2008).

CHAPTER 4

3. A Monte Carlo Study of the Second Virial Coefficient of the Regular Three-Arm Star Polymers; D. Ida and T. Yoshizaki, *Polym. J.*, in press.

CHAPTER 5

4. Some Comments on the Second Virial Coefficient of Semiflexible Polymers; D. Ida and T. Yoshizaki, *J. Chem. Phys.*, in press.

Acknowledgement

The present study has been carried out at the Department of Polymer Chemistry, Graduate School of Engineering, Kyoto University under the guidance of Professor Takenao Yoshizaki. The author would like to thank Professor Takenao Yoshizaki for his guidance, suggestions of the problems, numerous valuable comments, and constant encouragement, and his critical reading of the manuscript. The author has been learning from him not only many things about polymer solution science but also the true meaning of the word "scientific." This must also be acknowledged.

The author is indebted to Professor Emeritus Yoshiyuki Einaga of Nara Women's University for his valuable comments and constant encouragement throughout this work.

The author wishes to thank Associate Professor Yo Nakamura for his active collaborations and Lecturer Masashi Osa for his encouragement and helpful discussions. The author's thanks are also tendered to all the members in the laboratory of Polymer Molecular Science for their help.

Finally, the author wishes to thank his parents, Kazuhisa Ida and Eriko Ida, for their support and encouragement.